Electrical and Nonlinear Optical Studies of Specific Organic Molecular and Nonconjugated Conductive Polymeric Systems

by

Ananthakrishnan Narayanan

A dissertation submitted to the Graduate Faculty of
Auburn University
in partial fulfillment of the
requirements for the Degree of
Doctor of Philosophy

Auburn, Alabama
May 09, 2011

Keywords: Nonlinear optics, nonconjugated conducting polymer, electrical and optical characterization, spectroscopic studies, waveguides, photovoltaics

Approved by

Mrinal Thakur, Chair, Professor of Mechanical Engineering
Dan B. Marghitu, Professor of Mechanical Engineering
Lloyd S. Riggs, Professor of Electrical Engineering

Abstract

In this research, structural, electrical and nonlinear optical characteristics of: (a) single crystal films involving a noncentrosymmetric molecule DAST and a laser dye IR125 and (b) specific nonconjugated conducting polymers including poly(β-pinene) and polynorbornene have been studied.

4'-dimethylamino-N-methyl-4-stilbazolium tosylate (DAST) is a well known second order nonlinear optical material. This material has exceptionally high electro-optic coefficients, high thermal stability and ultrafast response time. In this work single crystal films involving a combination of DAST and IR125 have been prepared using modified shear method and the films have been characterized using polarized optical microscopy, X-ray diffraction, polarization dependent optical absorption and photoluminescence spectroscopy. The electro-optic coefficient of these films measured at 633nm was found to be 300pm/V. Since IR-125 has a strong absorption band from 500nm to 800nm, these films are promising for various applications in nonlinear optics at longer wavelength and for light emission.

Nonconjugated conducting polymers are a class of polymers that have at least one double bond in their repeat units. 1,4-cis polyisoprene, polyalloocimene, styrene butadiene rubber, poly(ethylenepyrrolediyl) derivatives, and poly(β-pinene) are some of the well known examples of nonconjugated conducting polymers. In this work, polynorborne, a new addition to the class of nonconjugated conducting polymers is discussed. Like other polymers in this class, polynorbornene exhibits increase in electrical conductivity by many orders of magnitude upon doping with iodine. The maximum electrical conductivity of this material is 0.01 S/cm. As

shown by using FTIR microscopy, the C=C bonds are transformed into cation radicals when polynorborne is doped. This is due to the charge-transfer from the double bond to the dopant (iodine). These materials like other nonconjugated conducting polymers have significant applications in electro-optics and photonics.

Electron paramagnetic resonance measurements on poly(β-pinene) before and after doping with iodine are reported in this work. The EPR signal of this polymer increases proportionally with the iodine concentration due to the formation of cation radicals upon doping and charge-transfer. The results agree well with the doping mechanism of nonconjugated conducting polymers discussed earlier in literature. Hyperfine splitting in heavily doped polymers is observed due to the reduced distance between the cation radical and the iodine anion.

Off-resonant electro-optic measurements in doped poly(β-pinene) at 790nm, 800nm, 810nm and 1.55μm using field-induced birefringence technique have been studied. The results show that this material exhibits the highest cubic nonlinearities of all known materials. The Kerr coefficient measured at 1.55μm is 1.6×10^{-10} m/V^2 which is about 30 times higher than that of conjugated polymers. Results of two photon measurements in this doped polymer using pump-probe technique with a pulsed, mode-locked (150 fs pulses) beam from a Ti-Sapphire laser are reported. The measured value of α_2 at 790 nm and 795 nm were found to be 2.28±0.1 cm/MW and 2.5±0.1 cm/MW respectively. The data confirms that the nonlinearity in this material is ultrafast and electronic in nature. Such large nonlinearities in these materials are attributed the charge confinement in these materials in a sub-nanometer domain (upon doping) resulting in a metal-like quantum dot structure.

Photovoltaic measurements in a composite involving poly(β-pinene) and C_{60} are discussed. This is the first time a nonconjugated conducting polymer based photovoltaic cell has

been fabricated. A composite involving 4% C_{60} by weight produced a photovoltage of 280mV for an incident light intensity of 6mW/sq.cm. These low cost devices have applications in solar cells, photodetectors etc.

A nonlinear optical waveguide was prepared by casting a thin film of poly(β-pinene) on bare multi-mode optical fiber and doping it with iodine. The doped fibers were of excellent optical quality. Two-photon absorption experiments were conducted using these waveguides and large changes in transmission upto 28% was observed in 15cm long fiber. More work needs to be done to confirm this result. This is a significant step in the direction of making these materials a viable choice for ultrafast (femtosecond time-scale) optical devices.

To summarize, these works included detailed investigations of structural, electrical and nonlinear optical characteristics of specific molecular crystal films and nonconjugated conducting polymers.

Acknowledgments

तमसो मा ज्योतिर्गमय |

O Lord! Lead me from darkness of ignorance to the light of knowledge

I consider completing this doctoral dissertation, the biggest accomplishment of my life thus far and as I write these lines, I am thrilled and full of gratitude. I dedicate this work to my family: my late grandmother for her love and affection; my parents for their immense sacrifice, support, prayers and their unstinting faith in me; my sister for her love, guidance and encouragement; my brother-in-law for being one of my best well-wishers; and to my year and a half old niece, for her priceless smiles.

The last phase of my graduate life was fraught with challenges. Looking back, I believe, I could not have done it without the moral support, encouragement and advice of Sonal.

This dissertation, without a doubt, is a culmination of the efforts all my teachers, right from the ones in kinder garden who taught all my alphabets, to those at Auburn who taught me complex concepts of quantum physics. I take this opportunity to thank them all. In particular, I thank my advisor, Dr. Mrinal Thakur, for his technical guidance and financial/infrastructural support; my doctoral committee members Dr. Marghitu and Dr. Riggs; Dr. Evert Duin for his help with the EPR measurements; Dr. Suhling and Dr. Flowers for helping me through very difficult times and Dr. Nels Madsen with whom I had the good fortune of working and learning as a Graduate Teaching Assistant.

It is a rare privilege to work in a place where every single colleague is a great friend. Jitto (you are the dude!), Swamy, Kutty, Harish, Vippa, Veera, Aditya and Sapana thank you for all the help. It was a pleasure knowing and working with all of you.

I thoroughly enjoyed my role as an instructor in Mechanical Engineering. I thank my students for their kindness and cooperation and for inspiring me to be a better teacher. I will also take this opportunity to thank my colleagues from Indian Student Association and International Student Organization, two student groups at Auburn that I have been closely associated with; I will always cherish the fond memories.

I want to express my sincere gratitude to a few individuals who have gone out of their way to help me: Ms. Nejla Orgen, Ms. Stephanie Bond, Mr. Bret Smith and Dr. James Wohl. I will miss you all.

My six year lodge at Auburn is a story of some wonderful memories, people and incidents. I thank everybody who made it an enriching and enjoyable experience. In particular, all my roommates and close confidants over the years: Bharath, Ganesh, Nono, Cheechu, Rahul, Tony, Manya, Aditya, Veera and Arjun. I would also like to thank all my friends back home for staying in touch and for being there when I needed them.

This section cannot accommodate an exhaustive list of all those who have made this dream come true. I will remember all of you. Thank you very much!

Table of Contents

List of Tables

List of Figures

CHAPTER 1

INTRODUCTION

The field of photonics has been constantly evolving and adapting to meet the ever-accelerating demands of the information age. Photonics brings together optics and electronics to efficiently handle and process enormous amount of data with exceptional speed. Development and characterization of reliable nonlinear optical materials have remained the focus in photonics for the past few decades. Organic materials in particular have attracted great research attention. Their low dielectric constants ensure that speed is never compromised. Further, the ease of fabrication and the freedom they offer to engineer them at molecular level have made them very popular. It is not difficult to predict that these materials will soon be the backbone of optical communication, information storage and other critical fields. But much waits to be explored and experimented in this field.

Ever increasing oil prices, global warming, climate change, efficient energy production and waste management are issues that have plagued today's policy makers around the globe. Finding a technological breakthrough to tap renewable sources of energy is clearly the only solution to all the problems, although, unfortunately not an easy one. Since solar energy is the most abundant and obvious of all renewable resources, development of photovoltaic materials to efficiently convert solar energy to electrical energy has been a key research initiative around the globe.

Despite their inherent advantages, organic photovoltaic materials are not widely used due to their low efficiency. Understanding the science, materials and methods involved in

organic photovoltaics could well be the solution to a problem that has economic, political, social and environmental repercussions.

The above-mentioned challenges are the key motivations for this research. The focus of this work can be divided into the following three broad categories:

1. Preparation and characterization of single crystal films involving a combination of DAST and laser dye IR125
2. Structural, electrical and nonlinear optical studies of nonconjugated conducting polymers: poly(β-pinene)and polynorbornene
3. Development and characterization of novel photovoltaic composites using nonconjugated conducting polymers and fullerene C_{60}

The contents of this dissertation are organized in 11 chapters. This chapter serves as an introduction and also briefly explains the contents and organization of this dissertation. Chapter 2 summarizes the background work related to this research. Its scope includes the history of nonlinear optics, fundamentals of electromagnetic propagation, nonlinear optical effects and processes, a brief overview of second order and third order nonlinear optical materials previously reported, a discussion on nonconjugated conducting polymers and the materials and methods involved in inorganic and organic photovoltaics.

Chapter 3 defines the objectives of this research work. Single-crystal films involving a combination of DAST and laser dye IR 125 for electro-optic applications are discussed in chapter 4. This chapter deals with the preparation of the films, their characterization using various techniques like polarized optical microscopy, optical absorption and X-ray diffraction. Experimental procedure and results of electro-optic measurements are also elaborated in this chapter.

In chapter 5, polynorborne, a nonconjugated conducting polymer, is discussed. The contents of this chapter include electrical, optical and structural properties of this polymer when doped with iodine. Electrical conductivity measurements, optical absorption, FTIR measurements, photoluminescence are discussed. The material's ability to behave like an organic quantum dot upon doping and its promise as a potential electro-optic material is also discussed.

Chapters 6 through 9 are dedicated to various experiments conducted on the non-conjugated conducting polymer, poly(β-pinene).

Chapter 6 discusses the structural characterization of doped and undoped poly(β-pinene) using Electron Paramagnetic Resonance. Relationship between dopant concentration and the formation of cation radicals is studied at room tempetarure and at lower temperature (100K). Hyperfine splitting observed in heavily doped polymers is also discussed.

Chapter 7 deals with the off-resonant electro-optic measurements at wavelengths including 1.55μm using field induced birefringence technique. Methods to protect sample life and improve the optical quality are discussed. The results are compared with other nonlinear optical materials.

Chapter 8 discusses the two-photon absorption measurements in doped poly(β-pinene) using time-resolved pump-probe technique performed with a Ti-Sapphire pulsed tunable laser.

A nonlinear optical waveguide based on a multi-mode silica fiber with a uniform thin film of the doped polymer as cladding layer is discussed in chapter 9. Experimental techniques and the results of two-photon absorption in these waveguides are also discussed.

Chapter 10 discusses photovoltaic effect in a composite involving nonconjugated polymer and C_{60}. Preparation and characterization of the photovoltaic cell and the results of the

photovoltaic measurements at different wavelengths are discussed.

Chapter 11 summarizes the overall conclusions of all works discussed in this dissertation

CHAPTER 2

BACKGROUND

2.1 Introduction to nonlinear Optics

Light is an electromagnetic radiation. The theory of electromagnetic propagation of light was first proposed by James Clerk Maxwell and was later confirmed by Heinrich Hertz.[1, 2] Electromagnetic waves consist of oscillating electric and magnetic field such that the direction of propagation of the wave, the electric field and the magnetic field are in mutually perpendicular directions. The propagation of light is governed by the following four equations, collectively known as the Maxwell's equations.

$$\boldsymbol{\nabla} \cdot \boldsymbol{D} = \rho \tag{2.1}$$

$$\boldsymbol{\nabla} \cdot \boldsymbol{B} = 0 \tag{2.2}$$

$$\boldsymbol{\nabla} \times \boldsymbol{E} = -\partial \boldsymbol{B}/\partial t \tag{2.3}$$

$$\boldsymbol{\nabla} \times \boldsymbol{H} = \boldsymbol{J} + \partial \boldsymbol{D}/\partial t \tag{2.4}$$

where $\boldsymbol{E}$ and $\boldsymbol{H}$ are the electric field and magnetic field vectors, $\boldsymbol{D}$ and $\boldsymbol{B}$ are the electric and magnetic displacement vectors, ρ and $\boldsymbol{J}$ is the charge and current density respectively. The Gauss law in equation (2.1) gives the relationship between the charge in a closed surface and the electric field. Gauss's law for magnetism in equation (2.2) states that the net magnetic flux in a closed surface is zero, owing to the fact that magnetic monopoles do not exist. Faraday's law of induction in equation (2.3) quantitatively defines the electric field caused due to change in magnetic field. Equation (2.4) is the Ampere's law which was later modified by Maxwell to its current form.

2.2 History

Nonlinear optics is a branch of science that deals with the interaction of an intense and monochromatic light source or applied electric field with a nonlinear optical (NLO) material. Although laser was invented in 1960 by Townes *et al.*[3], the genesis of nonlinear optics is traced to 1961 when Franklin *et al*. reported second harmonic generation after detecting ultraviolet light of wavelength 347.1 nm, when a ruby laser (wavelength 694.2 nm) was passed through a quartz crystal[4]. The following year, other optical nonlinear effects like third harmonic generation [5] and Raman scattering [6] were reported. Ever since then, this field has intrigued many scientists and in less than half a century, nonlinear optics has become one of the many promising fields of Physics.

2.3 Propogation of light in a medium

Optical media can be classified into two types:

1. Isotropic medium
2. Anisotropic medium

In an isotropic medium, the polarization $\boldsymbol{P}$ and the electric field displacement vector $\boldsymbol{D}$ do not depend of the direction of the applied electric field. The polarization in an isotropic medium is always parallel to the applied field and the linear relationship below holds.

$$\boldsymbol{P} = \varepsilon_o \chi \boldsymbol{E} \tag{2.5}$$

The relationship between the displacement vector and the susceptibility χ is given by

$$\boldsymbol{D} = \varepsilon_o \boldsymbol{E} + \boldsymbol{P} = \varepsilon \boldsymbol{E} \tag{2.6}$$

where ε is the dielectric constant and it depends on the susceptibility as under

$$\varepsilon = \varepsilon_o (1 + \chi) \tag{2.7}$$

In an isotropic molecular medium that is non-conducting and nonmagnetic, the electrons are tightly bound to their nucleus. When light interacts with such a medium, it may be considered as a dielectric subjected to an electric field. The polarization due to the dipole induced by the field is given by [7]

$$\boldsymbol{P} = -Ne\boldsymbol{r} \tag{2.8}$$

Where $\boldsymbol{P}$ is the polarization, e is the electronic charge, and $\boldsymbol{r}$ is the displacement induced by the field. Thus the wave equation for such a medium can be derived from the Maxwell's equations as

$$\boldsymbol{\nabla} \times \boldsymbol{\nabla} \times \boldsymbol{E} = -\frac{1}{c^2}\frac{\partial^2}{\partial t^2}\boldsymbol{D} \tag{2.9}$$

In a nonlinear anisotropic medium, the polarization is not necessarily parallel to the electric field. The polarization $\boldsymbol{P}$ is given by

$$\boldsymbol{P_1} = \varepsilon_o(\chi_{11}\boldsymbol{E_1} + \chi_{12}\boldsymbol{E_2} + \chi_{13}\boldsymbol{E_3}) \tag{2.10}$$

$$\boldsymbol{P_2} = \varepsilon_o(\chi_{21}\boldsymbol{E_1} + \chi_{22}\boldsymbol{E_2} + \chi_{23}\boldsymbol{E_3}) \tag{2.11}$$

$$\boldsymbol{P_3} = \varepsilon_o(\chi_{31}\boldsymbol{E_1} + \chi_{32}\boldsymbol{E_2} + \chi_{33}\boldsymbol{E_3}) \tag{2.12}$$

Where χ, the susceptibility is a tensor of rank 2. The electric displacement vector $\boldsymbol{D}$ is given by

$$\boldsymbol{D_i} = \varepsilon_o(1 + \chi_{ij})\boldsymbol{E_j} = \varepsilon_{ij}\boldsymbol{E_j} \tag{2.13}$$

where ε_{ij} is the permittivity tensor. If the co-ordinate system is chosen such that it coincides with the principal dielectric axes of the medium, we have

$$\begin{pmatrix} \boldsymbol{D_x} \\ \boldsymbol{D_y} \\ \boldsymbol{D_z} \end{pmatrix} = \begin{pmatrix} \varepsilon_x & 0 & 0 \\ 0 & \varepsilon_y & 0 \\ 0 & 0 & \varepsilon_z \end{pmatrix} \times \begin{pmatrix} \boldsymbol{E_x} \\ \boldsymbol{E_y} \\ \boldsymbol{E_z} \end{pmatrix} \tag{2.14}$$

The energy density due to the electric field is given by

$$\boldsymbol{U} = \frac{1}{2}\boldsymbol{E} \cdot \boldsymbol{D} \tag{2.15}$$

Since the x,y,z are chosen along the principal axes, we have

$$\boldsymbol{U} = \frac{1}{2}[\varepsilon_{11}\boldsymbol{E}_1^2 + \varepsilon_{22}\boldsymbol{E}_2^2 + \varepsilon_{33}\boldsymbol{E}_3^2] \tag{2.16}$$

$$2\boldsymbol{U} = \frac{\boldsymbol{D}_1^2}{\varepsilon_{11}} + \frac{\boldsymbol{D}_2^2}{\varepsilon_{22}} + \frac{\boldsymbol{D}_3^2}{\varepsilon_{33}} \tag{2.17}$$

$$If x = D_1\sqrt{2U}, y = D_2\sqrt{2U}, z = D_3\sqrt{2U} \tag{2.18}$$

$$\frac{x^2}{\varepsilon_{11}} + \frac{y^2}{\varepsilon_{22}} + \frac{z^2}{\varepsilon_{33}} = 1 \tag{2.19}$$

$$\frac{x^2}{n_x^2} + \frac{y^2}{n_y^2} + \frac{z^2}{n_z^2} = 1 \tag{2.20}$$

Equation (2.20) is known as the indicatrix equation, it relates the refractive index and the direction of polarization of a monochromatic light wave in a nonlinear anisotropic medium. Since the indicatrix equation traces the path of an ellipsoid, it is also called the refractive index ellipsoid.

2.4 Nonlinear optical processes

Before the advent of lasers, optical phenomena were considered to be linear. For instance, the relationship between polarization and electric field was considered to be linear. However, when lasers interacted with certain NLO materials, the linear relationship did not hold and a nonlinear dependence of polarization with applied electric field was reported[8, 9, 10, 11, 12]

$$\boldsymbol{P} = \boldsymbol{P_L} + \boldsymbol{P_{NL}} = P^{(1)}(\boldsymbol{E}) + \boldsymbol{P}^{(2)}(\boldsymbol{E}^2) + \boldsymbol{P}^{(3)}(\boldsymbol{E}^3)\ldots \tag{2.21}$$

where $\boldsymbol{P}$ is the total polarization, $\boldsymbol{P_L}$ is the linear part of the polarization and $\boldsymbol{P_{NL}}$ is the nonlinear part of the polarization caused by the electric field $\boldsymbol{E}$.

$$\boldsymbol{P_L} = \varepsilon_o\chi^{(1)}\boldsymbol{E} \tag{2.22}$$

$$\boldsymbol{P_{NL}} = \varepsilon_o\chi^{(2)}\boldsymbol{E}^2 + \varepsilon_o\chi^{(3)}\boldsymbol{E}^3\ldots \tag{2.23}$$

2.4.1 Second order nonlinear processes

NLO materials can be classified as centrosymmetric and non-centrosymmetric. Materials

in which the polarization is an odd function of electric field are called centrosymmetric materials. $(\boldsymbol{P}(-\boldsymbol{E}) = -\boldsymbol{P}(\boldsymbol{E}))$ In a centrosymmetric material

$$\chi^{(2)}\boldsymbol{E}^2 = -\chi^{(2)}\boldsymbol{E}^2 \tag{2.24}$$

This is possible only when the second order susceptibility, $\chi^{(2)} = 0$. Similarly $\chi^{(2n)} = 0$ where *n* is a positive integer. In a non-centrosymmetric material the polarization is an even function of applied electric field $(\boldsymbol{P}(-\boldsymbol{E}) = \boldsymbol{P}(\boldsymbol{E}))$ and hence the even terms of polarization can be nonzero. Clearly, to exhibit second order nonlinearities, an optical material must be non-centrosymmetric. We will now discuss the following second order nonlinearities.

1. Second harmonic generation
2. Sum frequency generation
3. Difference frequency generation
4. Optical rectification
5. Pockels effect

When a pump laser beam interacts with certain non-centrosymmetric materials, a laser beam with twice the frequency of the pump beam is produced. This phenomenon is called **second harmonic generation**. [13] If the electric field of the pump beam is [8]

$$\boldsymbol{E} = \boldsymbol{E}e^{-i\omega t} + c.c. \tag{2.25}$$

then the second order polarization $\boldsymbol{P}$ is given by

$$\boldsymbol{P} = \varepsilon_o\chi^{(2)}\boldsymbol{E}^2 \tag{2.26}$$

$$= 2\varepsilon_o\chi^{(2)}\boldsymbol{E}\boldsymbol{E}^* + (\chi^{(2)}\boldsymbol{E}^2e^{-2\omega t} + c.c.) \tag{2.27}$$

If two pump beams of frequency ω_1 and ω_2, with electric fields $\boldsymbol{E_1}$ and $\boldsymbol{E_2}$ interact with In the material is non-centrosymmetric material, we have

$$\boldsymbol{E} = \boldsymbol{E_1}e^{-i\omega_1 t} + \boldsymbol{E_2}e^{-i\omega_2 t} + \boldsymbol{E_1^*}e^{-i\omega_1 t} + \boldsymbol{E_2^*}e^{-i\omega_2 t} \tag{2.28}$$

$$\begin{aligned}\boldsymbol{P^{(2)}} = \varepsilon_o\chi^{(2)}[&\boldsymbol{E_1^2}e^{-2i\omega_1 t} + \boldsymbol{E_2^2}e^{-2i\omega_2 t} \\ &+\boldsymbol{E_1 E_2}e^{-i(\omega_1+\omega_2)t} + 2\boldsymbol{E_1 E_2^*}e^{-i(\omega_1-\omega_2)t} + c.c.] \\ &+2\varepsilon_o\chi^{(2)}[\boldsymbol{E_1 E_1^*} + \boldsymbol{E_2 E_2^*}]\end{aligned} \tag{2.29}$$

By carefully tuning the experimental conditions to achieve a particular phase matching condition, it is possible to efficiently convert the pump beam to a specific frequency. If the output frequency ω_3 is such that it is the sum of the two input frequencies ω_1 and ω_2 then the phenomenon is called **sum frequency generation** (SFG). In SFG the polarization $\boldsymbol{P}$ is given as

$$\boldsymbol{P}(\omega_1 + \omega_2) = 2\varepsilon_o\chi\boldsymbol{E_1 E_2} \tag{2.30}$$

If ω_3 is given by the difference of the pump beam frequencies, then the phenomenon is called **difference frequency generation** (DFG). The polarization $\boldsymbol{P}$ for such a nonlinear process is given by

$$\boldsymbol{P}(\omega_1 - \omega_2) = 2\varepsilon_o\chi\boldsymbol{E_1 E_2^*} \tag{2.31}$$

If the two electric fields interacting with the nonlinear crystal results in a static electric field then the process is called **optical rectification**. The polarization in this case is given by

$$\boldsymbol{P} = 2\varepsilon_o\chi(\boldsymbol{E_1 E_1^*} + \boldsymbol{E_2 E_2^*}) \tag{2.32}$$

The energy level diagram for the above three processes is shown in the figure below.

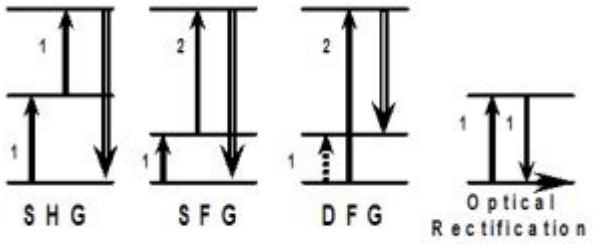

Figure 2.1 Energy level diagrams for different second order nonlinear processes

When an optical pump beam and a dc (or low frequency ac) electric field interact with a second order material, a change in refractive index proportional to applied dc (or low frequency ac) electric field is observed. This process is known as **linear electro-optic effect** or **Pockel's effect**. This was first observed by a German physicist Friedrich Pockel in 1906.[13] In a linear electro-optic effect the indicatrix equation shown in (2.20) is changed as shown. It must be noted that the x,y and the z axes cease to be the principal axes under the influence of the external field due to the presence of cross terms in the equation below.

$$\left[\frac{1}{n_x^2} + r_{1k}E_k\right]x^2+\left[\frac{1}{n_y^2} + r_{2k}E_k\right]y^2+\left[\frac{1}{n_z^2} + r_{3k}E_k\right]z^2 + 2r_{4k}E_kyz +$$

$$2r_{5k}E_kxz + 2r_{6k}E_kxy =1 \qquad (2.33)$$

where *r* is the electro-optic coefficient. Since the electro-optic tensor is symmetric about the first two indices, a shorthand notation r_{hk} is used in the above equation to denote r_{ijk} where [14, 8]

$$h=1\Rightarrow ij=11;\quad h=2\Rightarrow ij=22;\quad h=3\Rightarrow ij=33;\quad h=4\Rightarrow ij=23 \text{ or } 32;$$

$$h=5\Rightarrow ij=13 \text{ or } 31;\quad h=6\Rightarrow ij=12 \text{ or } 21 \qquad (2.34)$$

2.4.2 Third order nonlinear processes

Third order polarization in NLO materials consists of three distinct frequencies and is given by the equation below:

$$\boldsymbol{E(t) = E_1(t)e^{-w_1 t} + E_2(t)e^{-w_2 t} + E_3(t)e^{-w_3 t} + c.c.} \quad (2.35)$$

Different third order nonlinear process can be understood by separating the frequency components in the above equation. In this section we will discuss few common third order phenomena.

When some of these materials interact with an optical field and a slow time varying external field, the change in the indicatrix is quadratically related to the external field applied and is given by the relationship below:

$$\Delta n = K\lambda E^2 \quad (2.36)$$

Where Δn is the change in refractive index, K is the kerr co-efficient, λ is the wavelength of the laser beam and $\boldsymbol{E}$ is the magnitude of the slow time varying electric field. This effect was first reported by a Scottish physicist John Kerr in 1875. [15]

Kerr effect can also be observed when a highly intense laser beam propagates through a third order material. The change in refractive index is given by the equation below:

$$\Delta n = n_2 I \quad (2.37)$$

Where n_2 is the nonlinear refractive index and I is the intensity of the laser source. The nonlinear refractive index is related to the third order susceptibility $\chi^{(3)}$ per the equation below.

$$n_2 = \frac{12\pi^2\chi^{(3)}}{n_o c^2} \quad (2.38)$$

Where n_o is the weak field refractive index of the material and c is the speed of light. For glasses and some transparent crystals the nonlinear refractive index is about 10^{-16} - 10^{-14} cm/W. In 1990 Sheik Bahae reported [16] that the nonlinear refractive index in semiconductors is related to the fourth power of the energy gap and also the proximity of the energy of the laser source to the energy gap.

When a laser source whose transverse intensity propagates through a nonlinear material,

a phase delay due to Kerr effect deforms the wave front causing it to either focus or defocus depending on the sign of the nonlinear refractive index, n_2.[13] If n_2 is positive the material behaves like a positive lens and converges the beam, this is called self-focussing. When n_2 is negative an opposite effect is observed, where the material behaves like a negative lens and diverges the incident beam and this is known as self-defocusing.

Two-photon absorption is a third order nonlinear process where two photons (not necessarily of identical frequency) are excited to a higher energy level and the increase in energy is given by the sum of the energies of the two photons. The two-photon absorption co-efficient α_2 is given by

$$\Delta\alpha = \alpha_2 I \tag{2.39}$$

Where $\Delta\alpha$ is the change in linear refractive index and I is the intensity of the laser beam. Two-photon absorption is considered a nonlinear process because the strength of absorption varies as the square of the intensity of the source. This effect was first predicted by the Nobel laureate Goeppert-Mayerin[17] in her doctoral dissertation in the year 1931. However, the first experimental observation of this effect was reported three decades later after the advent of laser by two separate research groups who worked on europium doped crystal and cesium vapor.[18, 19]

2.4.3 Resonant Enhancement in Nonlinear Optical Materials

The quantum perturbation theory gives the relationship between the NLO susceptibility, transition dipole moment and the energy levels of the material. This is shown in equations below[8]

$$\chi^{(2)}_{ijk}(\omega_p + \omega_q; \omega_p, \omega_q) = \frac{NF}{\epsilon_o \hbar^2} \sum_{mn} \frac{P^i_{gn} P^j_{nm} P^k_{mg}}{(\omega_{ng} - \omega_p - \omega_q)(\omega_{mg} - \omega_p)} \tag{2.40}$$

$$\chi^{(3)}_{ijkl}(\omega_p + \omega_q + \omega_r; \omega_p, \omega_q, \omega_r) = \frac{NF}{\epsilon_o \hbar^2} \sum_{mno} \frac{P^i_{go} P^j_{on} P^k_{nm} P^l_{mg}}{(\omega_{og} - \omega_p - \omega_q - \omega_r)(\omega_{ng} - \omega_p - \omega_q)(\omega_{mg} - \omega_p)} \tag{2.41}$$

Where N is the number density of the atom, F is the permutation operator over the input frequencies, P_{jk}^{i} denotes the transition dipole moments. When the energy levels involved in the NLO process is close to the energy level of the material, the susceptibility increases significantly due to the strong coupling between the material and the light source.

2.4.4 Nonlinear Optics in Confined systems

Charge confinement is widely used in nonlinear optics to increase the optical nonlinearities. Charge confinement is achieved by artificially confining the valence electrons in regions smaller than delocalization length which results in discrete optical resonances and the characteristics of these resonances are determined by the extent of confinement. This effect has been demonstrated in various materials like metals, semiconductors and organic polymers.[20] There are two different kinds of confinements namely, quantum confinement and dielectric confinement. Both of these would be discussed in this section.

2.4.4.1Quantum Confinement

The de Broglie wavelength (λ_d) of electrons waves is given by[21]

$$\lambda_d = {}^{h}/_{p} \tag{2.42}$$

Where h is the plank's constant and p is the linear momentum. In a bulk material, free electrons can move in any direction and their thermal kinetic energy (E_T) is related to their linear momentum as

$$E_T = \frac{p_i^2}{2m_e^*} \approx \frac{1}{2} K_B T \tag{2.43}$$

Where p_i is the linear momentum along the i direction, m_e^* is the effective mass of the electron, K_B is the Boltzmann's constant and T is the absolute temperature. From the above two equations the de Broglie wavelength at a given temperature T can be expressed as

$$\lambda_d = \frac{h}{\sqrt{m_e^* K_B T}} \tag{2.44}$$

In bulk materials, the dimensions of the crystals are much larger than the de Broglie wavelength shown in equation 2.45. When the dimension of the crystal is reduced in any direction (x,y,or z), then the energy level ceases to be continuous and becomes quantized in that direction. This effect is called quantum confinement. Quantum confinement can be categorized into three groups depending on the number of directions in which the electron is confined. A one dimensional confinement can be achieved in semiconductors by sandwiching a thin layer of lower band gap material between two higher band gap materials thereby confining the electrons and holes in the lower band gap material in a finite potential well. This can be compared to a particle in a one dimensional box. Such a system is called a quantum well. Two-dimensional confinement is achieved in a quantum wires, were electrons are free to move along the direction of the wire. In a quantum wire, energy levels are quantized in the two directions perpendicular to the direction of the wire. In a three-dimensional confinement, the electron is confined in all three directions. Such a material behaves like an artificial atom. These systems are known as quantum dots. A quantum dot is an electron in a three dimensional box. Its energy is discretized in all three directions. The energy level of a simple quantum dot is as below[22, 20]

$$E_n = \frac{h^2}{8m_e}\left[\left(\frac{n_x}{l_x}\right)^2 + \left(\frac{n_y}{l_y}\right)^2 + \left(\frac{n_z}{l_z}\right)^2\right] \tag{2.45}$$

Where E_n energy level, h is the planks constant, m_e is the mass of the electron, n_i and l_i are quantum numbers and lengths respectively corresponding to the *i* direction. The figure below shows the density of states of electrons in bulk and confined structures.

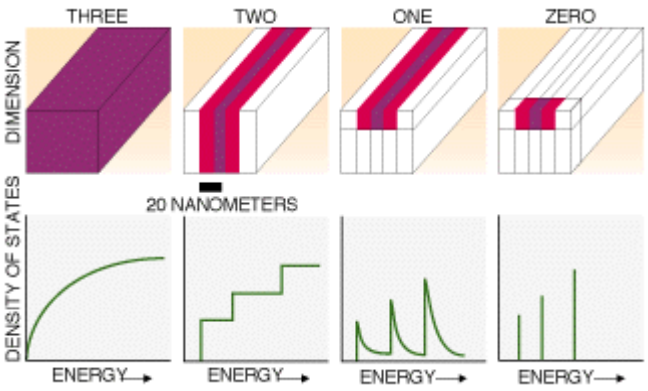

Figure 2.2: Density of states in confined systems from [20]

2.4.4.2 Dielectric confinement

In a confined system that has non-uniform charge density distribution, the electric field that polarizes the charges in the material may be different from the external field. Due to this disparity the field strength distribution varies at the interface between the confined region and the regions surrounding it. This creates an additional electric field inside the confined region due to the surface polarization and hence the dielectric constant of the surrounding area is significantly lesser that that on the confined area. When light is shined on such a system there could be an enhancement in the local field inside the confined system which would in turn affect the NLO properties of the system. [7]

2.4.4 .3 Effect of quantum confinement on third order susceptibility

The optical susceptibility in non-absorbing regions depends on the critical regions in the density of states. Since the density of states depends on the charge confinement (as can be seen in figure 2.2) the optical susceptibility is affected by charge confinement at the critical regions. In a one-dimensionally confined system (quantum well) with critical point E_o the third order susceptibility, $\chi^{(3)}$ can be expressed as [23]

$$\chi^{(3)} = \chi_{\sigma}^{(3)} \left(\frac{E_F}{E_o}\right)^6 \quad (2.46)$$

Where $\chi_{\sigma}^{(3)}$ is the third order polarizability of the non-confined structure, E_F is the Fermi level. The confinement length L dictates the ratio E_F/E_o.

In a quantum dot, where the electron is confined in all three directions with a critical surface E_2 the third order susceptibility is given by[24]

$$\chi^{(3)} \approx \frac{P_{cv}^2}{E_2^{9/2}} \quad (2.47)$$

Where P_{cv} is the interband transition dipole moment. The magnitude of P_{cv} depends on the extent of confinement. Equations 2.47 and 2.48 show that the artificial charge confinement has significant impact on the third order susceptibility

2.4.4.4 Effect of dielectric confinement on third order susceptibility

If spherical quantum dots of radius R $(R<\lambda)$ is dispersed in a dielectric medium of dielectric constant ε_0, the field (E_i) inside each particle is given by[25]

$$E_i = \frac{3\varepsilon_o}{\varepsilon+2\varepsilon_o} E \approx E f_1 \quad (2.48)$$

Where ε_o is the dielectric constant of the bulk (non-confined) material, E is the applied electric field and f_1 is a factor that approximately equals the ratio of electric field inside each particle to the applied electric field. If the polarization inside the quantum dot is of magnitude p, Maxwell and Garnett showed that the effective dipole moment of the composite $\tilde{\varepsilon}$ can be expressed as <agboyd34>

$$\tilde{\varepsilon} = \epsilon_o + 3p\varepsilon_o \frac{\epsilon-\epsilon_o}{\varepsilon+2\varepsilon_o} \quad (2.49)$$

If the frequency ω_s is such that

$$\varepsilon'(\omega_s) + 2\varepsilon_o = 0 \quad (2.50)$$

(where ε' is the real part of the bulk dielectric constant ε) the effective dielectric constant

significantly increase, correspondingly, at frequencies near ω_s there is a steep increase in the local field and such a phenomenon is called surface plasmon resonance(SPR). SPR has significant impact on the optical nonlinearities especially the optical Kerr effect. The optically induced change in dielectric constant is given by

$$\delta\tilde{\varepsilon} = 12\pi\chi^{(3)}|E(\omega)|^2 \tag{2.51}$$

Differentiating equation 2.50 and 2.51 and comparing it with equation 2.52 we have:

$$\tilde{\chi}^{(3)} = p|f_1|^2 f_1^2 \chi^{(3)} \tag{2.52}$$

where $\tilde{\chi}^{(3)}$ is the third order susceptibility of the composite. If the Kerr effect is measured at frequencies near the SPR frequency there is a substantial increase in $\tilde{\chi}^{(3)}$ in quantum dots due to dielectric confinement. This effect is over the above the enhancement caused due to quantum confinement. To summarize this discussion, the optical nonlinearities in confined nanostructures are significantly higher than their bulk counterparts due to a combination of dielectric and quantum confinements.

2.5 Nonlinear Optical Materials

The field of nonlinear optics has witnessed exponential growth since 1960 after laser was invented. The quest for materials with high optical nonlinearities has fueled the research in the field for about a half a century now. In this section we will discuss several NLO materials reported in the past. This section is divided into two subsections. The first subsection will discuss second order materials and the second will be dedicated to a discussion on third order materials.

2.5.1 Second Order Materials

During early 1960s when NLO material development and characterization was in its primitive stages, the following were taken into consideration while choosing an ideal device material.

1. The material must be non-centrosymmetric since the discussions in section 2.4 clearly shows that centrosymmetric materials do not have even order terms of susceptibility.
2. The materials must easily available
3. The materials must be birefringent to allow phase matching.
4. The material must have excellent optical quality and high refractive index
5. The material must have low dielectric constant to enable high bandwidth

The first reported optical nonlinearity was observed in quartz when Franklin and co-workers recorded a very weak second harmonic signal in quartz using a Q-switched ruby laser source [4]. The invention of phase matching was the next major breakthrough. In 1962 two research teams individually showed that phase matching in ammonium-dihydrogen phosphate (ADP) can result in significantly stronger second harmonic signals[26, 27]. Two years later Boyd and co-workers reported lithium meta-niobate ($LiNbO_3$) to be "An efficient phase matchable NLO material."[28] $LiNbO_3$ gained popularity as a photonic device material because of the several advantages it had over the then popular NLO materials ADP and KDP. Some of its advantages include its nonhygroscopic nature, hardness and ease to polishing [29]. However, the material had a notable shortcoming. In 1966 Ashkin and co-workers [30] showed that lithium meta-niobate was prone to mechanical damage when exposed to high power continuous wave gas lasers. Despite this shortcoming this material is perhaps the most popular inorganic NLO material. Other popular inorganic second order materials include potassium titanyl phosphate (KTP), lithium borate (LBO) and β-barium borate (BBO)[31].

Although some researchers reported the potential of organic materials in photonic devices, [32, 33] much attention was given to inorganic materials in 1960s. This trend changed in 1968 when Kurtz and his co-workers [34] demonstrated a powder technique to evaluate the optical

nonlinearities in powder samples of materials. Several investigators used Kurtz test to report a variety of organic materials with high optical nonlinearities [35, 36].

The shift in focus on organic nonlinear materials was due to the several advantages they have over their inorganic counterparts. Since NLO effects are electronic in nature, exceptionally high switching speeds can be attained.[37] The upper bound for bandwidth in electro-optic switches is determined by the dielectric constant of the material. The dielectric constant of the best-known inorganic nonlinear material $LiNbO_3$ is 29[38]. This limits the bandwidth of this material to 10GHz.cm. Organic polymers and single crystal films have dielectric constants as low as 3 and hence the upper bound for bandwidth for these materials go as high as 120 GHz.cm.[37] Organic materials also do not require high temperature processing and can be implemented in electrical circuitry[39]. Also, it was shown that organic materials can be optimized for NLO applications by tailoring their molecular structure [40, 41].

An ideal organic NLO material should possess a variety of characteristics like good physicochemical properties, large optical nonlinearities, wide optical transparency, flexibility in molecular design, ease of fabrication and phase matching, and must have the ability to withstand high laser intensities [7].

Some of the early organic materials investigated for second order nonlinearities were methyl 1-1,4-dinitrophenyl amino propionate (MAP) and 3-methyl-4-nitroaniline (MNA). In 1977 Oudar and co-workers reported [42] high optical nonlinearity in MAP. The researchers achieved 30% SHG conversion efficiency in a sample that was 1mm thick. The material showed promise because of its high damage threshold and large optical nonlinearity. More importantly the results showed that systematic molecular engineering approach could help achieve high optical susceptibilities. In 1979 Levine and co-workers [43] from Bell labs reported high optical

nonlinearities in MNA. The measured value of d_{12} was 45 times larger than $LiNbO_3$ and d_{11} was about 2000 times larger than $LiNbO_3$. Other early second order materials investigated were N-4-nitrophenyl-1-prolinol (NPP),[44] 2-cyclooctylamino-5-nitropyridine (COANP),[45] 3-methyl-4-methoxy-4'-nitrostilbene (MMONS)[46]. Although all the materials exhibited significantly high second order nonlinearities compared to organic materials like $LiNbO_3$, development of phase matachable high quality crystals with wide optical transparencies remained a challenge [47].

In 1983 Meredith and co-workers found that coulombic interactions in some organic salts could aid non-centrosymmetric crystallization in some organic salts [48]. Following this lead, Nakanishi [49] and Marder [50, 51] engineered crystalline salts by changing the anions in specific stilbazolium salts. Marder found [52] that 4-dimethyl amino-N-methyl-4 stilbazolium tosylate (DAST) showed that largest nonlinear coefficient among all the stilbazolium salts examined. DAST soon became one of the most widely investigated second order material. It crystallized noncentrosymmetrically. It had nearly optimal orientation of the chromophore which yielded a very high nonlinearity. The salt was found to be thermally very stable, with a melting point of 290^oC. More importantly its optical properties were found to be unaffected even when heated to 160^oC. DAST has practically no absorption at technologically significant wavelength and scientists believed that the material will be highly suited for electro-optic applications due to its ability to respond in terahertz range.

The initial hiccup with DAST was the non-availability of quality single crystal films. Bulks crystals or polycrystalline films of DAST cannot exploit the high optical nonlinearities of the molecule because of the following reasons[53]

1. Application of optical and electrical fields along a specific molecular axis is not feasible.
2. Loss of phase information due to scattering and destructive interference.

Due to the above reasons the electro-optic coefficient of DAST is about 100 pm/V measured at 750nm while the electro-optic coefficient of a single crystal film of DAST measured at the same wavelength is 445 pm/V[54, 55, 56]. The challenge then ahead was to prepare single crystal films of DAST with high optical quality. Several groups proposed different techniques to achieve this goal [57, 58, 59, 60, 61]. Thakur's technique to prepare single crystal films of polydiacetylene was revisited [62, 63]. This technique called the 'modified shear method' was successfully implemented to prepare single crystal films of DAST with excellent optical quality. His team subsequently followed this up by characterizing the electro-optic coefficients of single crystal films of DAST at different wavelengths. The results reported are reproduced in the table below [55, 64]

Wavelength (nm)	Electro-optic coefficient of DAST - r_{11} (pm/V)
633	770
720	530
750	445
1550	200

Table 2.1: Electro-optic coefficients of DAST as reported by Thakur *et al.*

The magnitude of imaginary part of imaginary part of the electro-optic coefficient was reported to be 280pm/V and 519 pm/V at 633nm and 488nm respectively [65]. DAST has absorption maxima at 550nm, [66] the high electro-optic coefficient at 633nm is attributed to the resonance enhancement due to the single photon absorption. However, as the wavelength increases, the electro-optic coefficient decreases due to the decrease in the resonance enhancement effect. The electro-optic coefficient of DAST at 1550nm is about 200pm/V. 1550nm is a technologically significant wavelength and very high electro-optic coefficients are desirable at this wavelength.

2.5.1.1 Dispersion of electro-optic coefficient and its figure of merit

The electro-optic coefficient is related to the macroscopic hyperpolarizabilities of the organic molecules and hence the wavelength dependence of electro-optic coefficients can be related to certain molecular parameters of the organic crystal. The electro-optic figure of merit is given by

$$n_3^1 = r_{IIK}^{\omega} \cong K_3 g \frac{\omega_{eg}^2(3\omega_{eg}^2-\omega^2)}{(3\omega_{eg}^2-\omega^2)^2} \quad 2.53$$

Where $g(\omega) = \frac{-4}{n_1(\omega)}\left(\frac{n_1^2(\omega)+2}{3}\right)^2$ accounts for the local field correction, ω_{eg} is the resonance frequency of optical transition, K_3 a parameter that depends on: the dielectric constant ε, number of molecules per unit volume *N*, the difference in dipole between the ground state and excited state μ, and the square of the transition dipole between the ground state and the excited state. The value for ω_{eg} can be obtained from the absorption measurements or the Sellmeier parameters [67], K_3 and g can be computed from ω_{eg} and the experimental value of n^3r at any wavelength. Thus, the figure of merit n^3r for organic materials can be computed as a function of the wavelength. Figure 2.4 shows the wavelength dependence of various NLO materials. Table 2.2 gives the parameters used to calculate the wavelength dependence of the organic materials shown in figure 2.5. Table 2.2 and figure 2.3 are reproduced from reference [37]

Material	**r (pm/V), n**	$\lambda_{eg} = 2\pi c/\omega_{eg}$ **of bulk (nm)**
DAST	r_{11}= 400 n_1=2.19 at 820nm	600
NMBA 4-nitro-4'-methylbenzylidene aniline	r_{11}= 37.2 n_1=2.283 at 488nm r_{11}= 36.4 n_1=2.216 at 514.5nm r_{11}= 25.2 n_1=2.078 at 632.8nm	353
PNP 2-(N-prolinol)-5-nitropyridine	r_{22}= 28.3 n_2=1.873 at 514.5nm r_{12}= 20.2 n_1=2.614 at 514.5nm r_{22}= 12.8 n_2=1.788 at 632.8nm	404
DAN 4-(N,N-dimethylamino)-3-acetamidonitrobenzene	r_{32}= 13 n_3=1.949 at 632.8nm	419
metanitroaniline	r_{33}= 16.7 n_3=1.875 at 632.8nm	400
COANP	r_{33}= 16.7 n_3=1.875 at 632.8nm	410
MMONS	r_{33}= 39.9 n_3=2.129 at 632.8nm	421
MNA	r_{11}= 67 n_1=2.00 at 632.8nm	414

Table 2.2: Electro-optic response of selected organic compounds

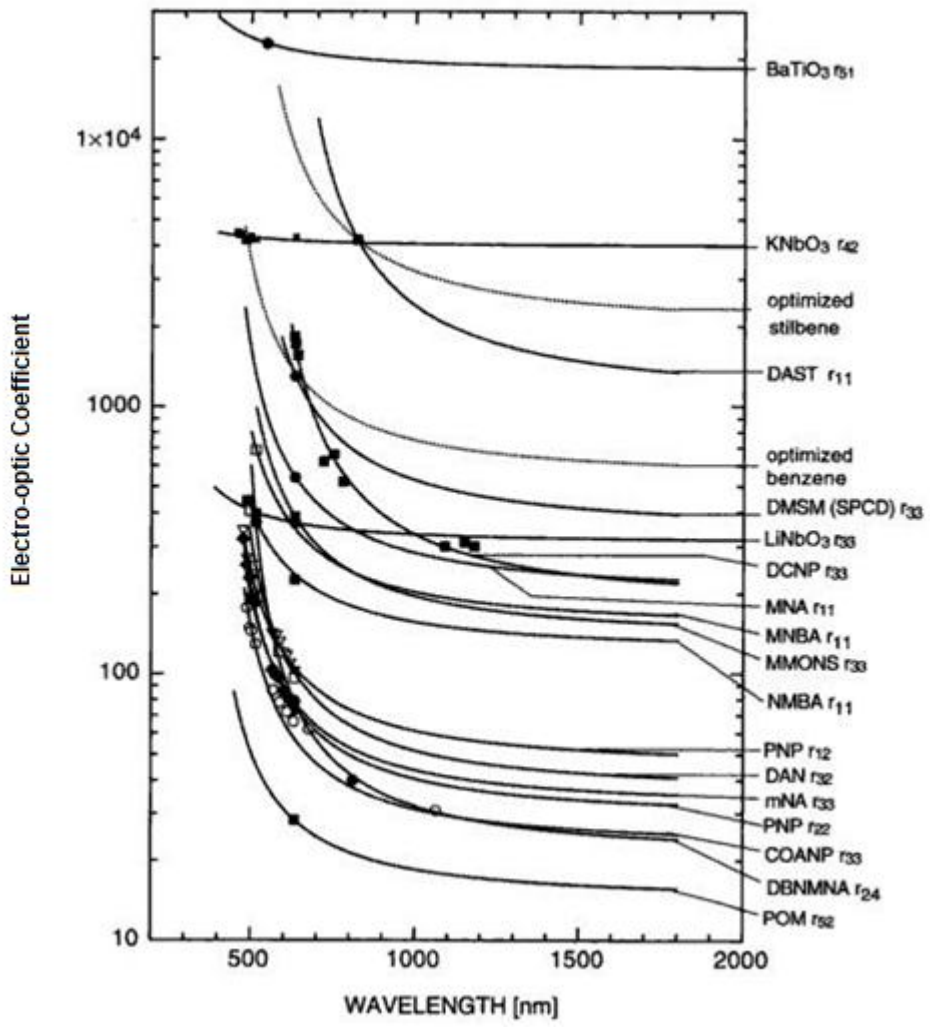

Figure 2.3: Electro-optic figure of merit of selected nonlinear materials as a function of wavelength

2.5.2 Third Order Materials

Since third order nonlinearities do not require symmetry conditions, a wide array of materials have been investigated for third order properties. Different techniques such as third harmonic generation (THG), degenerate four-wave mixing(DFWM), optical Kerr gate (OKG), and self-focusing techniques may be used to determine third order susceptibility and it is difficult to compare the results directly because different optical processes may use different experimental conditions. The magnitude of third order nonlinearity is reported to be dependent on the conjugation length of the material. Hence in 1970s several scientists conducted elaborate studies to

empirically determine the dependence.[68] In 1977 Ducuing and co-workers found the relationship between the delocalization length L and the number of electrons N. [69] Rustugi and co-workers deduced a relationship between microscopic polarizibility and delocalization length for one dimensional free electron gas model. In 1978 Agarwal and co-workers suggested third order susceptibility's dependence on the sixth power of π electron delocalization length for one dimensional π conjugated polymers. They further deduced that the third order susceptibility is inversely proportional to the sixth power of the energy gap. Other factors that affect the magnitude of third order susceptibility include donor-acceptor functionalities orientation of the polymer chain and packing density, conformation and its dimensionality. Several research groups worked on developing materials that have high third order nonlinearities and they can be broadly classified into the following categories: [68]

1. Inorganic materials
2. Organic liquids
3. Organic molecular solids
4. Organic charge transfer complexes
5. Organic π conjugated polymers
6. Organometallic compounds
7. Liquid crystals
8. Organic composites
9. Nano-metallic clusters and semiconductor nano-composites
10. Dye grafted polymers
11. Non-conjugated conducting polymers

Among the above organic π conjugated polymers and semiconductor and metallic nano-

particles have attracted keen attention in the recent past. Stauteret and co-workers reported exceptionally high third order nonlinearity in polydiacetylene *p*-toluene sulfonate (PDA-PTS). [70] This finding provided a major breakthrough for research in organic π conjugated polymers. The third order susceptibility of a single crystal film of PDA-PTS at 1890nm was reported to be as high as 8.5×10^{-12} esu. At resonance the imaginary part of $\chi^{(3)}$ was found to be 2.5×10^{-5} esu, which is one of the largest reported resonant values. [71] Other π conjugated polymers that were studied include (and are not limited to) poly (*p*-phenylenevinylene) (PPV), polyacetylenes, polythiophenes etc.

The high optical nonlinearity and ultra-fast response at non-resonant frequencies of π-conjugated polymers is attributed to the delocalization of π electrons along the conjugated chain or the quantum wire.

Metallic nanoparticles and semiconductor nano-clusters have also been pursued for third order properties. The cubic nonlinearities in synthetic materials can be increased by confining the valence electrons in a very small region typically within a few nanometers. These confinements fall into two categories namely quantum confinement and dielectric confinement. [72]

The high cubic nonlinearities in metallic clusters embedded in glass matrices are due to the surface Plasmon resonance effect (SPR). In such materials there exists a difference in dielectric constant between the metal clusters and the surrounding glass matrix which leads to a dielectric confinement in these materials. Large resonant cubic nonlinearities around SPR frequency are exhibited by these materials since the dielectric difference changes the field distribution and hence the optical properties. Optical nonlinearities of some metallic nanoparticles is shown in table below. [73]

Nanocluster	Size (nm)	Host	α (cm^{-1})	γ (m^2/W)	λ (nm)
Gold (Au)	5-30	SiO_2	10^4	4×10^{-14}	570-600
Copper Cu)	< 10	SiO_2	10^4	2×10^{-11}	532
Silver (Ag)	< 10	SLG	1	10^{-14}	591

Table 2.3: Cubic nonlinearities of select metallic nanoparticles

In semiconductor nanostructures the high cubic nonlinearity is due to the reduced particle size which increases the inter-particle spacing and hence the valence electron is confined in sub-delocalization dimensions. This changes the electron quantum states and the way they interact with applied optical fields. This effect is called the quantum confinement effect. Several materials like CdS, CdSe, ZnS, ZnSe have been reported to possess high third order nonlinearities due to quantum confinement effect.

Recently Thakur and co-workers have shown that a new class of conducting polymers called nonconjugated conducting polymers (NCP) exhibit exceptionally high cubic nonlinearities upon doping. These materials also have interesting electrical properties. The following subsection is discusses the electrical properties and their potential in the field of nonlinear optics.

2.5.3 Nonconjugated conducting polymers as third order materials

Conjugated polymers were the first known conducting polymers. In 1977 Shirakawa and co-workers reported that the conductivity of conjugated polymer polydiacetylene increased about a billion times when doped with iodine. [74] The electrical properties of several doped conjugated polymers were reported thereafter. In 1988 Thakur provided a breakthrough in understanding the conductivity theory of conducting polymers. He showed that specific polymers with at least one double bond in their repeat unit could be electrically conducting upon doping with electron donors or acceptors. Conducting polymers do not necessarily need to have a conjugated backbone and hence a new class of conducting polymers called nonconjugated conducting polymers (NCP) came

into existence. The first reported NCP by Thakur and co-workers was 1-4, cis(polyisoprene). [75] Its conductivity increased by about ten orders when doped with iodine. Thakur's team and others subsequently reported other NCPs that showed similar behavior such as poly(β-pinene) [76], styrene butadiene rubber (SBR), [77] poly(ethylenepyrroledyl) (PEP) [78] and polyaniline furfural [79].

When NCPs are doped, the dopants interact with the double bond to form a radical cat ion or a polaronic state since electron transfer from the double bond to dopant occurs creating a hole or an electron vacancy. When the concentration of the dopant increases the number of double bonds transformed into cat ion radicals increase proportionally. The electrical conductivity saturates when almost all available double bonds are transformed into cat ion radicals. It must be noted that in doped NCPs the electrical conductivity is due to the holes that are loosely bound to the dopant. Doping causes charges to be confined in sub-nanometer domains. Further, the loosely bound hole can be modeled as a spring mass arrangement that has a quartic term in its potential energy. Such a system shows a great promise as a third order material. These materials unlike conjugated polymers do not have extended delocalizations, their optical nonlinearity is solely attributed to the charge confinement. Thakur and co-workers first reported third order nonlinearities in the NCP 1,4-cispolyisoprene. A change in refractive index of 4×10^{-4} was reported in iodine doped1,4-cispolyisoprene at 633nm for an applied voltage of 2V/μm. The corresponding Kerr coefficient was reported to be 1.6×10^{-10} m/V^2 which is about 66.67 times higher than that of nitrobenzene measured at 589nm.[80] A modulation depth of 0.12% was reported in iodine Poly(β-pinene) at 633nm. The Kerr coefficient at this wavelength was about 1.2×10^{-10} m/V^2 and the measured $\chi^{(3)}$ was reported to 0.65×10^{-8} esu. [81]. Susequently two-photon measurements were performed in this polymer using a 150fs Ti-Sapphire laser and maximum two-photon absorption coefficient of

2.6cm/MW was reported at 810nm [82]. The Kerr co-efficient of another doped NCP, poly(ethylenepyrroleiyl) (PEP) was reported to be 1.2×10^{-10} m/V^2 at 633 nm [78].

These reports prove without doubt that NCPs have a great potential in the field of nonlinear optics due to their exceptionally high cubic nonlinearities. These materials are cheap and thin films of these materials with exceptional optical quality can be prepared easily.

2.6 Photovoltaics

Photovoltaics is the branch of science that deals with the conversion of light energy to electrical energy. Modern day photovoltaic (PV) cells can be divided into two broad categories: inorganic and organic. An inorganic PV cell normally acts like a PN junction. When light strikes the junction, electron hole pairs are created; electrons flow to the positive side and holes flow to the negative side and this constitutes a flow of current. The driving forces in this process are the built-in potential and the work functions of the contacts. In organic PV cells a different mechanism is used. They consist of composite involving a polymer and an electron acceptor. Light of appropriate wavelength excites the electrons in the polymer and these electrons are accepted by the electron acceptor and are carried through a low work function electrode while the holes are carried through an electrode that has a higher work function. PV cells have distinct advantages over the conventional power generation methods. They are [83]:

1. Photovoltaic cells are driven by solar power, an abundant, renewable resource. This reduces the pressure on our depleting fossil fuel reserves.
2. PV cells do not produce any harmful radiations; it is the safest means of energy production.
3. PV technology does not leave any traces. No by products are wastes. Hence waste management is not an issue.
4. PV technology is the most environmentally friendly technology

5. The PV cells can be used both in centralized and decentralized power plants
6. PV cells have no moving parts, hence no wear, no replacement. This results in reduced maintenance cost

However, the current PV technology also suffers from the following shortcomings:

1. The PV grids and arrays are very expensive. Their installation is extremely capital intensive. Although the unit does not have any recurring cost, it takes an extremely long time to break even. The general perception is that solar cells are extremely capital intensive.
2. The electricity produced is dc and it needs to be converted to ac. This again adds to the cost.
3. Solar cells bring along an element of uncertainty. It depends on the climatic and geographical conditions. Hence it can only be used to compliment a conventional power system.

In the early days of PV technology, the cells were necessarily inorganic. The first PV cells was demonstrated using Selenium by Fritts in 1883 [84]. Gold electrodes served as the higher work function electrodes and the iron electrodes served as the lower work function electrodes. When photons strike Fritts' Selenium based cell, the electron hole pairs are generated. The golds electrode accepts the holes while the lower work function iron electrodes accept the electrons to constitute a photocurrent. [85] The PN junction based PV cell was a chance discovery at Bell labs in 1954 that revolutionized the field of inorganic photovoltaics. The first demonstrated junction based solar cell had 6% efficiency. [86] This lead to a great research attention in this field. Subsequently several other semiconductor materials were investigated for PV properties. Some of them include Cu_2S, CdS, CdTe, GaAs etc. [87, 88, 89]

Some of the milestones in inorganic PV technology are listed below

1. In 1973 a violet cell was demonstrated that had improved efficiency in shorted wavelength region. [90]
2. In 1980 thin film solar cells were successfully demonstrated. [83]
3. In 1985 efficiency as high as 20% was achieved under normal sunlight condition and over 25% using 200X concentration[91, 92]
4. In 1990 PV technology reported a growth rate of 33%. [83]
5. In 2004 solar power accounted for 0.04% of total power generated and in 2010 this is tipped to go up to 0.4%. [93]

2.6.1 Organic materials in Photovoltaic Technology

Although the work in organic photovoltaics began as early as in 1950, commercially viable organic cells still seem to be in their nascent stages. The first organic PV cell was reported in 1958. The issue with organic PV technology has been the efficiency. The high efficiency inorganic PV cells have reached an efficiency of 40%. Much work needs to be done in organic materials to attain such high efficiencies. But this technology has significant advantages over the inorganic PV technology. They are:

1. Organic PV composites are easy to process and fabricate. They do not require sophisticated high temperature fabrication facilities
2. PV composites are extremely inexpensive.
3. Large area PV composites can be easily produced
4. Organic materials extend the possibility of extremely high optical absorption coefficients.

In 1980s organic materials like mercocyanine and phthalocyanine based PV cells were reported. A maximum efficiency of 1% was achieved for small area cells. [94, 95] Organic conjugated

polymers and electron acceptor based configuration was then tested for PV cells. Buckminster fullerene, C_{60} has been widely used as an electron acceptor in organic PVs [96]. Tang and coworkers achieved a breakthrough in organic PV technology by developing a cell using copper phthalocyanine and perylene tetracarboxylic derivative. [97] Several groups studied a polyphenylene vinylene (PPV) based PV cells. [98, 99, 100] Phthalocyanine has also generated wide research interest as a potential PV material. [101] Many other conjugate polymer, electron acceptor based PV composites were studied. [102] The structures of PPV and specific electron acceptors are shown below.

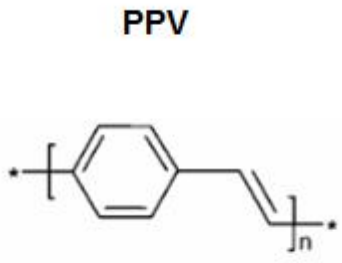

(a)

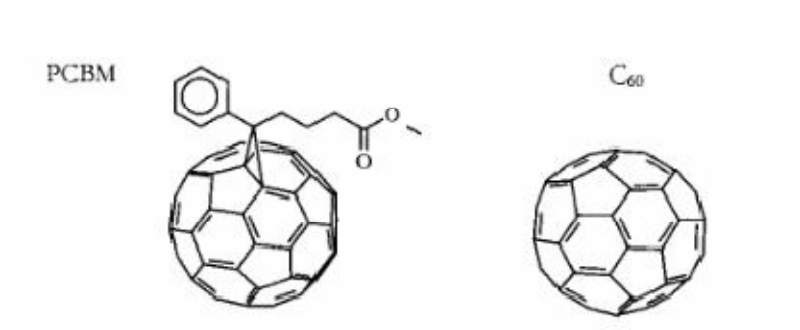

(b)

Figure 2.4: Molecular structure of (a) PPV and (b) electron acceptors [102]

In 1992 Saricifti and coworkers reported a strong photoinduced charge transfer between MEH-PPV and C_{60} [103]. This result was further bolstered by Morita and coworkers who observed a similar effect in other fullerene composities [104, 105] The mechanism of photoinduced charge transfer is pictorially illustrated below.

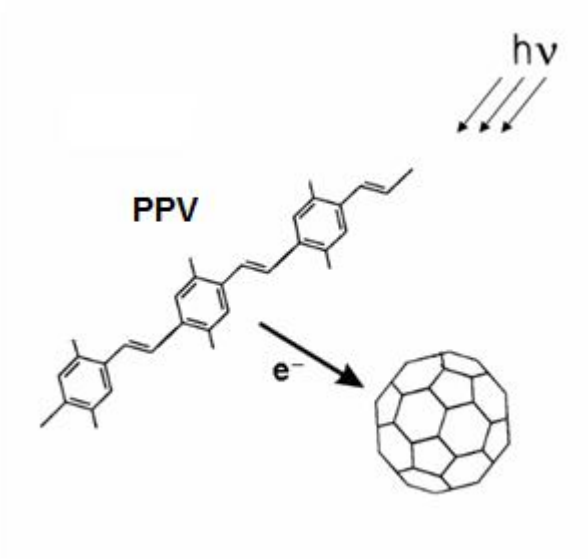

Figure 2.5 Schematic of photoinduced electron transfer between PPV and fullerene [85]

In summary the field of organic PVs has experienced a great progress in the past few decades. Organic PV technology due to its low cost is the only viable route to accomplish widespread solar cell penetration. It is believed that a 5% efficiency is organic solar cells is attainable [106]. Clearly the tradeoff between inorganic and organic solar cells boils down to a cost versus efficiency. If the efficiency of organic solar cells can be increased, it can change the way world perceives the energy crisis.

CHAPTER 3

OBJECTIVES

The objective of the proposed research work is to study the structrural, electrical and nonlinear optical properties of specific organic materials that have applications in the field of photonics. The second order optical material discussed in this work is a novel single-crystal film involving a combination DAST and IR125. This material is expected to have a high electro-optic coefficient at technologically significant wavelengths like 1550nm. Third order optical materials discussed fall under the class of conducting materials called nonconjugated conducting polymers. In particular, poly(β-pinene), polynorbornene and trans-polyisoprene will be discussed. Photovoltaic composites of nonconjugated conducting polymers and C_{60} will also be discussed. The specific objectives of this research are:

1. to develop a single crystal film of DAST and IR125 using modified shear method; characterize the single crystal film using polarized optical microscopy, x-ray diffraction and optical absorption; determine the electro-optic coefficients of the film at 633nm using the field induced birefringence method and compare the results obtained with that of single crystal films of DAST
2. to measure the electrical conductivities of iodine doped polynorbornene and trans-polyisoprene as a function of dopant concentration; characterize polynorbornene and trans-polyisoprene using optical spectroscopy, Infrared spectroscopy (FTIR) and optical microscopy

3. to perform electron paramagnetic resonance studies on poly(β-pinene) at different temperatures and dopant concentrations of iodine and explain the effect of doping in this nonconjugated conducting polymer.
4. prepare doped poly(β-pinene) samples to be used for electro-optic measurements; optimize doping duration and ambience to enhance optical quality of the doped polymer samples; find a technique to preserve the doped polymer samples for longer durations; monitor the protected sample to determine the shelf life
5. to perform electro-optic measurements in poly(β-pinene) at off-resonant wavelengths including 1.55μm; find the electro-optic Kerr coefficients at these wavelengths, compare the results so obtained with other third order material and explain the behavior
6. to perform time resolved interferometry measurements on doped poly(β-pinene) to determine the two-photon absorption coefficient at 790nm and 795nm using pump probe technique.
7. to improve the interaction length of the polymer with light using nonlinear optical wave-guiding and demonstrate large modulation.
8. to prepare thin film composites of nonconjugated conducting polymers poly(β-pinene) and buckminsterfullerene, C_{60}; measure the optical absorption and photoluminescence characteristics of these composites; fabricate photovoltaic cells using thin film composites of poly(β-pinene) and buckminsterfullerene, C_{60}

CHAPTER 4

ELECTRO-OPTIC EFFECT IN A NOVEL SINGLE CRYSTAL FILM INVOLVING DAST AND IR125

Organic single crystal films have attracted significant research attention due to a wide range of applications in electronics and photonics. Exceptionally large optical nonlinearities have been observed in specific organic single-crystal films. Extensive research has been performed on organic films for electronics, owing to their lower cost and easier processibility. Field-effect-transistors based on several organic single crystalline materials such as rubrene, pentacene, tetrazene, BP2T etc[107, 108] have been reported. Organic single-crystal materials are known have significantly higher electronic mobility compared to solution-cast and evaporated organic/polymeric films.

4.1 Material and Methods

Single-crystal films of DAST were prepared using modified shear method. [62] The electro-optic coefficients of single-crystal films of DAST at different wavelengths have already been reported[55, 65, 66].

The values are exceptionally large due to the optical uniformity of the films. The unit cell [109] of DAST crystal is monoclinic with the lattice parameters: a=10.365A, b= 11.322A, c=17.892A, β=92.24^{o}. Single-crystal films of DAST were prepared by the modified shear method at a higher temperature to obtain larger areas (~ 1 cm^2 and larger).[55] The film has a [001] surface orientation. The dipole axis of DAST molecules or the overall orientation of DAST

molecules is along the a-axis. In the present report, we discuss growth and characterization of single-crystal film of a combination of materials including DAST and a laser dye, IR-125 (molecular structure shown in Fig.4.1b). The DAST single-crystal film exhibits the largest electro-optic coefficient among all materials reported so far. At 633nm its electro-optic coefficient is 770pm/V. At 1.55 μm the electro-optic coefficient of DAST film is about 200pm/V.

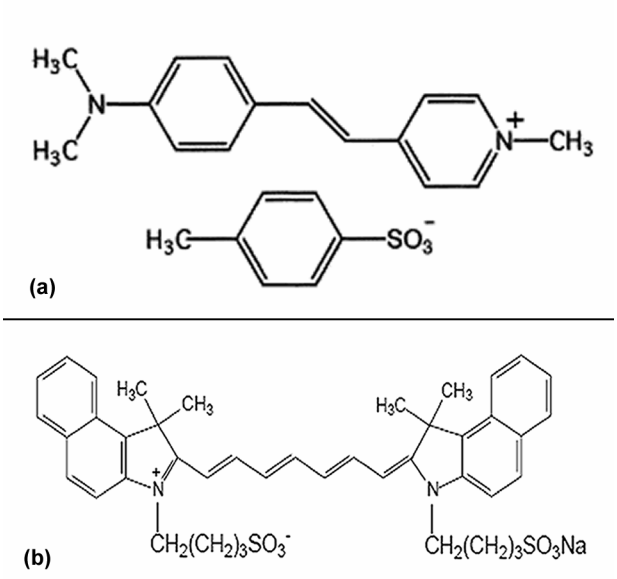

Figure 4.1: Molecular structure of DAST (a) and IR125(b)

The optical absorption spectra of DAST single-crystal film ([001] orientation) for different incident polarizations have been reported. DAST has strong optical absorption (inset of Fig.4.3) over the wavelength range of 400 to 600nm with a peak at around 550nm. [66] The electro-optic coefficient is largest at 633nm due to resonance enhancement. The magnitude of the electro-optic coefficient reduces at off-resonant wavelengths. Despite this reduction the value is still higher compared to other organic and inorganic materials (lithium niobate, r_{33} = 30pm/V). In this work, a single-crystal film involving a combination of two organic materials: DAST and IR-125, is reported. This material is expected to exhibit novel electronic and optical characteristics that DAST by itself may not have.

Single-crystal films of a combination of DAST and the laser dye, IR-125 (molecular structure shown Fig.4.1b) were grown using the modified shear method [62, 63] at a higher temperature. Solid DAST and IR-125 samples were dissolved in methanol, with DAST in super-saturation. The amount of IR-125 was about 15% of the weight of DAST. A small amount of this solution was introduced between two opposing flat substrates and the substrates were moved with respect to each other to impart a shear. The shear method leads to molecular organization induced by polar forces (strong capillary effect) at the interface and shear between two opposing substrates. The capillary effect between two opposing substrates is critical for such controlled orientation crystal growth. As the solvent is slowly evaporated in a controlled environment, single-crystal films of predictable orientation are formed on the substrate. The single-crystal films obtained by this method have excellent optical qualities. This is the first report on single-crystal film of a combination of two organic materials.

The single-crystal film of a combination of DAST and IR-125 (we will call this DAST-IR125 film) was characterized using: 1. polarized optical microscopy, 2. polarization-dependent optical absorption spectroscopy, and 3. x-ray diffraction. Electro-optic measurement of the films was made using field-induced birefringence technique.

4.2 Results and Discussion

4.2.1 Polarized optical microscopy:

The DAST-IR125 single-crystal films were characterized using polarized optical microscopy. An optical micrograph of a single-crystal film prepared using the modified shear method is shown in Fig.4.2. These crystal-films are bright red in color. They have excellent optical quality and uniform surfaces. The single-crystal films grown have a thickness in the range of 0.5 to 3μm and areas of about $1cm^2$ (micrograph below does not show the whole film).

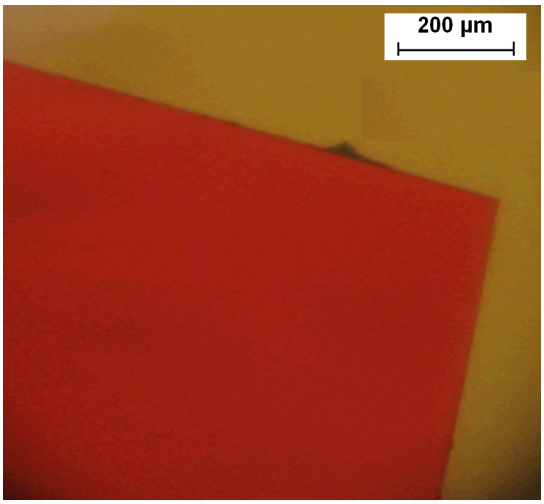

Figure 4.2: Optical micrograph of a single crystal film of DAST and IR125

4.2.2 Polarization-dependent optical absorption spectroscopy:

Optical absorption spectroscopy was performed on these films at different polarizations of the incident beam. The spectra are shown in Fig.4.3. Two distinct bands are observed: one

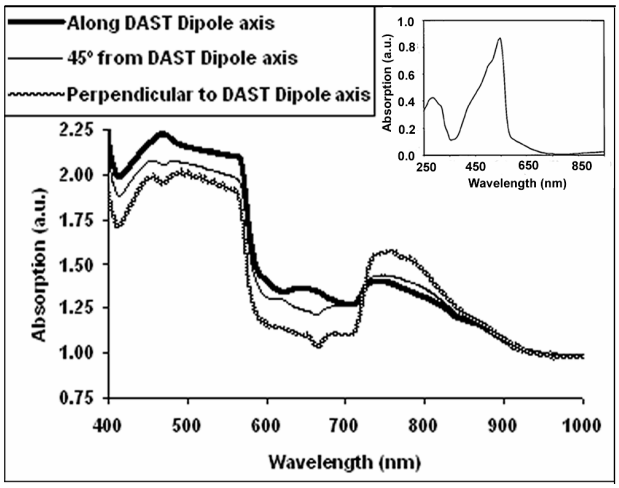

Figure 4.3: Optical absorption spectra of DAST-IR125 single-crystal film. Figure in the inset: Optical absorption spectrum of DAST single-crystal film

corresponding to DAST from 400 to 600nm and the other corresponding to IR-125 from 600nm to 900nm. The absorption spectrum along the dipole axis of DAST shows a strong DAST peak and a weaker IR-125 peak. When measured with polarization perpendicular to the dipole of

DAST, the IR-125 absorption (600 to 900 nm) becomes prominent (optical gap ~ 1.4eV). For polarization at 45^{o} with respect to the dipole-axis, both DAST and IR-125 peaks are observed. The dipole axis of DAST is along a-axis. The optical absorption spectra indicate that the IR-125 molecule is oriented perpendicular to the a-axis. Since these single-crystal films have high absorption at longer wavelengths, high electro-optic coefficients at longer wavelengths can be expected. In addition, this may be the first example of an organic single-crystal film with a low band-gap.

4.2.3. X-ray diffraction

X-ray diffraction was performed on these films. Fig.4.4 shows the X-ray diffraction (XRD) data for DAST-IR125 single-crystal film. The amorphous background in the XRD data of single-crystal film of DAST IR-125 is due to the quartz substrate. Comparing with known XRD data of DAST single-crystal film, the DAST-IR125 film appears to have a [001] surface orientation.

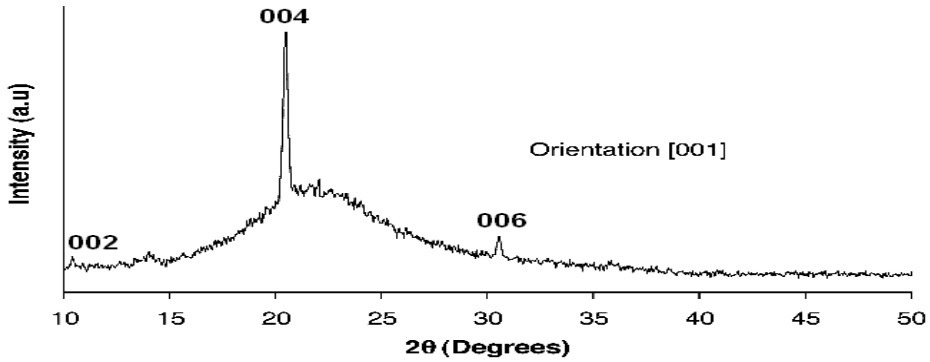

Figure 4.4: X-ray diffraction (XRD) data for DAST-IR125 single-crystal film.

4.2.4. Electro-optic Measurement

Electro-optic measurements were performed on the DAST-IR125 single-crystal films at 633 nm wavelength. The samples were prepared using a shadow mask technique. The dipole axis of DAST was determined and Al electrodes were deposited on the sample using vacuum

deposition technique. The electrodes were deposited perpendicular to the dipolar axis and a slit (50-100μm) was formed. A sample prepared by this technique is shown in Fig.4.5a. The electro-optic measurements were performed using field-induced birefringence technique at 633nm. A cross-polarized geometry was achieved using a polarizer oriented at 45º from the incident laser beam polarization. An analyzer was oriented orthogonally to the polarizer and was placed after the sample. Electric field was applied along the dipole axis of DAST using the electrodes deposited on the sample. A photo detector was used to measure the output beam. The signal was analyzed using an oscilloscope or a lock-in amplifier. A schematic of the experimental setup is shown in Fig.4.5b.

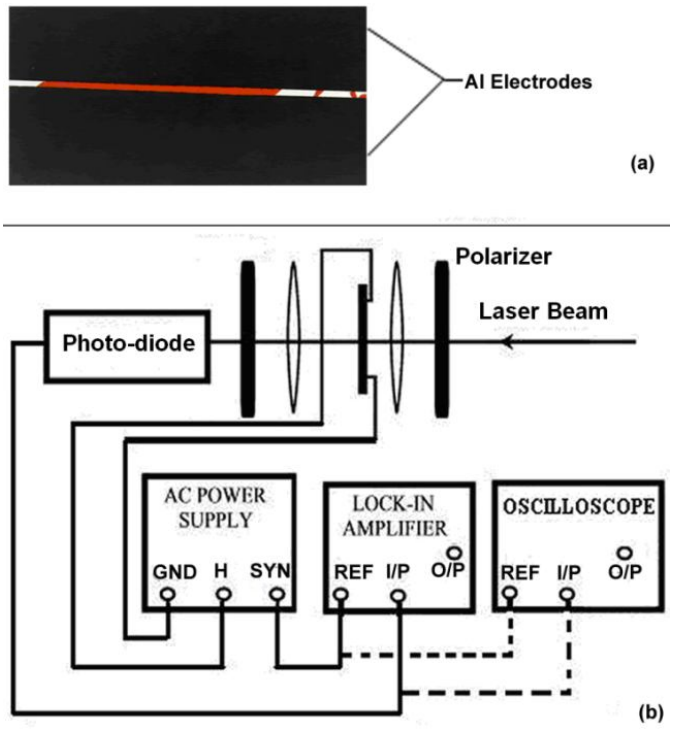

Figure 4.5 a) Aluminum electrodes evaporated (with shadow-masking) on a DAST-IR125 single-crystal film for use in the electro-optic measurement, b) Schematic of experimental set-up for electro-optic measurement

An exceptionally high modulation depth of about 14% was observed at 633 nm for a 2.7μm thick film when an ac field of 1V/μm was applied. An oscilloscope trace of the

modulation signal is shown in Fig.4.6. Calculation of the electro-optic coefficient requires values of refractive indices and absorption coefficients at these wavelengths. In the absence of those data at the present, we can determine an approximate value using known refractive indices of DAST by itself. The magnitude of the electro-optic coefficient (r_{11}) of DAST-IR125 film as obtained is about 300 pm/V at 633 nm.

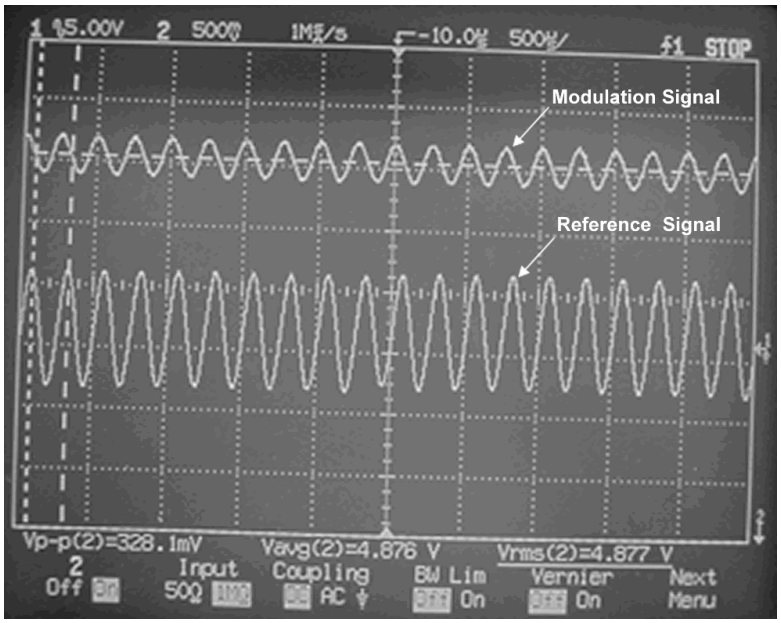

Figure 4.6 Oscilloscope trace of electro-optic modulation signal of DAST-IR125 single-crystal film. The waveform above is the electro-optic modulation signal and the waveform below is the reference signal.

4.3. Conclusions

In conclusion, single-crystal film involving a combination of two organic materials: DAST and IR-125, is reported for the first time. This film has been characterized using polarized optical microscopy, polarization-dependent optical absorption and x-ray diffraction. The film has a [001] surface orientation. The IR-125 molecule is oriented close to perpendicular to the DAST dipole-axis. The film has a low optical gap of about 1.4 eV for polarization perpendicular to the DAST dipole-axis. Along the dipole-axis, the optical gap is about 2 eV. The optical absorption

characteristics of DAST-IR125 film is significantly different than that of DAST film. The electro-optic coefficient of DAST-IR125 film as measured is about 300 pm/V at 633 nm. These novel materials have a wide variety of applications in organic electronics and photonics.

CHAPTER 5

POLYNORBORNENE: NONCONJUGATED CONDUCTING POLYMER

5.1 Introduction

In this discussion electrical and optical properties of a novel nonconjugated conducting polymer polynorbornene is discussed. Polynorbornene is synthesized from the monomer norbornene using ring opening metathesis reaction. Like other nonconjugated conducting polymers, the conductivity of this polymer increases by several orders upon doping with iodine. this material is also expected to exhibit high cubic nonlinearities due to the charge confinement in sub-nanometer domains.

5.2 Experimental

5.2.1 Electrical Conductivity

As discussed previously, the maximum conductivity of a nonconjugated conducting polymer depends on the number fraction of its double bonds per repeat unit. The maximum conductivity of polyisoprene[80] which has a double-bond number fraction of 1/4, is 0.1 S/cm. Poly(alloocimene)[110], which has a double bond number fraction of 1/3 reaches a maximum conductivity of 1S/cm, while poly(β-pinene)[76] with double bond number fraction of 1/6, has a maximum electrical conductivity of 0.008 S/cm.

In this report, we discuss electrical conductivity of polynorbornene which has a double-bond number fraction of 1/5. For this polymer, we expect a maximum conductivity between those of polyisoprene and poy(β-pinene).

Table 5.1 shows the maximum electrical conductivity and the corresponding double bond

number fraction of specific conducting polymers

Polymer	Double bond number fraction	Electrical Conductivity (S/cm)
Poly(β-pinene)[76]	1/6	0.008
Polynorbornene	1/5	0.01
Cis-poly(isoprene)[80]	1/4	0.1
Poly(alloocimene)[110]	1/3	1
Polyacetylene (Conjugated polymer)	1/2	100

Table 5.1: Conductivity of nonconjugate conducting polymers

Polynorbornene samples obtained from Aldrich (average Mw> 2,000,000) was powdered and dissolved in benzene. The polymer solution was then used to cast a thin film on a glass slide. Initial weight of the polymer and the conductivity of the film were measured. The film was then doped with iodine; the weight uptake of iodine and the corresponding conductivity of the film were noted at regular intervals. The conductivity of the polymer was observed to increase with increase in dopant concentration. A maximum conductivity of 0.01S/cm was observed corresponding to an iodine concentration of about 1.5 molar. This value is in between those of poly(β-pinene) and polyisoprene. The conductivity of polynorbornene as a function of molar concentration of dopant is shown in Fig.5.1. A comparison of the conductivities of some of these nonconjugated conductive polymers are shown in Table 5.1. It should be noted that the double bond number fraction of polynorbornene is 1/5 and its conductivity lies between that of cis-poly(isoprene) and poly(β-pinene) as one might have expected.

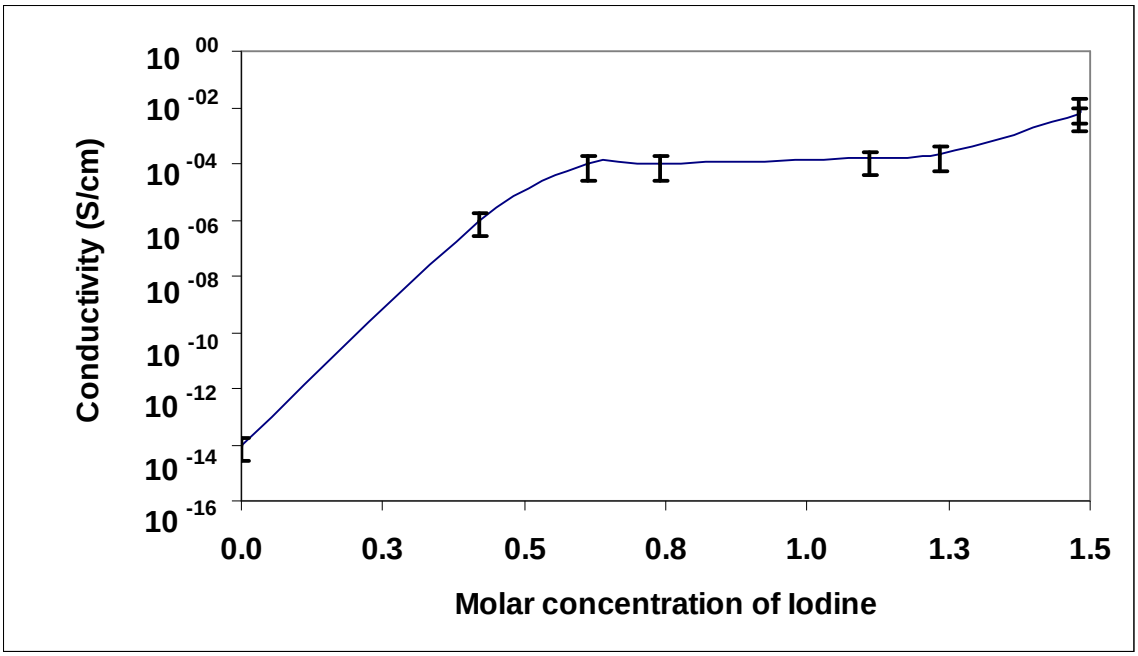

Figure 5.1: Conductivity of polynorbornene as a function of molar concentration of iodine

When the polymer is doped with iodine, cation radicals are formed. The number of cation radicals formed is directly proportional to the molar concentration of iodine. The holes formed when the polymer is doped are responsible for the increased conductivity. Molecular structure of doped polynorbornene with the cation radicals formed due to iodine doping is shown in figure 5.2.

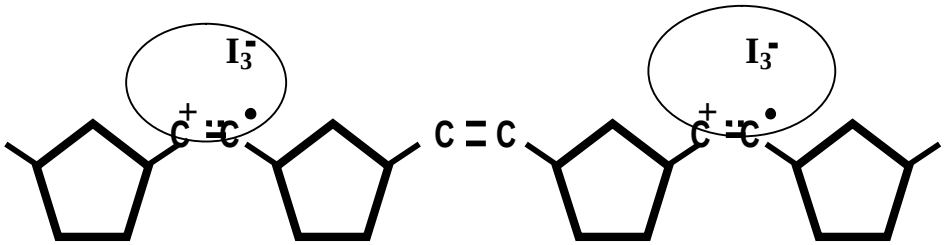

Figure 5.2: Cation radicals in doped polynorbornene

5.2.2 Optical absorption

The undoped film of polynorbornene is transparent. The film turns brownish green upon doping with iodine. Optical absorption measurements were performed on polynorbornene film at

different dopant concentrations using thin films cast on quartz substrates. The spectra are shown in Fig. 5.3.

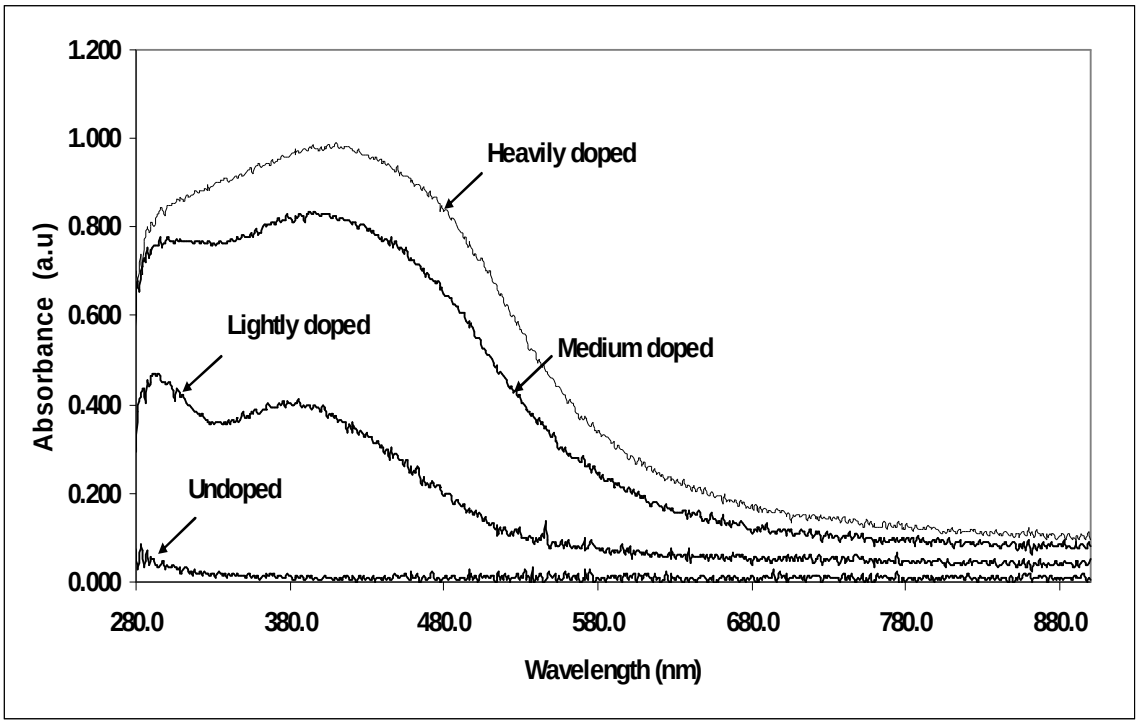

Figure 5.3: Optical absorption spectra of polynorbornene at different iodine doping level

The lightly doped polymer has two peaks at 295nm (5.3eV) and 396nm (3.13eV). The peak at 5.3eV corresponds to the cation radicals formed due to doping and the peak at 3.13eV corresponds to the charge transfer between the double bond and the dopant. When the dopant concentration is increased, the intensity of the peak at 5.3eV increases and the peak corresponding to charge transfer broadens and undergoes a red shift. This behavior is observed in other nonconjugated conducting polymers such as poly(β-pinene)[76] and cis-poly(isoprene). [80]

The optical absorption of doped polynorbornene is comparable to that of metallic nanoclusters. Figure 5.4 shows the absorption spectra of silver nanocrystals.[111]

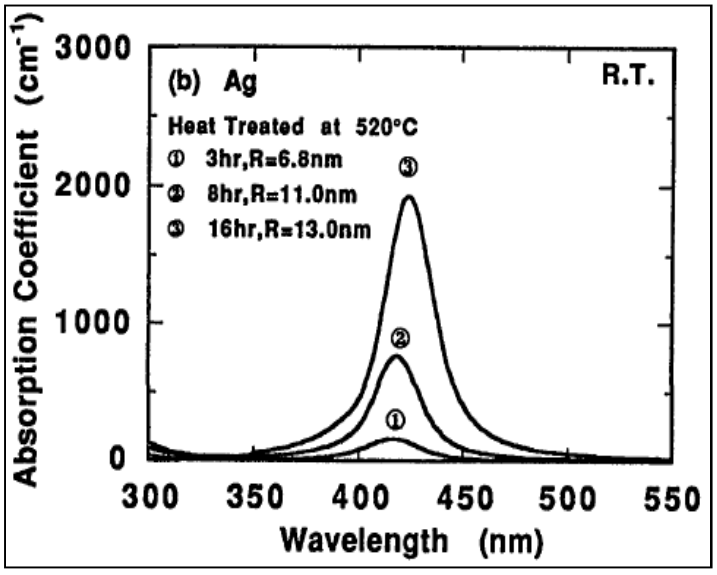

Figure 5.4: Optical absorption spectra of silver nanocrystals

The absorption peak of the nanocrystal is a function of the particle size. With increase in particle size the absorption peak broadens and red shifts. A similar effect can be found is the absorption peak corresponding to charge transfer in polynorbornene. In doped nonconjugate polymers, charges are confined in subnanometer domains and hence doped polymers behave like nanometals or quantum dots. These nano-optical materials exhibit exceptionally high optical nonlinearities.

5.2.3 FTIR Spectroscopy

FTIR spectroscopic studies of polynorbornene as a function of dopant concentration (iodine) were done using a Nicolet 5PC FT-IR spectrometer. Pellets of doped and undoped polynorbornene were made using potassium bromide. FTIR studies show a decrease in the peak intensities at 1718 cm^{-1} and 967 cm^{-1}corresponding to C=C stretching and =C-H bending vibration bands respectively, upon doping (Fig.5.5). The C=C transforms into cation radicals upon doping and charge-transfer. The decrease in the peak at 1718 cm^{-1} is directly related to the dopant concentration.

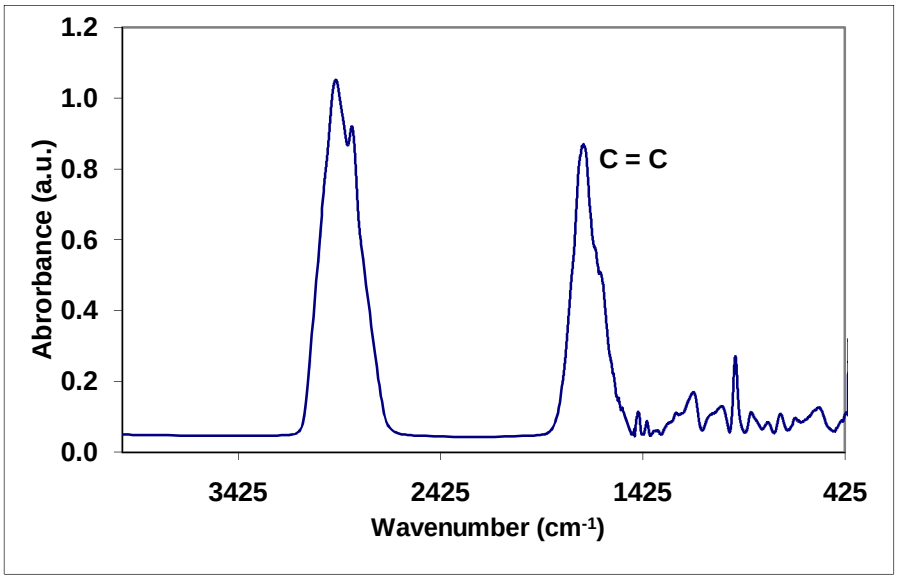

(a)

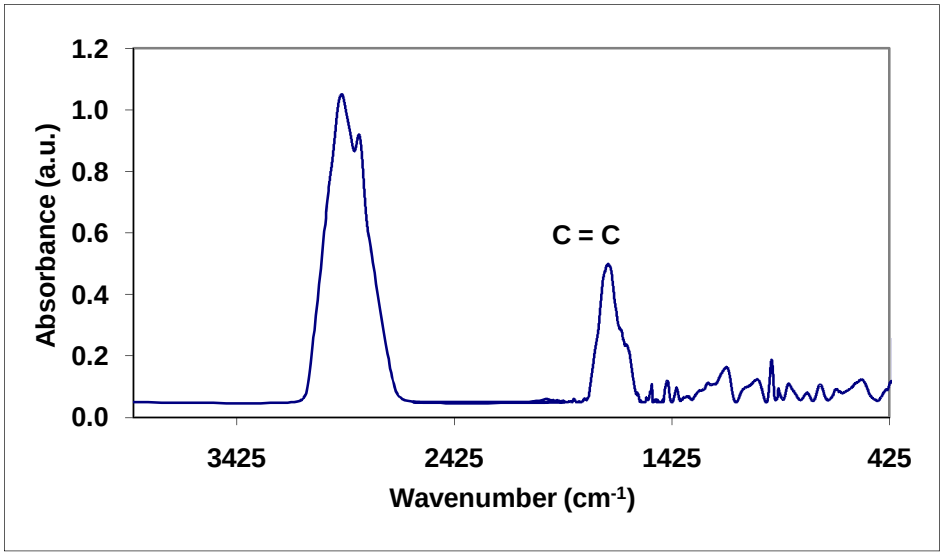

(b)

Figure 5.5: FTIR spectra of undoped (a) and doped (b) polynorbornene

5.2.4 Photoluminescence

Photoluminescence measurements were performed on polynorbornene using a Perkin Elmer LS-55 spectrometer. When the undoped polymer was excited at 280nm an emission band from 400nm to 480nm was observed with a peak at 425nm. The spectrum is shown in figure 5.6. The

undoped polymer has a weak absorption at 300nm. In doped polynorbornene the emission was quenched due to iodine.

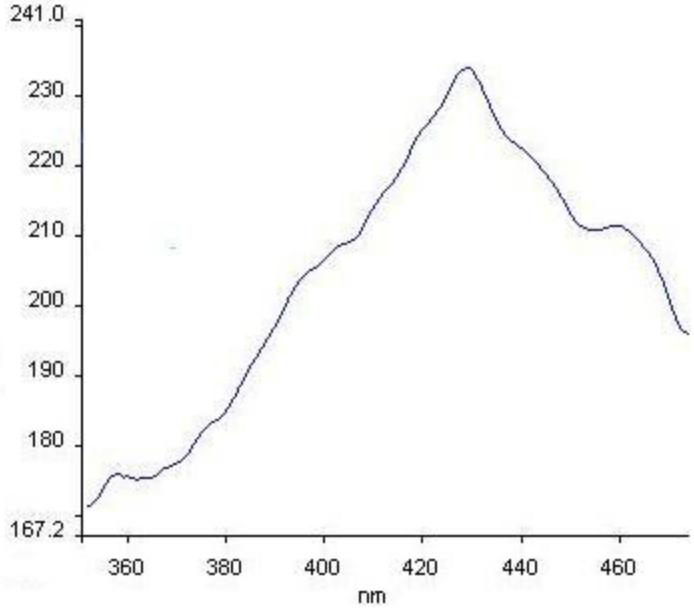

Figure 5.6 Photoluminescence in undoped polynorbornene

5.3.Results and Discussions

Polynorbornene is a novel polymer in the class of nonconjugated conducting polymer. Undoped polynorbornene is non-conducting. When doped with iodine, its electrical conductivity increases by several orders of magnitude. The maximum conductivity of this polymer was found to be 0.09 S/cm corresponding to iodine molar concentration of 1.5. Optical absorption spectrum of lightly doped polymer has two distinct peaks. One at 5.4eV corresponding to cation radicals and the other at 3.13 eV corresponding to charge transfer between double bond and dopant. When the dopant concentration is increased, the intensity of the peak due to cation radicals increases and the peak due to charge transfer broadens and undergoes a red shift. FTIR measurements show a decrease in C=C peak at 1718 cm-1 when the polymer is doped. Photoluminescence measurements show an emission peak at 425nm when the undoped polymer is excited at 300nm. Electrical and optical properties of polynorbornene are comparable with

other nonconjugate conducting polymers.

5.4 Conclusions

Electrical and optical properties of a novel nonconjugated conducting polymer polynorbornene are discussed. Upon doping the polymer behaves like a nano-metal. Like other nonconjugated conducting polymers, polynorbornene seems to be a promising nonlinear optical material.

CHAPTER 6

EPR SPECTROSCOPIC STUDIES OF RADICAL CATIONS IN A NONCONJUGATED CONDUCTIVE POLYMER, POLY(β -PINENE)

6.1 Introduction

Electronic and optical polymers have attracted significant research attention because of the fundamentally interesting characteristics and a wide range of potential applications. Nonlinear optical properties of organic and polymeric materials have various applications in photonics. The research on nonconjugated conductive polymers was initiated in 1988. [75] The field has attracted significant research interest since then [79, 78, 76] . Detailed studies of nonconjugated conductive polymers have been made using various spectroscopic methods including optical absorption, FTIR, Raman, ^{13}C-NMR, Mossbauer and EPR[112]. Various applications of these polymers have been demonstrated. Nonconjugated conductive polymers such as doped polyisoprene are important materials having confined electronic or nano-optical structures [80]. Exceptionally large quadratic electro-optic effect (third order optical susceptibility) has been reported for iodine-doped polyisoprene.[80] Electrical conductivity, FTIR spectroscopic and photoluminescence characteristics of a novel nonconjugated conductive polymer, poly(β-pinene) have been recently reported [76]. Large quadratic electro-optic effect in iodine-doped poly(β-pinene) due to formation of nano-optical domains has been recently reported. The molecular structures of poly(β-pinene) before and after doping with iodine are shown in Figs.6.1(a) and 1(b) respectively. The doping leads to a charge-transfer from the isolated double bond to iodine forming radical cations. In this discussion, the results of electron

paramagnetic resonance (EPR) measurements of poly(β-pinene) for different doping levels to confirm formation of radicals are discussed.

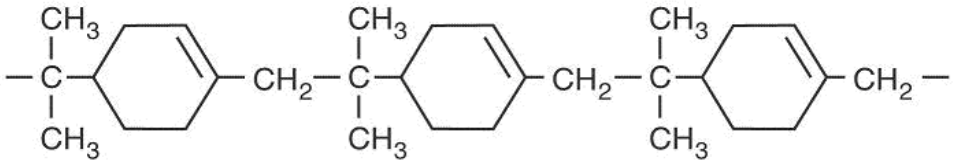

(a)

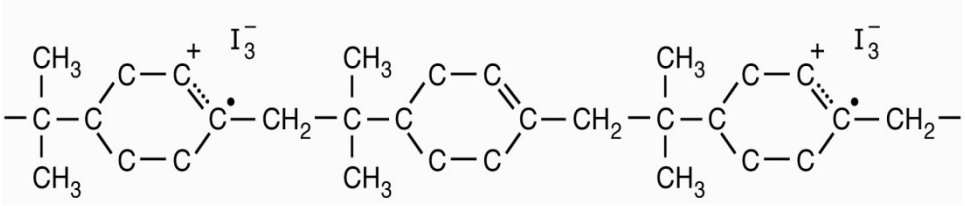

(b)

Figure 6.1: Molecular structure of undoped (a) and doped (b) poly(β-pinene)

The electrical conductivity of poly(β-pinene) increases by more than ten orders of magnitude upon doping with iodine. Undoped poly(β-pinene) has conductivity less than 10^{-12} S/cm. Upon doping with iodine the conductivity increases rapidly. When the molar concentration of iodine reaches about 0.85 the conductivity saturates [76] at ~ $8x10^{-3}$ S/cm.

Optical absorption and FTIR spectroscopic results of poly(β-pinene) have been reported. The optical absorption spectra for different dopant concentrations are shown in Fig.6.2. Two major optical absorption peaks have been observed for lightly doped samples: one at 4 eV corresponding to cation radicals and the other at 3.1eV due to the charge transfer between the donor and the acceptor. The lower energy peak undergoes a red shift when the dopant concentration increases. This is due to the reduction of the average distance separating the radical cation and the iodine anion [76, 81].

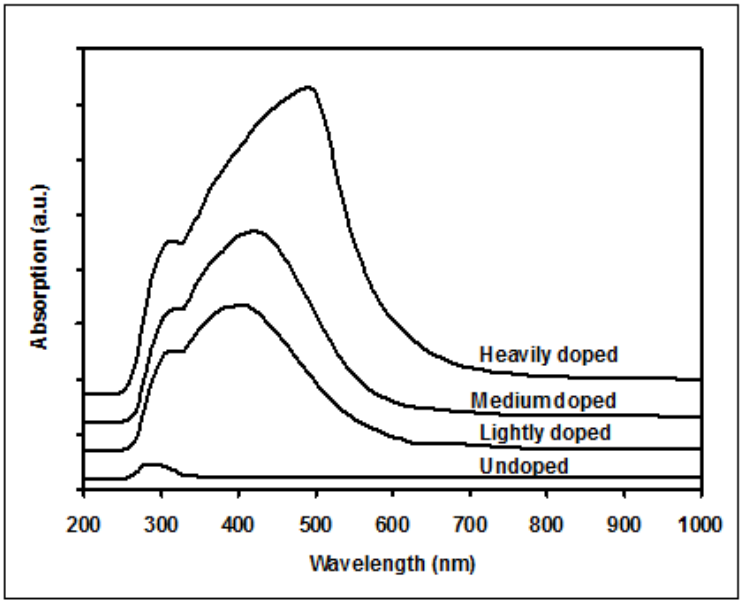

Figure 6.2: The optical absorption spectra of poly(β-pinene)for different dopant concentrations

FTIR spectra of the polymer before and after doping are shown in Fig. 6.3. Upon doping, there is a decrease in the FTIR peaks at 1610 cm^{-1} and 728 cm^{-1} corresponding to C=C stretching vibration and =C-H bending vibration respectively. This decrease is due to charge-transfer from the isolated double-bond to the dopant and formation of radical cations (Fig.1b). In the present report, we discuss results of EPR measurements to show that cation radicals are formed upon doping of poly(β-pinene).

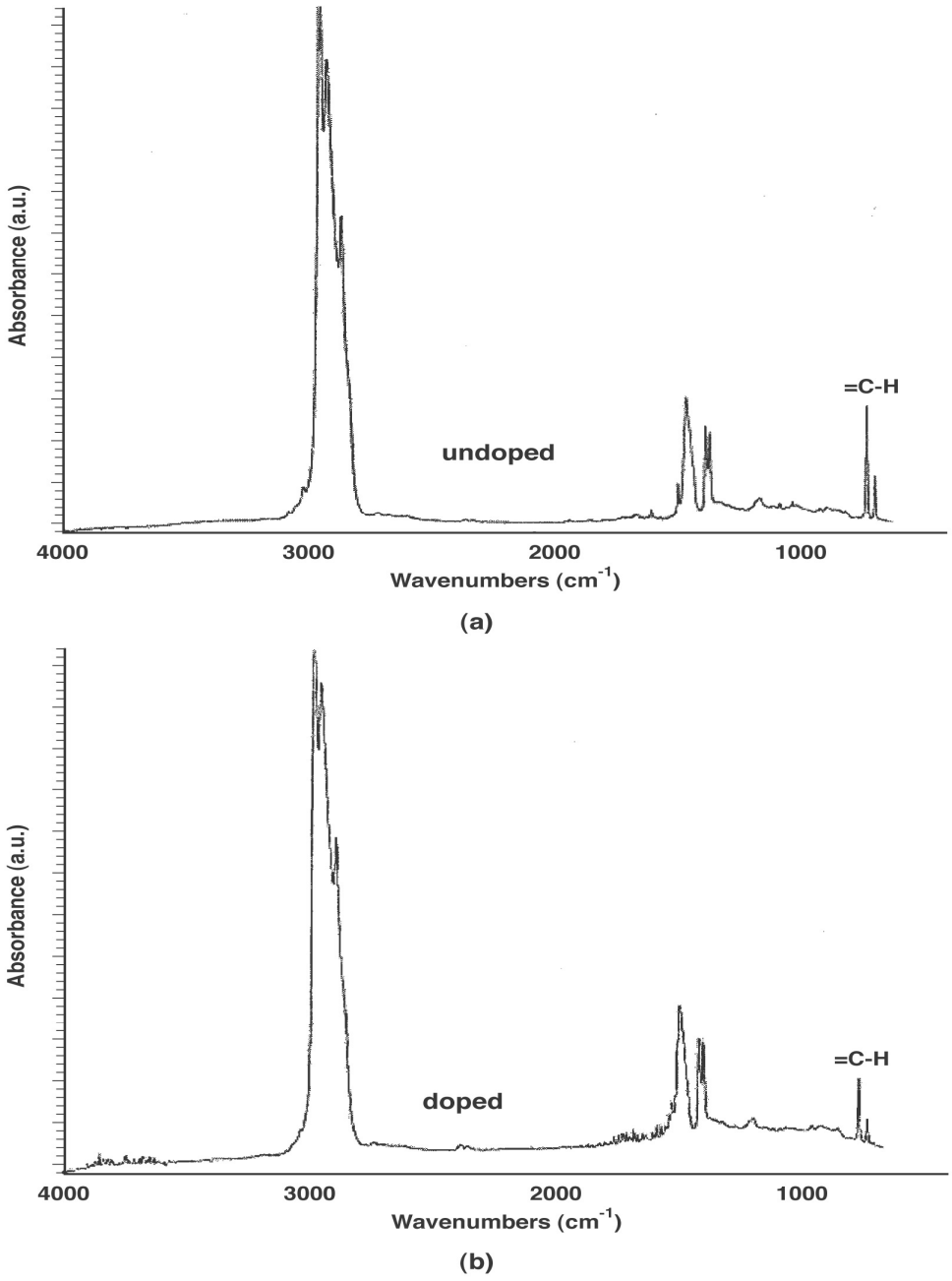

Figure 6.3: FTIR spectra undoped (a) and doped(b) poly(β-pinene)**[76]**

6.2 Experimental

The EPR measurements were performed on poly(β-pinene) at different doping levels of iodine. The poly(β-pinene) samples used in this work were purchased from Aldrich Chemicals Corp. Films of poly(β-pinene) were prepared on a glass substrate from a toluene solution. The

films were then doped with iodine at different concentrations. The molar concentrations were calculated by measuring the weight uptake of iodine in the film. The powder samples obtained from the doped films were used to perform the EPR measurements. Undoped poly(β-pinene) samples were also prepared as a powder and weighed to perform the EPR measurement. The EPR experiment was conducted at X-band (9 GHz) using a Bruker EMX spectrometer at room temperature as well as at a lower temperature (100 ^{o}K). Cooling of the sample was performed with an Oxford Instruments ESR 900 flow cryostat with an ITC4 temperature controller.

6.3 Results and Discussion

The undoped poly(β-pinene) sample showed a very weak EPR signal due to the methyl radicals. Significant EPR signals increasing in proportion to the dopant concentration have been observed and the results are shown in Fig. 6.4.

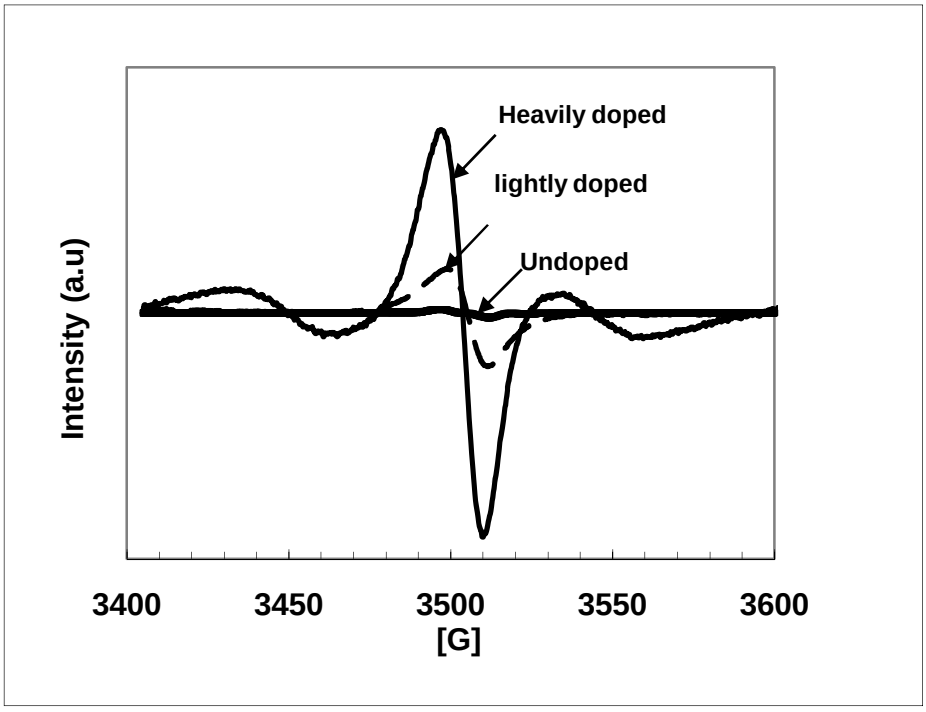

Figure 6.4: EPR data of poly(β-pinene) at different dopant concentrations

Clearly, the EPR signal of the heavily doped sample is large. As these results have shown, g =

2.0042 and the EPR line-width (ΔH_{pp}) of the doped samples is about 13 G. These values compare well with those of doped cis-polyisoprene reported earlier [112]. The line-width is larger compared to that in conjugated conductive polymers[113] because the radical is less mobile (confined) in the case of the nonconjugated conductive polymer. The EPR signals of a lightly doped and a heavily doped sample are shown in Figs.6.5 and 6.6 respectively.

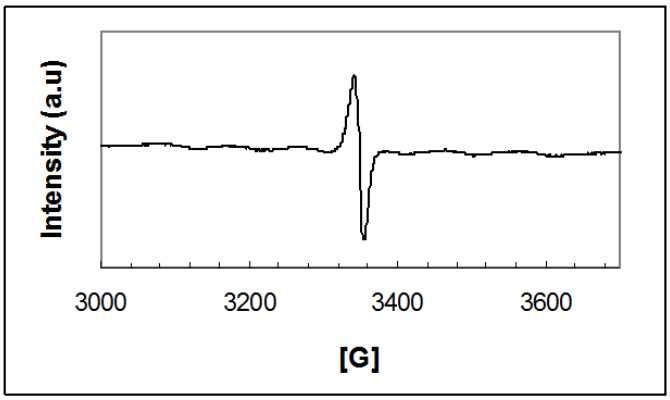

Figure 6.5: EPR signal of undoped poly(β-pinene)

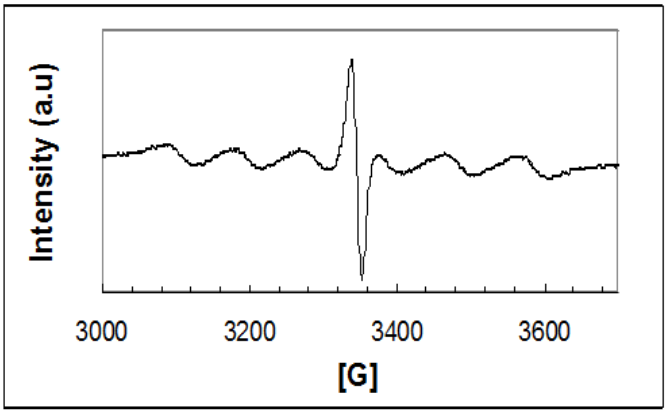

Figure 6.6: EPR signal of lightly doped poly(β-pinene)

Hyperfine splitting was observed in the EPR signal particularly in the case of heavily doped samples (Fig.6.6). Six peaks due to hyperfine splitting were observed. If there are 'n' nuclear spin halves, n+1 distinct peaks due to hyperfine splitting are expected in the EPR signal. Iodine has a nuclear spin of 5/2. Therefore, six peaks as a result of hyperfine splitting can be expected

and were observed. At the high dopant concentration, there is a reduction in the distance between the cation radical and the iodine anion leading to the hyperfine splitting as observed.

The area under the curve in the EPR signal (at 100^{o}K) was plotted as a function of molar concentration of iodine, and the correlation is shown in Fig.6.7. The area per gram varies linearly with the molar concentration of iodine. Since the area is proportional to the spin concentration, the results show that the concentration of radicals increases proportionally with the dopant concentration. These results clearly show that cation radicals are formed upon doping and consequent charge-transfer from the isolated double bonds to the dopants.

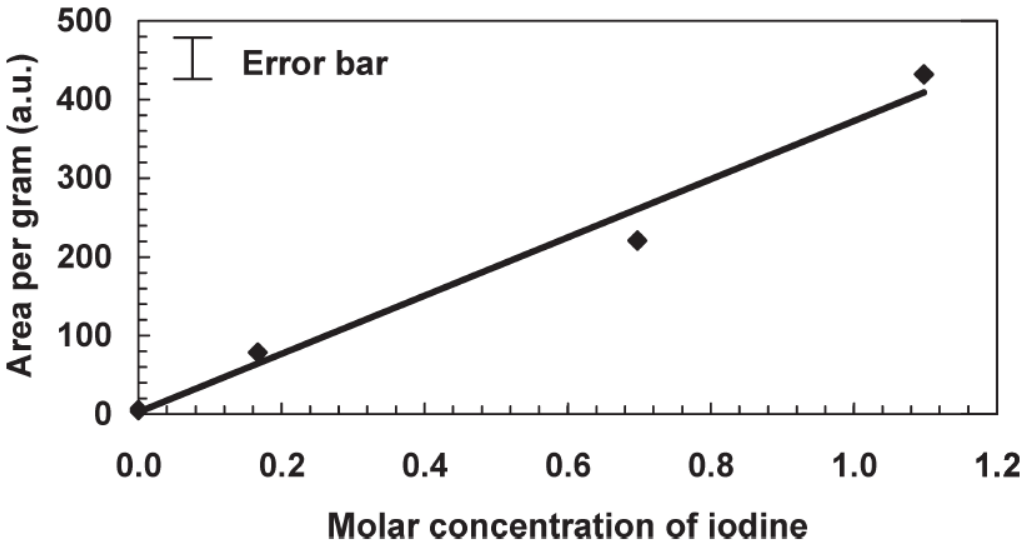

Figure 6.7: Area of EPR signal per gram of poly-(β-pinene) as a function of molar concentration of iodine

6.4 Conclusions

In summary, EPR measurements have been performed on poly(β-pinene) at different concentrations of iodine. The signal was found to increase proportionally with the iodine concentration due to the formation cation radicals upon doping and charge-transfer. The results are consistent with the FTIR and optical absorption data. The g-value and the EPR line-width (ΔH_{pp}) compares well with that of another nonconjugated conductive polymer, doped 1,4-*cis*-

polyisoprene.[112] Hyperfine splitting in the EPR signal has been observed for heavily doped samples because of reduced distance between the cation radical and the iodine anion.

CHAPTER 7

OFF- RESONANT ELECTRO-OPTIC MEASUREMENTS IN DOPED POLY(β-PINENE)

7.1 Introduction

Third-order optical materials have attracted significant research attention due to their applications in ultrafast switching, electro-optic modulation, optical phase conjugation, optical limiting, etc.[7, 8]Various classes of third-order materials have been investigated. High optical nonlinearities have been reported on conjugated polymers such as polydiacetylenes.[14] The optical nonlinearities in these polymers are attributed to the delocalized electrons along their backbones forming quantum wires. Metallic nanoparticles (quantum dots) have been widely investigated for their large third-order nonlinearities.[114] In metallic quantum dots, the high optical nonlinearity is due to the surface plasmon resonance and associated characteristics of the confined systems. Recently, exceptionally high third-order optical nonlinearities have been reported in doped nonconjugated conductive polymers.[80, 81, 78] Nonconjugated conducting polymers have been discussed in detail.[76, 110] Optical nonlinearities in nonconjugated conducting polymers have been attributed to the charge confinement in subnanometer domains (subnanometer metallic quantum dots) formed upon doping.

The magnitude of the Kerr coefficient of iodine-doped poly(β-pinene) as measured at 633nm is 50 times that of the standard Kerr-electro-optic material, nitrobenzene [81]. The two-photon absorption coefficient of this iodine doped polymer measured using an open aperture z-scan technique at 810 nm was reported [82] to be 2.6 cm/MW. Here, we discuss the electro-optic

measurements performed at 790 - 810 nm and 1.55 μm.

7.2 Experimental

Poly(β-pinene) samples purchased from Sigma Aldrich was used in this work. A measured quantity of the polymer was dissolved in toluene at room temperature. A thin (~ 1 μm thick) transparent film of poly(β-pinene) was cast on a glass slide from this solution. The film was then doped with iodine by evaporation at room temperature. The duration of doping determined the dopant concentration in the films. Heavily doped films looked dark and had high electrical conductivity of about 10^{-2} S/cm. Electro-optic measurements were performed on medium doped samples with electrical conductivity of ~ 10^{-3} S/cm. The doping time was found to be critical to produce better quality films. Figure 7.1 shows the optical micrographs of an over-doped and an optimally doped film. The over-doped film developed cracks producing poor optical quality.

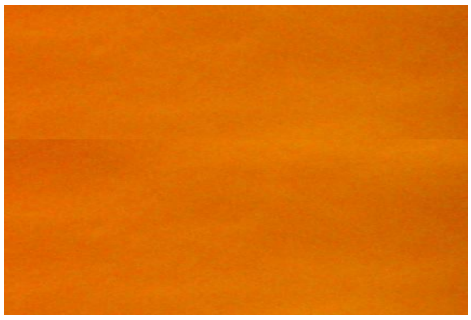

(a)

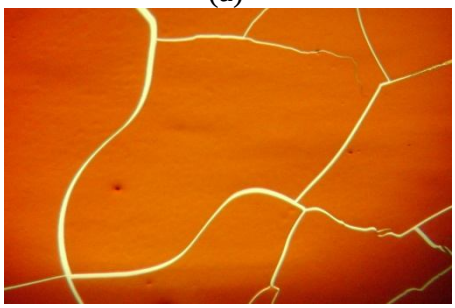

(b)

Figure 7.1: (a) Optical micrograph (100x) of an optimally doped and processed film of poly(β-pinene) showing excellent optical quality.
(b) Optical micrograph (100x) of typical doped film with poor optical quality.

Therefore, emphasis was placed on optimizing doping time. The sample was then covered with a film of optical glue to preserve it for longer duration. Two copper electrodes were then applied to the sample to form a narrow slit of about 100 μm.

Besides iodine-doped poly(β-pinene) a number of other polymers were investigated for quadratic electro-optic effect at 1.55 μm using the same sample configuration and measurement techniques. This was to provide sufficient background check-up and eliminate the possibilities of measuring slow processes including: electrostriction, molecular movements, capacitive effect and other potential mechanical effects resulting from application of electric fields. The polymers used include: undoped polyisoprene (natural rubber), undoped polybutadiene, undoped polystyrene, dye-doped polystyrene, undoped poly(β-pinene), PTS-polydiacetylene and also silicon.

Field-induced birefringence technique was used to make the electro-optic measurements. A schematic of the setup is shown in Fig.7.2 The sample was placed between a polarizer and an analyzer which were oriented orthogonal to each other and at an angle of 45° to the polarization of the incident laser beam. An ac voltage at 4 kHz was applied between the two copper electrodes to create an electric field on the sample. The modulation in optical intensity due to field induced birefringence in the sample was measured using a photo-diode and a lock-in amplifier latched to twice the frequency of the applied field. A Ti-Sapphire laser in cw mode was used to make measurements at 790, 800 and 810nm. Measurements at 1.55 μm were performed using a semiconductor laser (BW-Tek). The applied ac electric field (at 4kHz) was varied from 0.2 - 2.2 V/μm.

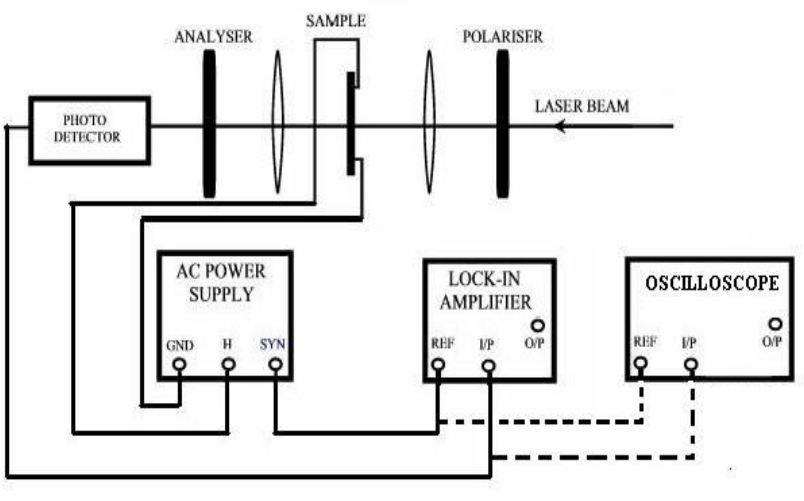

Figure 7.2: Schematic of field induced birefringence experiment

7.3 Results and Discussion

An exceptionally large quadratic electro-optic effect was recorded in doped poly(β-pinene). The electro-optic modulation depth at 1.55 μm for different applied electric fields are shown in Fig. 7.3a. A modulation depth of ~ 0.1% was observed in a 1 μm thick sample for an applied field of 1V/μm at 1.55 μm. Therefore, the Kerr-coefficient as determined is 1.6×10^{-10} m/V^2. The Modulation depths at 790, 800 and 810 nm were also very large leading to exceptionally large Kerr coefficients (Table 7.1). The Kerr coefficient at 810 nm is slightly smaller since this wavelength coincides with the two-photon resonance peak [82]. Two-photon absorption coefficient is the imaginary part of nonlinear refractive index, while the measurement reported here corresponds to the real part of nonlinear refractive index.

Wavelength (nm)	**Kerr Coefficient** (m/V^2)
790	1.3×10^{-10}
800	1.8×10^{-10}
810	1.5×10^{-10}
1550	1.6×10^{-10}

Table 7.1: Kerr coefficient of poly(β-pinene) at different wavelength

The background materials including: undoped polyisoprene (natural rubber), undoped polybutadiene, undoped polystyrene, dye-doped polystyrene, undoped poly(β-pinene), polyethylene and silicon did not show any appreciable quadratic electro-optic effect. As expected, only PTS-polydiacetylene showed significant quadratic electro-optic signal since that is known to have large and ultrafast optical nonlinearity. Therefore, the observed nonlinearity in doped poly(β-pinene) is not due to slow effects. The modulation signal observed for PTS-polydiacetylene film showed a quadratic dependence on the applied field (Fig.7.2 b). The Kerr-coefficient as determined for PTS-polydiacetylene is ~ $3x10^{-12}$ m/V^2 at 1.55 μm.

The studies as discussed in this report have been performed under ambient conditions. The results were repeatable even seven months after the sample preparation partly because of the coating with the optical glue.

The nonlinear index of refraction, n_2 and the third order nonlinear susceptibility, χ^3 can be approximately estimated from the magnitude of Kerr coefficient utilizing known correlations. The estimated χ^3 is about $3x10^{-8}$ esu which is exceptionally large, larger than that of known metallic quantum dots.

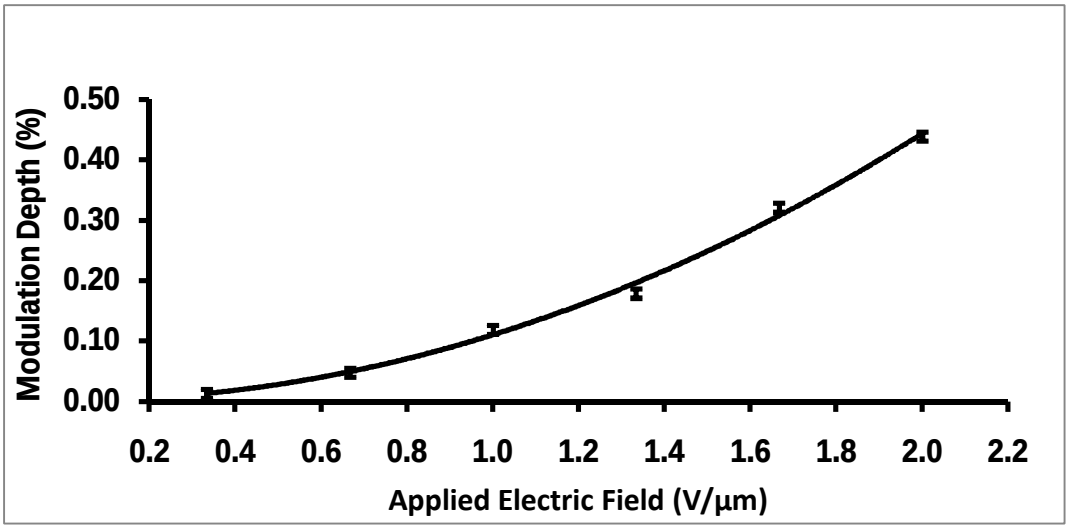

The exceptionally large nonlinearity as observed has been attributed to the metallic (a)

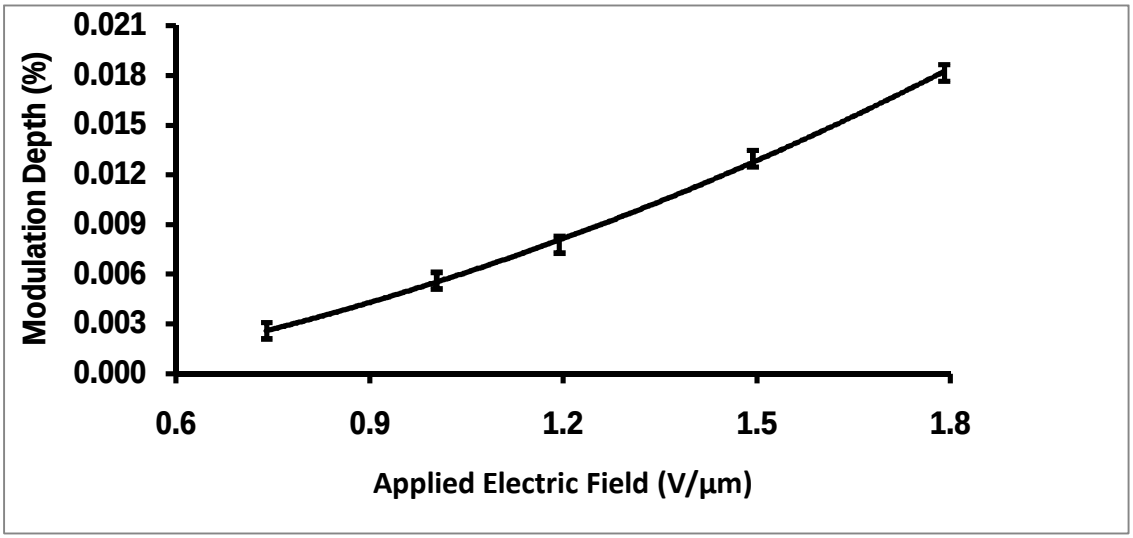

(b)

Figure 7.3: Modulation depths observed at 1.55 μm as a function of applied electric field for: (a) iodine-doped poly(β-pinene) film, and (b) PTS-polydiacetylene single-crystal film.

quantum dots of subnanometer dimension that are formed upon doping of a nonconjugated conductive polymer such as poly(β-pinene). The quantum dot structures are schematically presented in Fig.7.4(encircled regions).

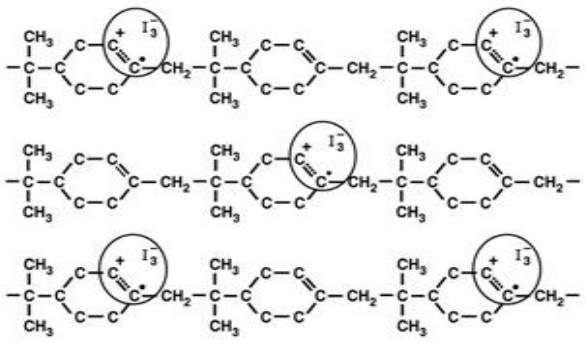

Figure 7.4: Organic quantum dots of sub-nanometer dimension formed by doping and charge-transfer of poly(β-pinene).

The wavelength of maximum absorption in the optical absorption spectrum of doped poly(b-pinene) is shorter compared to that of 5 nm size metallic quantum dots as would be expected. The encircled regions in Fig.7.4 are less than one nanometer in dimension. In addition doped poly(β-pinene) is known to have a broad two-photon absorption peak at ~ 810 nm. The optical nonlinearity (Kerr coefficient) at 1.55 μm is enhanced partly because of the position of the two-photon absorption peak. The improved film quality as achieved by optimized doping and processing is another reason for the enhanced nonlinearity.

The results at 1.55 μm are significant considering applications in ultrafast electro-optic, all-optical switching and modulation for telecommunication. Such high third order optical nonlinearities at technologically significant wavelengths are being reported for the first time. The Kerr coefficient at 1.55 μm as measured is the largest known at this wavelength considering all materials including metallic and semiconductor quantum dots and conjugated polymers [115, 7].

7.4 Conclusions

Quadratic electro-optic effect in iodine-doped poly(β-pinene) at off resonant wavelengths have been measured using field-induced birefringence technique. The magnitude of the Kerr coefficient at 1.55 μm is 1.6×10^{-10} m/V^2, which is the largest known for any material. At 790 -

810 nm the magnitudes are also very large. The magnitude is slightly smaller at 810 nm since this wavelength coincides with the two-photon resonance peak. These exceptionally large nonlinearities are attributed to the sub-nanometer size metallic quantum dots formed upon doping and charge-transfer involving poly(β-pinene). The large nonlinearity at 1.55 μm is important for ultrafast device applications in telecommunication.

CHAPTER 8

TIME RESOLVED TWO-PHOTON ABSORPTION MEASUREMENTS IN DOPED POLY(β-PINENE)

8.1 Introduction

Organic and inorganic quantum dots have attracted wide research attention due to their potential applications in photonics. Significant advances have been made in the development and characterization of inorganic quantum dots. Optical nonlinearities in inorganic quantum dots are due to a combination of quantum and dielectric confinements.[20] A variety of inorganic systems like CdS, As_2S_3, ZnS etc. have shown high cubic nonlinearities, however their response is slow when compared to organic third order materials. [14] Organic-inorganic hybrid materials have also been reported to possess high third order nonlinearities.[116] In the recent years the focus has shifted to organic polymers because of their ultrafast response, high damage threshold and the freedom they provide in engineering their structures to increase optical nonlinearities. Conjugated polymers; a class of conducting polymers with alternating single and double bonds, have been widely studied by various groups for their cubic nonlinearities. Optical nonlinearities in these materials are due to the presence of delocalized electrons in their sp_2 hybridized carbon atoms.[7] These materials behave like organic quantum wires. Nonconjugated conducting polymers based quantum dots are the first known metal-like organic quantum dots. These polymers do not have alternating single and double bonds. The electrical and nonlinear optical properties of various doped nonconjugated conducting polymers like 1-4 cis-polyisoprene[80], polyalloocimene[110], poly(ethylenepyrrolediyl) derivative[78], polynorbornene[117], and

poly(β-pinene)[81] have been previously reported. Electro-optic coefficients of iodine doped poly(β-pinene) at 1.55μm is higher than that of the best known conjugated polymer polydiacetylene[118]. When a nonconjugated polymer is doped with iodine, the double bonds (C=C) are transformed into cation radicals which are confined in a subnanometer domain resulting in a quantum dot like structure. Optical nonlinearities in these systems are attributed to the charge confinement in these systems.

Recently, Titus and co-workers reported an exceptionally high two-photon absorption coefficient (~2.6 cm/MW at 810 nm) in iodine doped poly(β-pinene) using open aperture Z-scan technique.[82] The two-photon absorption in this material is higher than or comparable to many semiconductor and metallic quantum dots. It is critical to confirm the origin of optical nonlinearities in these materials. In this chapter time resolved interferometry measurements of iodine doped poly(β-pinene) are discussed. This experiment measures both the magnitude and response time of two-photon absorption in doped poly(β-pinene).

8.2 Experimental

8.2.1 Sample preparation

Poly(β-pinene) pellets purchased from Sigma-Aldrich were used in this experiment. Known mass of these pellets was dissolved in measured quantity of toluene at room temperature. A thin and uniform film of poly(β-pinene) was cast on a micro cover glass slides (average thickness 150μm) using this solution. The average thickness of the film varied from 1μm to 4μm. The thickness of the film was controlled by changing the solute to solvent ratio. These films were then doped in iodine for 9 to 11 hours. The duration of doping was found to be critical because over doped samples resulted in surface cracks that adversely affected the optical quality of the films. After doping the sample was left in fume hood for about 30 minutes to get rid of the

surface iodine. The resistance of the doped samples used in this experiment was about 35MΩ. A coating of optical glue on the doped sample may be used to preserve it for a longer duration.

8.2.2 Pump-probe setup

The experiment setup for time resolved interferometry technique using the pump probe method is shown in figure 8.1. A tunable (710nm – 940nm) Ti-Sapphire laser (Tsunami model 3950-L1S) producing 150fs pulses was used in this experiment.

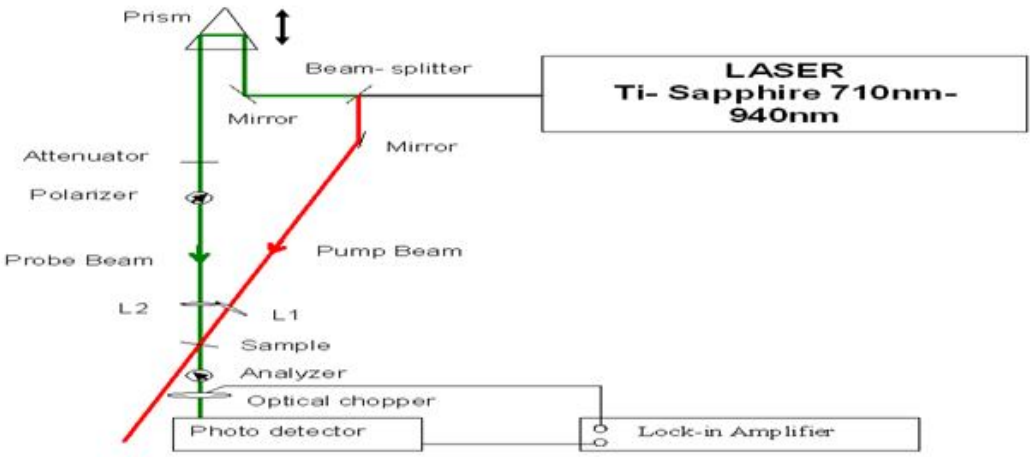

Figure 8.1 Schematic of the experimental set-up for pump probe technique

The beam from the laser was split into two using a beam splitter. One of the beams was used as the probe and the other as the pump.

8.2.2.1 Probe alignment

In figure 8.1 the path of the probe beam is traced by the green line. An optical attenuator was used to reduce the intensity of the probe beam to a desired level. A prism based retro-reflector as shown in the figure was used to change the path length of the beam. The motion of the prism was controlled using a precision motion controller. The beam then passed through a polarizer oriented parallel to the polarization of the incident laser beam. A focusing lens (5X) was used to focus the beam on the doped poly(β-pinene) sample. The beam from the sample passed through

an analyzer and was then detected using a photodiode. The orientation of the analyzer was also parallel to the polarization of the incident laser beam. The photodiode was connected to a lock-in amplifier that recorded the probe signal. The amplifier also received a reference signal from an optical chopper placed in the path of the probe beam. The lock-in amplifier only recorded signal from the photodiode that matched the frequency of the chopper, thereby eliminating spurious signals or noise.

8.2.2.2 Pump alignment

The pump beam is traced by a red line in figure 8.1. After the beam splitter the pump beam passed through multiple mirrors before being focused on the sample using a 5X lens. The pump beam and probe beam were made to overlap on the sample. The pump beam was not detected by the photodiode.

8.2.3 Data collection

The retro-reflector was aligned such that the path length of the two beams matched exactly which resulted in a spatial and temporal overlap of the beams right at the sample. The intensity of the probe beam was reduced to about 5% of the pump beam using the attenuator. The signal in the lock-in amplifier was recorded when the pump beam was incident on the sample and when the pump beam was blocked from the sample. The path length of the probe was then changed using the retro-reflector to produce a delay between the pump and the probe, and the signal from the lock-in was recorded. The ratio of change in transmission to normalized transmission was plotted as a function of the path difference.

8.3 Results and discussion

The two-photon absorption data measured at mode-locked condition (150 fs) at 790nm and 795nm are shown in figure 8.2 and 8.3 respectively.

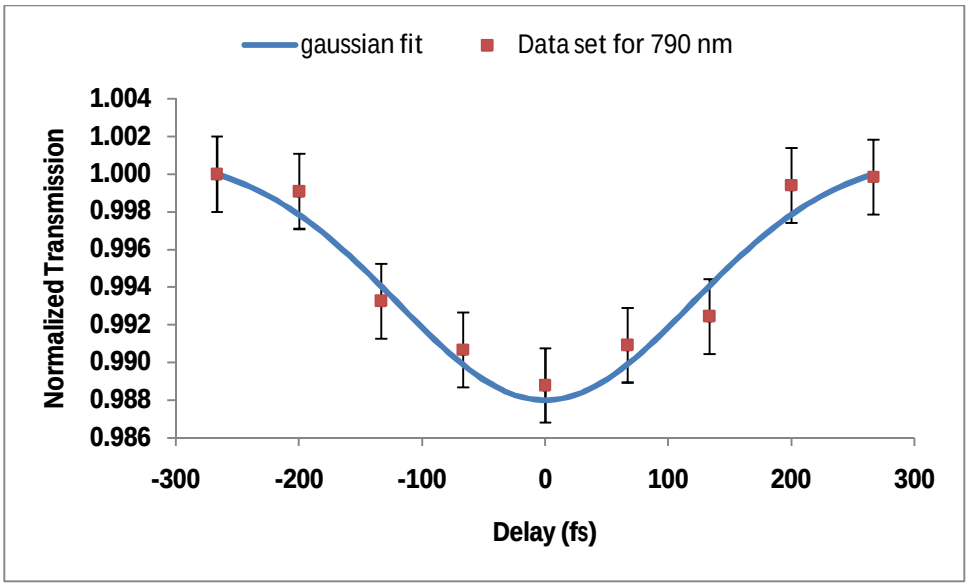

Figure 8.2: Two-photon absorption data measured at 790 nm using pump-probe technique

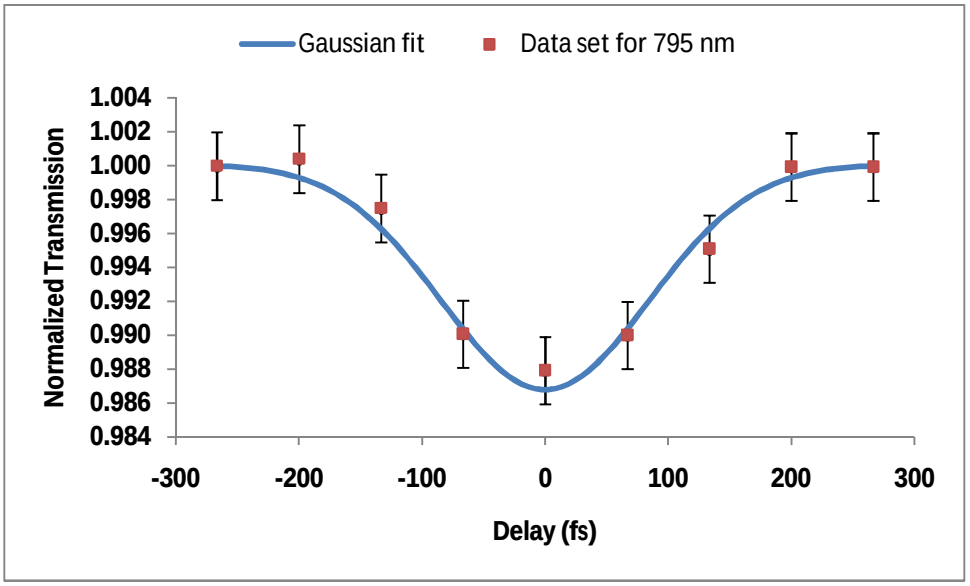

Figure 8.3: Two-photon absorption data measured at 795 nm using pump-probe technique

When the intense pump beam interacts with the sample it induces a change in the local linear absorption. This causes a change in transmission which is detected by the probe beam and measured in the lock-in. The plots in figures 8.2 through 8.3 clearly show that this effect is ultrafast since the response time is pulse width (150fs) limited. Thus the optical nonlinearity in this material is clearly electronic in nature and is not caused due to excited state absorption or

thermal effects. In metallic nanoparticles as a consequence of dielectric confinement, surface plasmon resonance enhances the optical nonlineartities at specific wavelengths. Time resolved experiments in these systems have been reported by other research groups.[119, 120] Their results show that the response is longer (~2ps) than the pulse-width used (30fs) and that the change in transmission is positive at 532nm. In doped poly(β-pinene) we find that the response is less than the pulse width used (150fs) and hence much faster than the effects observed in nanometals. This makes doped poly(β-pinene) well suited for high speed all-optical switching applications.

The magnitude of two-photon absorption coefficient (α_2) can be calculated from the change in transmission ($\Delta T/T$) as below.

$$\Delta T/T = -l\Delta\alpha \tag{8.1}$$

where $\Delta T/T$ is ratio of change in transmission to normalized transmission, $\Delta\alpha$ is the change in linear absorption coefficient and l is the thickness of the sample. The two-photon absorption coefficient α_2 is related to $\Delta\alpha$ through the equation below

$$\Delta\alpha = \alpha_2 I \tag{8.2}$$

Using the above equations the value of two-photon absorption coefficients found at 790nm and 795nm were found to be 2.28±0.1 cm/MW and 2.50±0.1 cm/MW respectively. The magnitude of α_2 of doped poly(β-pinene) shown above is exceptionally high and also consistent with the previously published results obtained using Z-scan.[82] Table 8.1 lists the two-photon absorption reported in metallic and semiconductor nanosystems.

Material	**Wavelength (nm)**	**α_2 (cm/MW)**
GaAs nanocrystals [121]	527 1064	0.03 0.05
Cu nanoclusters in fused silica [122]	532	0.01
ZnO beaded MWNT[123]	780	0.02
Iodine doped poly(β-pinene) (this work)	790 795	2.28 2.50

Table 8.1: Comparison of nonlinear absorption coefficients in various nanomaterials

Clearly the two-photon absorption coefficient in doped poly(β-pinene) is significantly higher than the these systems. This can be explained by examining the transformation that occurs in the polymer upon doping. Doping changes the electronic, structural and optical properties of conducting polymers. In case of conjugated polymers there is a significant decrease in optical nonlinearities upon doping because conjugated polymers transition to metallic state upon doping. In nonconjugated conducting polymers, doping leads to a quantum dot like structure. When nonconjugated conducting polymers are doped, the C=C bonds are transformed into cation radicals and there is a charge transfer between the double bond and the dopant. Optical absorption spectra, EPR and FTIR measurements in doped poly(β-pinene) and other nonconjugated systems have confirmed this phenomenon. The structure of doped poly(β-pinene) is shown in the figure below

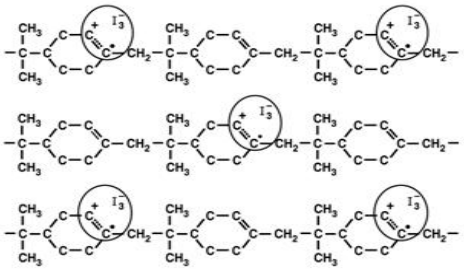

Figure 8.4: Quantum dots (encircled regions) in doped poly(β-pinene)

From the above figure and from the bond length calculations it is evident that the charge transfer

sites are confined in sub-nanometer domains resulting in an organic quantum dot structure. The work by Nimtz and coworkers on three dimensional size induced metal insulator transition (SIMIT) offers an interesting comparison. Nimtz *et. al* measured the electrical conductivity of indium nanocrystals as a function of the particle diameter. [124] They observed that when the diameter of the nanoparticle is comparable to the electron wavelength (~1μm) the electrical conductivity is inversely proportionally to the third power of the particle diameter. The bulk indium material is highly electrically conductive but as the particle size is reduced to 10^{-8} m, the indium quantum dots are far less conducting. This is shown in figure 8.5 (reproduced from reference [126]). In nonconjugated conducting polymers the electrical conductivity is at a similar level as in indium quantum dots. The charge transfer sites formed upon doping are of subnanometer dimension resulting in the organic quantum dot structure.

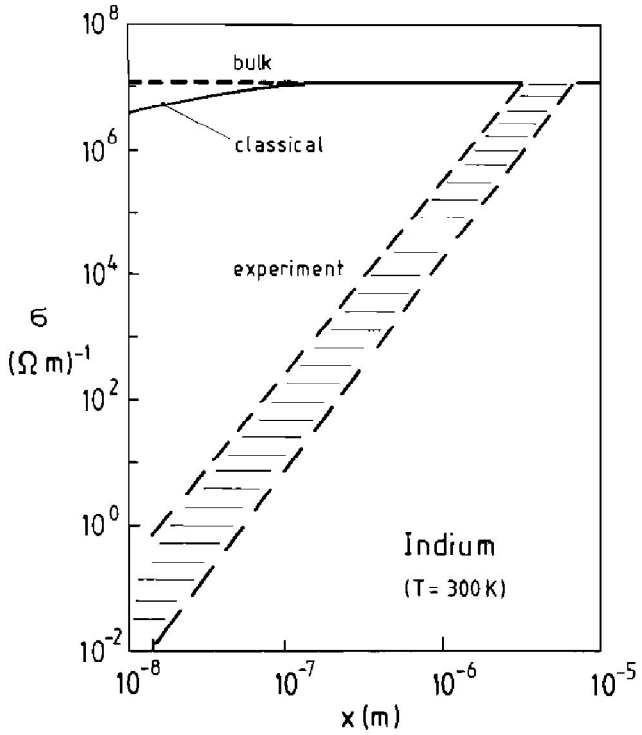

Figure 8.5: Size dependent electrical conductivity measurements in indium nanocrystals [124]

8.4 Conclusions:

Exceptionally high two-photon absorption coefficient, α_2 was measured in doped poly(β-pinene) at 790nm and 795 nm using pump probe technique using a mode locked Ti-Sapphire laser with 150 fs pulses. The response time of α_2 was ultrafast clearly indicating that the nonlinearities in this material are of electronic origin. Such high nonlinearities are attributed to the quantum dot like structure formed upon doping. This material has a wide variety of applications in photonics.

CHAPTER 9

NONLINEAR OPTICAL WAVEGUIDING IN DOPED POLY(β-PINENE)

9.1 Introduction

There has been increasing interests in nonlinear optical waveguides due to their ability to provide exceptional beam confinement for large propagation lengths.[125] Nonlinear optical waveguides in several materials like polymeric hosts, glass substrate, crystal cored fibers and Langmuir Blodgett films have been reported.[37] A nonlinear optical waveguide increases the interaction length of the optically active material and the lights source. In the previous chapters the exceptionally high optical nonlinearities in doped poly(β-pinene) were discussed using various techniques like field induced birefringence and time resolved interferometry. These experiments were conducted on thin films (1μm -6μm) of doped poly(β-pinene). Increasing their interaction lengths and demonstrating higher modulation depths is desired to ensure that these materials have applications in various nonlinear optical devices. However, the conventional sample preparation discussed previously cannot be used to prepare thick film suitable for nonlinear optical applications because of the inability of the dopants to penetrate deep into thick films. Since the optical nonlinearities in nonconjugated systems heavily depend on the dopant interaction, uniform and optimal concentration of the dopant through the entire thickness of the film is essential. Also, thick films often have poor optical quality and large scattering losses. Alternatively, a thin and uniform layer of doped poly(β-pinene) on a bare glass fiber can provide long interaction between the sample and the laser without compromising on the dopant homogeneity or the optical quality. In this chapter a nonlinear optical wave-guide based on

doped poly (β-pinene) is discussed.

9.2 Experimental

Several techniques were tried to increase the interaction length. A poly(β-pinene) pellet was one of the first approaches. The undoped polymer was finely ground and spread evenly on a glass slide. The powder was then doped with iodine for 9 to 12 hours. The doped polymer powder was then placed on a dye and pressed using a hydraulic press at 1500 psi. The resulting pellet was about 15 mm thick. However, the pellet yielded poor light throughput and accounted for large scattering losses and hence could not be used for the nonlinear optical experiments. Another technique was to draw fibers of desried length using the undoped poly(β-pinene). Pellets of undoped fiber were heated above the melting point. Thin uniform fibers were drawn out of the molten polymer using a sharp needle. The diameter of the fiber could be altered by the temperature of the polymer. Thin fibers of about 30μm could be drawn at about 75º C. Although these fibers were uniform, had no pores and were of exceptional optical quality (before and after doping) they could not be used to nonlinear optical measurements for the following reasons:

1. The polymer fiber became very brittle after doping and handling doped fibers was extremely difficult.
2. Their thermal damage threshold was extremely poor and could not withstand high intensities of laser beam.

To overcome these shortcomings, a fiber-optic waveguide was prepared. Multi-mode optical fiber with a numerical aperture of 0.37 and core diameter 200μm purchased from Thorlabs was used to prepare the waveguide. The fiber had a silica core, an acetone soluble TEQS cladding and Tefzel outer jacket. A 15 cm long fiber was sliced with flat edges on both sides. The outer jacket and the cladding was burned using a flame torch. The bare fiber was then left in acetone

for about an hour to dissolve any remnants of the cladding and to purge other contaminants. The dry fiber was then dipped in a thick solution of poly(β-pinene) and toluene. The fiber was then taken out of the solution and dried in room temperature. Thus, a uniform "cladding" of the polymer was cast on a bare multi-mode silica fiber. The fiber was then doped with iodine for required amount to time. Pictures of poly(β-pinene) cladded fibers before and after doping is shown in figure 9.1. The poly(β-pinene) cladded fibers were of excellent optical quality making them ideal candidates for nonlinear optical measurements. The optical micrographs of doped and undoped fibers are shown in figure 9.2.

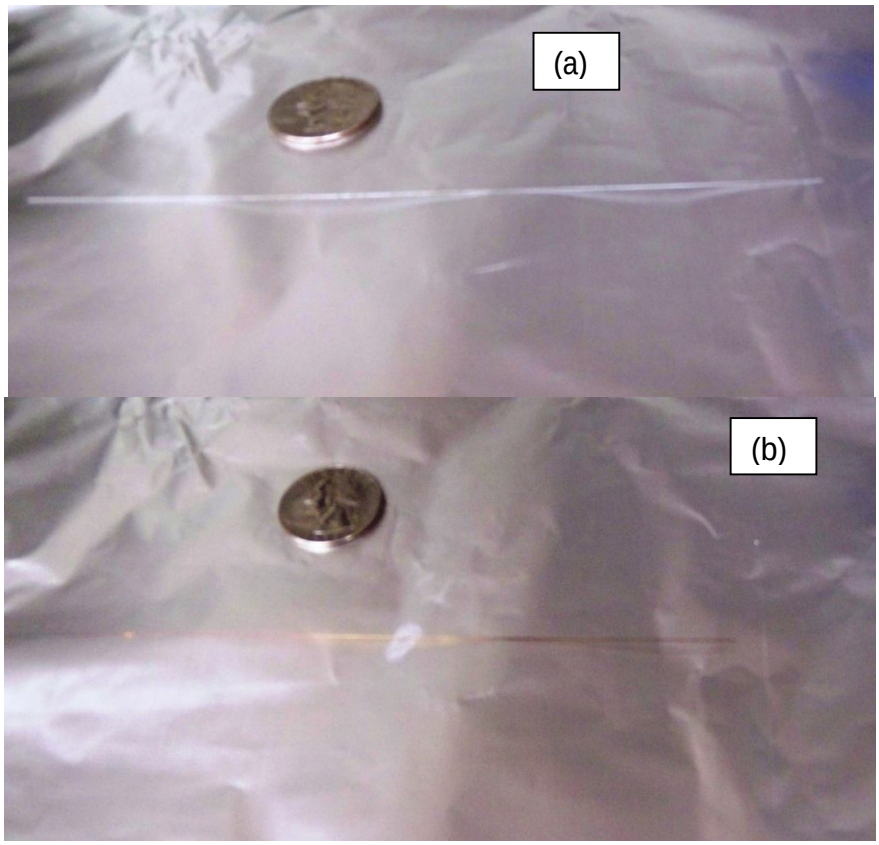

Figure 9.1 photographs of (a) undoped and (b) doped fiber-optic waveguide

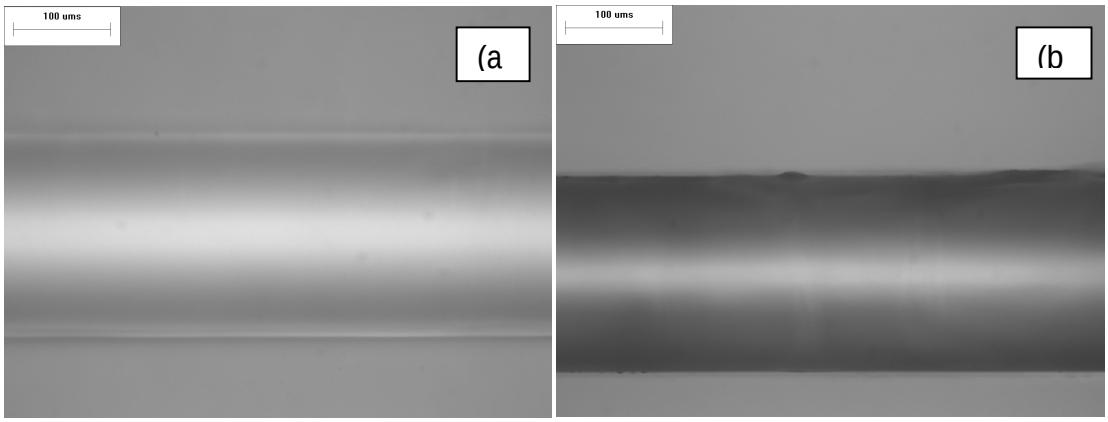

Figure 9.2: Optical micrographs of (a) undoped and (b) doped fiber-optic waveguides

Figure 9.3 shows the schematic of the experimental setup for measuring two-photon absorption in doped optical fiber.

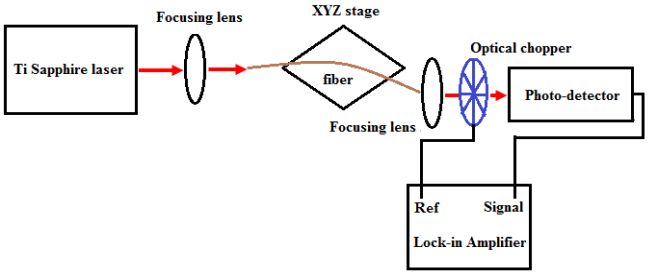

Figure 9.3: Experimental setup for two-photon absorption in a fiber-optic waveguide.

All measurements in this report were performed using a mode-locked, pulsed Ti-Sapphire Tsunami laser with 150 fs pulse at 790nm. The optical power of the laser was adjusted using an attenuator, the beam was then focused on the doped fiber using a 40x lens. The fiber was mounted on a precision stage whose motion could be controlled along all the three axes. The fiber was carefully aligned to achieve maximum throughput. The beam from the other end of the fiber was focused using a 20X lens on to a photodiode. An optical chopper placed in the path of the beam chopped the beam at a set frequency. The photodiode and the optical chopper were connected to a lock-in amplifier. The lock-in amplifier recorded the signal from the photodiode

that matched the frequency of the chopper. The input power was measured using a power meter. The input power was varied from 10 mW to 60 mW in cw and mode-locked conditions; the corresponding output power recorded by the lock-in amplifier was noted.

9.3 Results and discussions

A light throughput of about 1.3% is observed in a 15cm long doped fiber at an input power level of 10mW. The normalized transmission of the optical waveguide plotted as a function of input power is shown in figure 9.4.

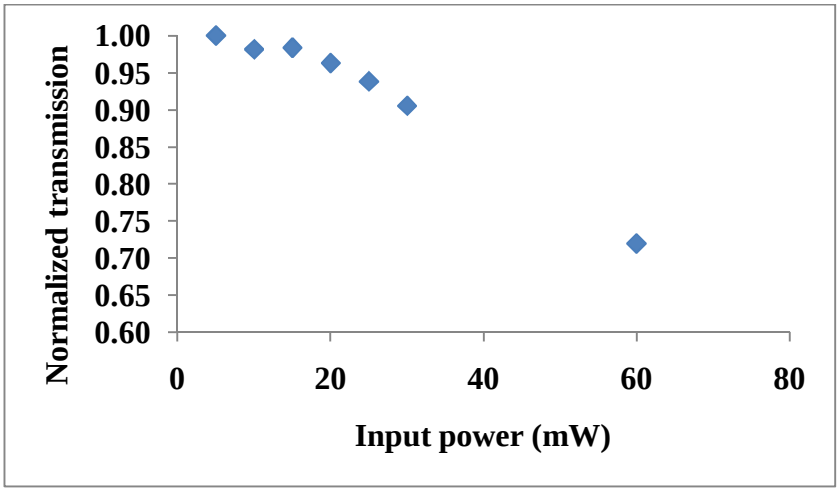

Figure 9.4: Normalized transmission in the optical waveguide at different input power levels

The data shows a clear decrease in the transmission at higher power levels. No change in transmission was recorded in undoped fibers. The experiment was also repeated in the cw mode and little or no change in transmission was observed. This decrease in transmission in doped fibers under mode-locked conditions is due to the two-photon absorption in doped poly(β-pinene). A maximum decrease of 28 % is observed at 60 mW input power. The peak intensity within the guide was about 2.5MW/cm^2. The observed change in transmission in the waveguide is more than 200 times that observed in doped thin films of poly(β-pinene). More work needs to be done to confirm this result.

The magnitude of two-photon absorption in this material can be computer from the change in transmission.

$$\frac{\Delta T}{T} = -l\Delta\alpha \qquad 9.1$$

where $\Delta T/T$ is ratio of change in transmission to normalized transmission, $\Delta\alpha$ is the change in linear absorption coefficient, l is the thickness of the sample. Equation 9.1 gives the change in linear absorption. This was discussed in chapter 8 for thin films. The two-photon absorption coefficient α_2 is given by

$$\Delta\alpha = \alpha_2 I \qquad 9.2$$

9.4 Conclusions

In conclusion, a nonlinear optical waveguide was prepared by casting a uniform cladding of poly(β-pinene) on a bare multi-mode fiber and doping it. The waveguide was of excellent optical quality and could withstand a peak intensity of 2.5 MW/cm^2 without damage. Two photon absorption measurements were made using this fiber at 795 nm. A maximum decrease in transmission of 28% was observed at an input power level of 60mW in mode-locked condition. The observed change is higher compared to thin films by a factor of over 200. The result is significant considering its potential applications in high speed (femtosecond timescale), optical limiting and others. More work needs to be done to confirm this result.

CHAPTER 10

PHOTOVOLTAIC EFFECT IN NONCONJUGATED CONDUCTING POLYMER

10.1 Introduction

Organic polymers have attracted a great deal of interest in the area of photovoltaics. These materials show promising results and can serve as lower cost alternatives to inorganic photovoltaic materials [85]. The first two-layer organic photovoltaic system appears to have been reported in 1958 [94]. Poly(p-phenylene vinylene) (PPV) has been widely studied in the research area of organic photovoltaic devices [98, 99, 100]. Reports have been made on photovoltaic devices based on polythiopene [96].

Composites involving conjugated organic polymers and electron acceptors have been widely studied for photovoltaics. Buckminsterfullerene, C_{60} and its derivatives have been widely used in the area of photovoltaics since its discovery [103]. Photo-induced electron-transfer between conjugated polymer and C_{60} leading to photovoltaic effects have been investigated in detail [104, 105].

10.2 Experimental

In this discussion, the photo-induced electron-transfer and resulting photovoltaic effect in a composite involving a *nonconjugated* conductive polymer and fullerene will be discussed. Such effect involving a nonconjugated conducting polymer is being reported for the first time. The solutions of composites were prepared by dissolving weighed quantities of poly(β-pinene) and C_{60} in toluene. Composites having different concentrations of C_{60} ranging from 0% to 8% by weight were prepared. The films of these composites were cast on a glass slide under normal

environmental conditions. Fig. 10.1 shows the optical micrographs of these films.

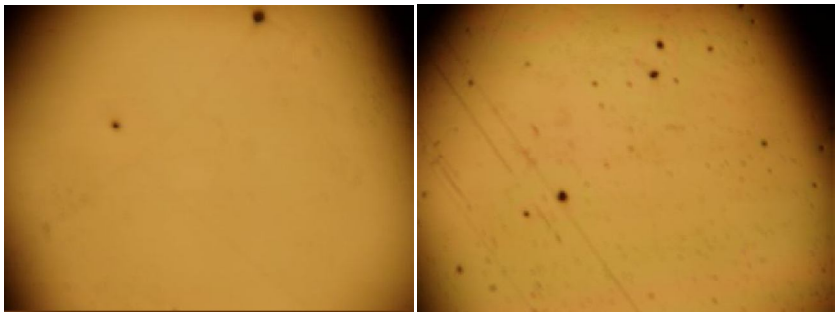

(a) (b)

Figure 10.1: Optical micrographs (magnification 50x) of the composite films. The composite with 4% by weight (a) of C_{60} is more homogeneous than that with 8% by weight (b) of C_{60}

It was observed that the composite films having about 4% C_{60} by weight or less were more homogeneous compared to films having a higher weight percent of C_{60}. This is because the solution is saturated when the C_{60} added is more than 4% by weight. As a consequence, the film with 8% by weight of C_{60} is less homogeneous. The optical absorption, photoluminescence spectra and photovoltaic effects in these composite films were measured for different concentrations of C_{60}.

10.3 Results and Discussions:

Thin films of the composites were cast on glass substrates and the absorption spectra of the films were studied. Pristine poly(β-pinene) has an absorption peak at about 270 nm. The optical absorption spectra of the composites formed by poly(β-pinene) and C_{60} at different concentrations is shown in Fig.10.2. The composites show two distinct peaks, one at ~ 270nm and the other at ~ 335 nm. The inset in Fig.10.2 shows the absorption spectrum of C_{60}. The peak at 270 nm observed in the composite is due to poly(β-pinene) and C_{60}, while the peak at 335nm is due to C_{60} alone. The intensity of the absorption peak for the composite film increases with increase in the concentration of C_{60} (by % weight). As shown in the Fig.10.2, the bottom most

spectrum corresponds to the composite with 0% C_{60} by weight (pristine poly(β-pinene)). The spectrum above it corresponds to the composite having 1% C_{60} by weight. The top-most spectrum corresponds to the composite having 8% C_{60} by weight. As these spectra show, the absorption characteristics of poly(β-pinene) does not change in association with C_{60} since no new peak appears in the composite spectra other than those of the components. Therefore, no charge-transfer between the polymer and C_{60} occurs at the ground state.

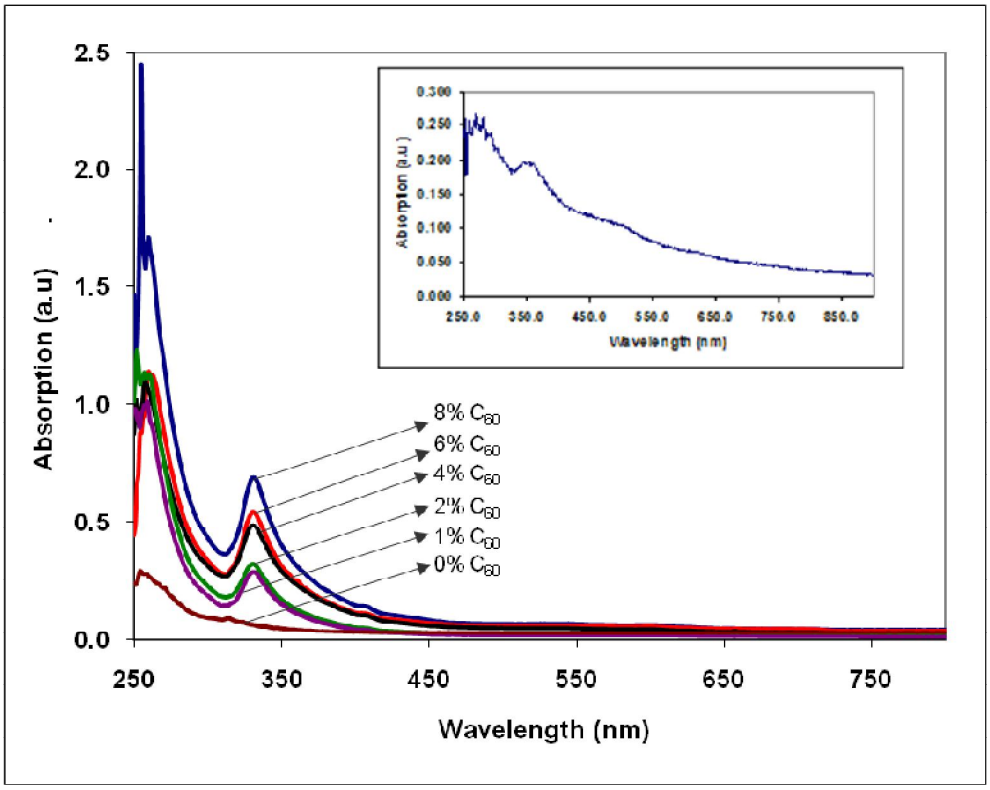

Figure 10.2: Optical absorption spectra of the composites involving poly(β-pinene) and different weight percents of C_{60}. The inset shows the absorption spectrum of C_{60} alone.

The photoluminescence of the composite films has been studied (Fig.10.3) using Perkin Elmer LS-55 spectrometer. As shown in the inset of Fig.10.3, pristine poly(β-pinene) has an emission peak at 360 nm for an excitation wavelength of 280 nm =[76]==[76]==[76]=[76]. The photoluminescence is quenched in the composite involving poly(β-pinene) and C_{60}. This is

because the photo-excited electron in poly(β-pinene) is transferred to C_{60} leading to no luminescence. These results confirm photo-induced charge-transfer in the composite involving poly(β-pinene) and C_{60}.

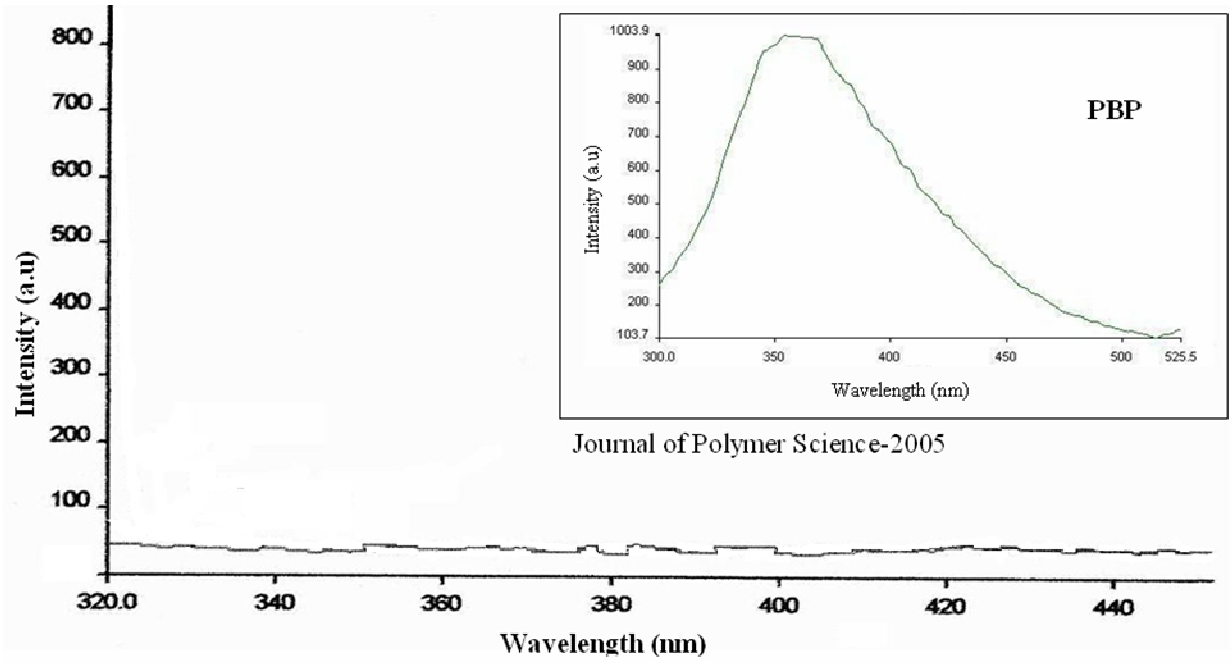

Figure 10.3 Quenching of photoluminescence of the composite involving poly(β-pinene) and C_{60} (2% by weight) for excitation at 280 nm. The inset shows the photoluminescence spectrum of poly(β-pinene) by itself for excitation at 280 nm

Photovoltaic cells used in the report were formed by sandwiching the composite film between two electrodes. Aluminum coated glass slide was used as one electrode and indium-tin-oxide coated glass slide was used as the other electrode. The film of the composite involving poly(β-pinene) and C_{60} was cast on the aluminum electrode and the indium-tin-oxide electrode was placed on it. Pressure was applied to keep the composite and the electrodes in contact. The film thickness was about 1 μm. Films thinner than that were not used in these experiments to avoid short-circuit between the electrodes. Aluminum electrode was connected to the negative terminal of a high impedance electrometer (Keithley 617 Programmable Electrometer) and the

indium-tin-oxide electrode was connected to the positive end of the electrometer to measure the photovoltage. The indium-tin-oxide electrode was placed face-up to ensure that the light is incident on the polymer through this electrode. The experimental setup is shown in Fig. 10.4. The inset in the Fig.10.4 shows the spectrum of the white light source used in these measurements. In addition, a nitrogen laser (325 nm and 425 nm) was used as a light source for these measurements. Besides the composite samples, poly(β-pinene) by itself and C_{60} by itself were also used in the sandwiched structure for photovoltaic measurement as control experiments.

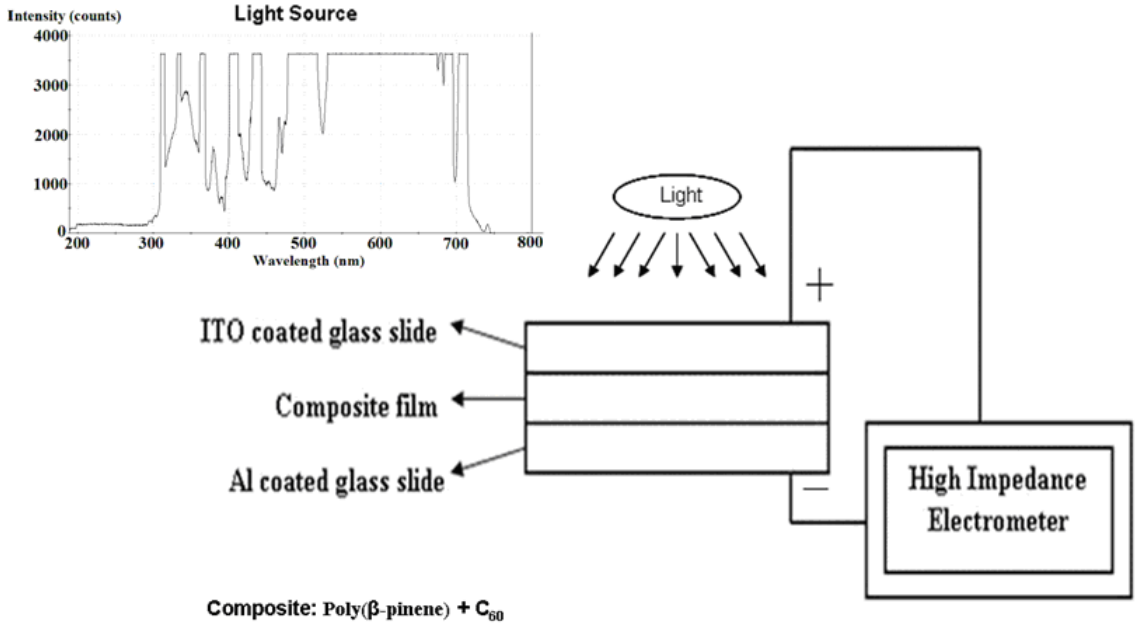

Figure 10.4: Schematic of the photovoltaic experimental setup

The photovoltage produced for a composite involving poly(β-pinene) and 4% C_{60} by weight was recorded for different intensities of the incident light. White light source with a wavelength range of 300-700nm was used. It was observed that the photovoltage produced increased with increase in the intensity of the incident light as shown in the Figure 10.5. A light intensity of 6mW/cm^2

yielded a photovoltage of 280mV. For poly(β-pinene) by itself and C_{60} by itself no appreciable photovoltage was observed. This shows that the measured photovoltage is due to the interaction between poly(β-pinene) and C_{60}.

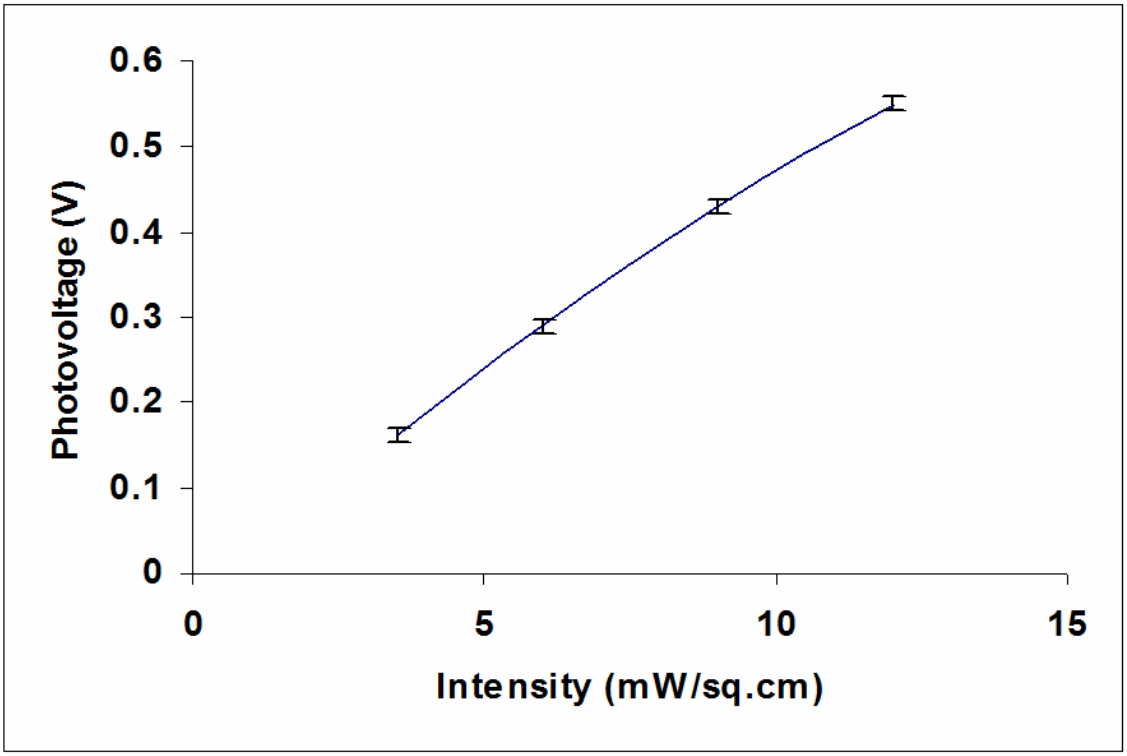

Figure 10.5: Photovoltage as a function of incident light intensity for a composite containing 4% C_{60} by weight

Photovoltages were recorded for the composites having different concentrations of C_{60} at different intensities of incident light. Table 10.1 shows the photovoltage produced for composites having different concentrations of C_{60} at different intensities of the incident light.

Intensity Of Incident light (mW/cm^2)	Photo-voltage (mV)			
	Composite with 8% C_{60}	Composite with 6% C_{60}	Composite with 4% C_{60}	Composite with 2% C_{60}
3.5	110	190	162	80
6	200	290	280	130
9	210	380	430	170
12	255	420	550	210

Table 10.1: Photo-voltages produced for composites

Measurements were also performed for composites having different concentrations of C_{60} using Nitrogen laser operating at 325 nm with a fixed intensity of 2mW/sq.cm. The results are shown in the Table 10.2. In addition, another line from the nitrogen laser with wavelength of 425 nm was used for such experiments but no measurable photovoltage was observed. This is because pristine poly(β-pinene) does not absorb significantly at 425 nm.

Sample	Photo-voltage (mV)
Composite with 2% C_{60}	20
Composite with 4% C_{60}	80
Composite with 6% C_{60}	39
Composite with 8% C_{60}	18

Table 10.2: Photo-voltages produced for composites with different concentrations of C_{60} using Nitrogen laser as light source (intensity 2 mW/cm^2)

It was observed that the composite involving poly(β-pinene) and 4% C_{60} by weight showed better performance when compared to the composites involving poly(β-pinene) with other concentrations of C_{60}. This is due to the better homogeneity of the composite involving poly(β-

pinene) and 4% C_{60} by weight when compared to other composites. For composite films with higher weight percentages of C_{60}, clusters of C_{60} were formed leading to lower interaction with the polymer double bonds. As a result, less photo-induced charge-transfer and smaller photo-voltages were observed (Table 10.1 and Table 10.2). The photovoltaic device under the present configuration can be used in photo-detector application in the ultraviolet regime. Photovoltaic cells for power generation will need a more refined configuration involving thinner composite films that will allow larger currents for the devices.

In the composite involving poly(β-pinene) and C_{60}, the polymer, poly(β-pinene) acts as an electron donor and the C_{60} acts as an electron acceptor. When light is incident and absorbed by the polymer, electron hole pairs are produced. From this excited state of the polymer, electron is transferred to C_{60} as shown in the Fig.10.6. The electrons are then transported to the aluminum electrode by the C_{60} and the holes are transported to indium tin oxide electrode. This transportation of electrons and holes produces the observed photovoltage. The observation that the nitrogen laser at 325nm produces photovoltage while the same laser at 425nm does not produce significant photovoltage implies that electron-transfer occurs only from the polymer to C_{60} but not vice-versa. Further studies on efficiency and current ratings of the cells are under progress.

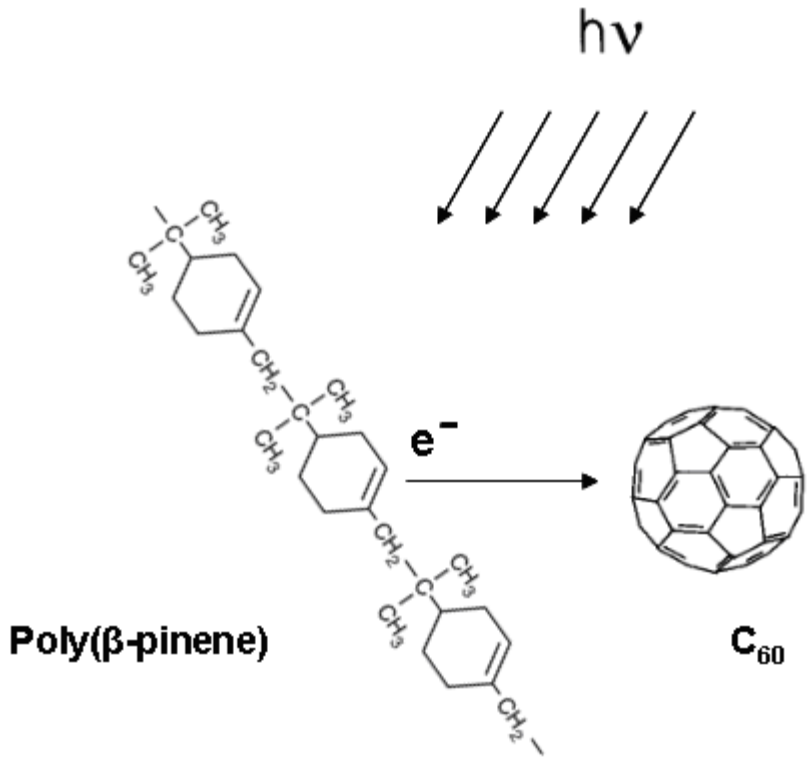

Figure 10.6: Schematic of photo-induced electron transfer from poly(β-pinene) to C_{60}

10.4 Conclusions

Photo-induced charge-transfer and resulting photovoltaic effect in composite films involving a nonconjugated conductive polymer and C_{60} have been observed for the first time. It was observed that the composite 4% C_{60} by weight produced a photovoltage of 280mV for an incident light intensity of 6mW/cm^2. The photovoltage produced increases with increase in the intensity of the light. It was also observed that the composite with 4% C_{60} showed better performance when compared to the composites having other concentrations of C_{60}. This photovoltaic cell has many applications at a lower cost in the areas of solar cells, photo-detectors, photo-sensors, etc. While pristine poly(β-pinene) has significant photoluminescence (peak at 360 nm) for excitation at 280 nm, the photoluminescence is quenched when C_{60} is added to poly(β-pinene) to form the composite. This shows that the observed photovoltaic effect is due

to photo-induced charge-transfer from the isolated double-bond of the polymer to C_{60}.

CHAPTER 11

CONCLUSIONS

Single crystal films involving a combination of DAST and laser dye IR125 of excellent optical quality were prepared using the modified shear method. Polarized optical absorption spectra show that the IR 125 molecules are aligned perpendicular to the DAST dipole axis. The optical absorption characteristics of DAST-IR125 film are significantly different than that of DAST film. The electro-optic coefficient of DAST-IR125 film as measured is about 300 pm/V at 633 nm. These novel materials have a wide variety of applications in organic electronics and photonics.

Electrical and optical properties of nonconjugated conducting polymer, polynorbornene were studied. When doped with iodine, its electrical conductivity increases by several orders of magnitude. The maximum conductivity of this polymer was found to be 0.01 S/cm corresponding to iodine molar concentration of 1.5. Optical absorption spectrum of lightly doped polymer has two distinct peaks. One at 4.21eV corresponding to cation radicals and the other at 3.13 eV corresponding to charge transfer between double bond and dopant. When the dopant concentration is increased, the intensity of the peak due to cation radicals increases and the peak due to charge transfer broadens and undergoes a red shift. FTIR measurements show a decrease in C=C peak at 1718 cm^{-1} when the polymer is doped. Photoluminescence measurements show an emission peak at 425nm when the undoped polymer is excited at 300nm. Electrical and optical properties of polynorbornene are comparable with other nonconjugate conducting polymers.

EPR measurements were performed on poly(β-pinene) at different concentrations of iodine. The EPR signal was found to increase proportionally with the iodine concentration due to the formation cation radicals upon doping and charge-transfer. The results are consistent with the FTIR and optical absorption data. The g-value and the EPR line-width (ΔH_{pp}) compare well with that of another nonconjugated conductive polymer, doped 1,4-*cis*-polyisoprene. Hyperfine splitting in the EPR signal was observed for heavily doped samples due to reduced distance between the cation radical and the iodine anion.

Quadratic electro-optic effect in iodine-doped poly(β-pinene) at off resonant wavelengths was measured using field-induced birefringence technique. The magnitude of the Kerr coefficient at 1.55 μm was found to be 1.6×10^{-10} m/V^2, which is the largest known for any material. At 790 - 810 nm the magnitudes are also very large. The magnitude is slightly smaller at 810 nm since this wavelength coincides with the two-photon resonance peak. These exceptionally large nonlinearities are attributed to the sub-nanometer size metallic quantum dots formed upon doping and charge-transfer involving poly(β-pinene). The large nonlinearity at 1.55 μm is important for ultrafast device applications in telecommunication.

Exceptionally high two-photon absorption coefficient, α_2 was measured in doped poly(β-pinene) at 790nm and 795 nm using pump probe technique using a mode locked Ti-Sapphire laser with 150 fs pulses. The response time of α_2 was ultrafast clearly indicating that the nonlinearities in this material are of electronic origin. Such high nonlinearities are attributed to the quantum dot like structure formed upon doping. This material has a wide variety of applications in photonics.

A nonlinear optical waveguide was prepared by casting a uniform cladding of poly(β pinene) on a bare multi-mode fiber and doping it. The waveguide was of excellent optical quality

and could withstand a peak intensity of 2.5MW/cm^2 without damage. Two photon absorption measurements were made using this fiber at 795 nm. A maximum decrease of 28% in transmission was observed at an input power level of 60mW in mode-locked condition. The observed change is higher than that observed in thin films by a factor of over 200. More work needs to be done to confirm this important result. Nonlinear waveguiding has significant applications in photonics including high speed switching and optical limiting.

Photo-induced charge-transfer and resulting photovoltaic effect in composite films involving a nonconjugated conductive polymer and C_{60} were studied. It was observed that the composite involving 4% C_{60} by weight produced a photovoltage of 280mV for an incident light intensity of 6mW/sq.cm. The photovoltage produced was found to increase with increase in the intensity of the light. This photovoltaic cell has many applications at a lower cost in the areas of solar cells, photo-detectors, photo-sensors, etc. While pristine poly(β-pinene) has significant photoluminescence (peak at 360 nm) for excitation at 280 nm, the photoluminescence is quenched when C_{60} is added to poly(β-pinene) to form the composite. This shows that the observed photovoltaic effect is due to photo-induced charge-transfer from the isolated double-bond of the polymer to C_{60}.

In conclusion, detailed structural, electrical and nonlinear optical properties of specific important organic molecular and nonconjugated conductive polymeric systems have been studied.

REFERENCES

[1] M. Born and E. Wolf. *Principles of optics: electromagnetic theory of propagation, interference and diffraction of light*. Cambridge University Press, 1999.

[2] D. L. Sengupta and T. K. Sarkar. *Maxwell, Hertz, the Maxwellians and the early history of electromagnetic waves*, volume 1. 2001.

[3] C. H. Townes. Lasers. *Frontiers of Science: In Celebration of the 80th Birthday of CN Yang*, page 1, 2003.

[4] P. A. Franken; A. E. Hill; C. W. Peters and G. Weinreich. Generation of optical harmonics. *Phys. Rev. Lett.*, 7:118, 1961.

[5] R. W. Terhune; P.D. Maker and C.M. Savage. Optical harmonic generation in calcite. *Phys. Rev. Lett.*, 8(10):404–406, 1962.

[6] R. W. Hellwarth. Theory of stimulated Raman scattering. *Phys. Rev.*, 130(5):1850, 1963.

[7] P. N. Prasad and D. J. Williams. *Introduction to nonlinear optical effects in molecules and polymers*. Wiley New York, 1991.

[8] R. W. Boyd. *Nonlinear Optics*. Academic Press, 2003.

[9] E. G. Sauter. *Nonlinear optics*. Wiley-Interscience, 1996.

[10] Y. R. Shen. *The Principles of Nonlinear Optics*. John Wiley and Sons, Newyork, 1984.

[11] A. Yariv and P. Yeh. *Optical waves in crystals*. Wiley New York, 1984.

[12] N. Bloembergen. *Nonlinear optics*. World Scientific, 1996.

[13] R. Paschotta. *Encyclopedia of laser physics and technology*. Vch Pub, 2008.

[14] H. S. Nalwa and S. Miyata. *Nonlinear optics of organic molecules and polymers*. CRC press, 1997.

[15] P. Weinberger. John Kerr and his effects found in 1877 and 1878. *Philosophical Magazine Letters*, 8(12):897–907, 2008.

[16] M. Sheik-Bahae; A. A. Said; T. Wei; D. J. Hagan and E. W. V. Stryland. Sensitive

measurement of optical nonlinearities using a single beam. *IEEE J. Quantum Electron*, 26:760, 1990.

[17] M. Goeppert-Mayer. Double beta-disintegration. *Ann Phys.*, 9:273, 1931.

[18] W. Kaiser; C. G. B. Garrett and D. L. Wood. Fluorescence and optical maser effects in caf2: Sm++. *Phys. Rev. Lett.*, 123:766, 1961.

[19] I. D. Abella. Optical double-photon absorption in cesium vapor. *Phys. Rev. Lett.*, 9:453, 1962.

[20] G. P. Agrawal and R. W. Boyd. *Contemporary Nonlinear Optics*. Academic Press, 1992.

[21] A. M. Fox. *Quantum Optics: An Introduction*. Oxford University Press, 2006.

[22] P. N. Prasad. *Nanophotonics*. John Wiley & Sons, 2004.

[23] G. P. Agarwal; C. Cojan and C. Flytzanis. Nonlinear optical properties of one-dimensional semiconductors and conjugated polymers. *Phys. Rev. Lett.*, B15:904, 1978.

[24] D. Chemla and J. Zyss, editors. *Nonlinear Optical Effects in Organic Molecules and Crystals*. John Wiley & Sons, 1987.

[25] J. D. Jackson. *Classical Thermodynamics*. John Wiley & Sons, 1980.

[26] P. D. Marker; R. W. Terhune; M. Nisenoff and C. M. Savage. Effects of dispersion and focusing on the production of optical harmonics. *Phys. Rev. Lett.*, 8:21, 1962.

[27] J. A. Giordmaine. Mixing of light beams in crystals. *Phys. Rev. Lett.*, 8:19, 1962.

[28] G. D. Boyd and C. K. N. Patel. Linbo3: An efficient phase matchable nonlinear optical material. *Appl. Phys. Lett.*, 5:234, 1964.

[29] F. Zernike and J. E. Midwinter. *Applied Nonlinear Optics*. Wiley New York, 1973.

[30] A. Ashkin; G. D. Boyd; J. M. Dziedzic; R. G. Smith; A. A. Ballman; J. J. Levinstein and K. Nassau. Optically-induced refractive index inhomogeneities in $LiNbo_3$ and $LiTao_3$. *Appl. Phys. Lett.*, 9:72, 1966.

[31] Committee on Optical Science and National Research Council Engineering. Harnessing light: Optical science and engineering for the 21st century. Technical report, National Academy Press, Washinton D.C., 1998.

[32] P. M. Rentzepis and Y. H. Pao. Laser-induced optical second harmonic generation in organic crystals. *Appl. Phys. Lett.*, 5:156, 1964.

[33] G. H. Heilmeir; N. Ockman; R. Braunstein and D. A. Kramer. Relationship between optical second harmonic generation and the electro-optic effect in the molecular crystal hexamine. *Appl. Phys. Lett.*, 5:229, 1964.

[34] S. K. Kurtz and T. T. Perry. A powder technique for the evaluation of nonlinear optical materials. *Appl. Phys.*, 39:3798, 1968.

[35] D. S. Chemla; J. L. Oudar and J. Jerphagnon. Origin of the second-order optical susceptibilities of crystalline substituted benzene. *Phys. Rev. B*, 12:4534, 1975.

[36] J. L. Oudar and D. S. Chemla. Hyperpolarizabilities of the nitroanilines and their relations to the excited state dipole moment. *J. Chem. Phys.*, 66:2664, 1977.

[37] C. Bosshard; K. Sutter; P. Pretre; J. Hulliger; M. Florsheimer; P. Kaatz and P. Gunter. *Advances in Nonlinear Optics*. Gordon and Breach Publishers, 1995.

[38] M. C. Gupta, editor. *Handbook of Photonics*. CRC press, 1997.

[39] M. B. J. Diemeer; F. M. M. Suyten; E. S. Trommel; A. McDonach; J. M. Copeland; L. W. Jenneskens and W. H. G. Horsthuis. Photoinduced channel waveguide formation in nonlinear optical polymers. *Electron. Lett.*, 26:379, 1990.

[40] B. L. Davydov; L. D. Derkacheva; V. V. Dunina; M. E. Zhabotinskii; V. F. Zolin; L. G. Koreneva and M. A. Samokhina. Spectroscopy techniques. *Opt. Spectrosc.*, 30:274, 1971.

[41] J. S. Lalama and A. F. Garito. Origin of the nonlinear second-order optical susceptibilities of organic systems. *Phys. Rev. A*, 20:1179, 1979.

[42] J. L. Oudar and R. Hierle. An efficient organic crystal for nonlinear optics: methyl- (2,4-dinitrophenyl) -aminopropanoate. *J. Appl. Phys.*, 48:2699, 1977.

[43] B. F. Levine; C. G. Bethea; C. D.Thurmond; R. T. Lych and J. L. Bernstein. An organic crystal with an exceptionally large optical second?harmonic coefficient: 2-methyl-4-nitroaniline. *J. Appl. Phys.*, 50:2523, 1979.

[44] J. Zyss and J. L. Oudar. Relations between microscopic and macroscopic lowest-order optical nonlinearities of molecular crystals with one- or two-dimensional units. *Phys. Rev. A*, 26:2028, 1982.

[45] P. Gunter; C. Bosshard; K. Sutter; H. Arend; G. Chapuis; R. J. Twieg and D. Dobrowolski. 2-cyclooctylamino-5-nitropyridine, a new nonlinear optical crystal with orthorhombic symmetry. *Appl. Phys. Lett.*, 50:486, 1987.

[46] K. Ogawa; M. Kaji; H. Kagawah; M. Sagawa and A. Kakuta. Structure of 8-(4-acetylphenyl)-1,4-dioxa-8-azaspiro[4,5]decane: a new potential nonlinear optical

material. *Acta. Cryst.*, C50:95, 1994.

[47] A K Bhowmik. *Nonlinear Optical and Light Emission Studies of Special Organic Molecules and Crystals*. PhD thesis, Auburn University, 2000.

[48] G R Meredith. Nonlinear optical properties of organic and polymeric materials. In *ACS Symposium Series, American Chemical Society, 233*, 1983.

[49] S. Okada; A. Masaki; H. Matsuda; H. Nakanishi; M. Kato; R. Maramatsu and M. Otsulka. Synthesis and crystal structure of a novel organic ion-complex crystal for second-order nonlinear optics. *Jap. J. of Appl. Phys.*, 29:1112, 1990.

[50] S. R. Marder; J. W. Perry and C. P. Yakymyshyn. Organic salts with large second-order optical nonlinearities. *Chem. Mater.*, 6:1137, 1994.

[51] S. R. Marder; J. W. Perry and W. P. Schaefer. Synthesis of organic salts with large second-order optical nonlinearities. *Science New Series*, 245:626, 1989.

[52] U. Meier; M. Bosch; C. Bosshard and P. Gunter. Dast a high optical nonlinearity organic crystal. *Synth. Met.*, 109:19, 2000.

[53] S G Kutty. *Enhanced Electro-optic Modulation Using a Single Crystal Film of an Organic Molecular Salt Placed Inside a Fabry-Perot Cavity*. PhD thesis, Auburn University, 2005.

[54] F. Pan; G. Knopfle; C. Bosshard; S. Follonier; R. Spreiter; M. S. Wong and P. Gunter. Electro-optic properties of the organic salt 4-n,n-dimethylamino-4-n-methyl-stilbazolium tosylate. *Appl. Phys. Lett.*, 69:13, 1996.

[55] M. Thakur; A. Mishra; J. Titus and A. C. Ahyi. Electro-optic modulation at 1.5 ghz using single-crystal film of an organic molecular salt. *Appl. Phys. Lett.*, 81:3738, 2002.

[56] M. Thakur; J. Titus and A. Mishra. Single-crystal thin films of organic molecular salt may lead to a new generation of electro-optic devices. *Opt. Eng.*, 42:456, 2003.

[57] H. Adachi; Y. Takahashi; J. Yabuzaki; Y. Mori and T. Sasaki. High-quality organic 4-dimethylamino-n-methyl-4-stilbazolium tosylate (DAST) crystals for thz wave generation. *J. Cryst. Growth*, 198:568, 1999.

[58] F. Tsunesada; T. Iwai; T. Watanabe; H. Adachi; M. Yoshimura; Y. Mori and T. Sasaki. High-quality crystal growth of organic nonlinear optical crystal dast. *J. of Cryst. Growth*, 237:2104, 2002.

[59] R. Mohan Kumar; D. Rajan Babu; G. Ravi and R. Jayavel. Growth and characterization of 4-dimethylamino-n-methyl-4-stilbazolium tosylate (DAST) single crystals. *J. of Cryst. Growth*, 250:113, 2003.

[60] S. R. Forrest; P. E. Burrows; A. Stroustrup; D. Strickland and V.S. Ban. Intense second harmonic generation and long-range structural ordering in thin films of an organic salt grown by organic vapor phase deposition. *Appl. Phys. Lett.*, 68:1326, 1996.

[61] S. Sohama; H. Takahashi; T. Taniuchi and H. Ito. Organic nonlinear optical crystal dast growth and its device applications. *Chem. Phys.*, 245:359, 1999.

[62] M. Thakur and S. Meyler. Growth of large-area thin-film single crystals of poly(diacetylenes). *Macromolecules*, 18:2341, 1985.

[63] M. Thakur; Y. Shani; G. C. Chi and K. O' Brein. Thin single crystal films of organics; waveguiding in pts films. *Synth. Met.*, 28:D595, 1989.

[64] S. P. Kutty and M. Thakur. Electro-optic modulation using single-crystal film of an organic molecular salt in a fabry-perot cavity. *Appl. Phys. Lett.*, 87:191111/1, 2005.

[65] R. Swamy; S. P. Kutty; J. Titus; S. Khatavkar and M. Thakur. Electroabsorption in single-crystal film of a second-order optical material. *Appl. Phys. Lett.*, 85:4025, 2004.

[66] A. K. Bhowmik; J. Xu and M. Thakur. Polarized optical absorption and photoluminescence measurements in single-crystal thin films of 4-dimethylamino-n-methyl-4-stilbazolium tosylate. *Appl. Phys. Lett.*, 75:3291, 1999.

[67] W. Sellmeier. Zur erklärung der abnormen farbenfolge im spectrum einiger substanzen. *Annalen der Physik und Chemie*, 219:272, 1871.

[68] H. S. Nalwa. Fabrication of organic nanocrystals for electronics and photonics. *Adv. Mater.*, 5:341, 1993.

[69] K. C. Rustagi and J. Ducuing. Third-order optical polarizability of conjugated organic molecules. *J.Opt. Commun.*, 10:258, 1974.

[70] C. Sauteret; J. P. Herman; R. Frey; F. Pradere; J. Ducuing; R. H. Baughman and R. R. Chance. Identification and role of two-photon excited states in a ?-conjugated polymer. *Phys. Rev. Lett*, 36:956, 1976.

[71] J. Bolger; T. G. Harvey; W. Ji; A. K. Kar; S. Molyneux; B. S. Wherrett; D. Bloor and P. Norman. Near-resonant third-order optical nonlinearities in p-toluene sulfonate polydiacetylene. *J. Opt. Soc. Am. B*, 9:1552, 1992.

[72] D. Arivuoli. Fundamentals of nonlinear optical materials. *Pramana - J. Phys.*, 57:871, 2001.

[73] H. S. Nalwa, editor. *Handbook of Nanostructured Materials and Nanotechnology*. Academic Press, 2000.

[74] H. Shirakawa; E. J. Louis; A. G. MacDiarmid; C. K. Chiang and A. J. Heeger. The electronic structures of-polyacetylene. *J. Chem.Soc., Chem. Comm.,*, 16:578, 1977.

[75] M. Thakur. A class of conducting polymers having nonconjugated backbones. *Macromolecules*, 21:661, 1988.

[76] H. Rajagopalan; P. Vippa and M. Thakur. Quadratic electro-optic effect in a nano-optical material based on the nonconjugated conductive polymer poly (? -pinene). *Appl. Phys. Lett.*, 88:033109/1, 2006.

[77] M. Thakur. Nonconjugated conductive polymer. *J. Mac. Mol. Sci. A*, A38:1337, 2001.

[78] R. Swamy; H. Rajagopalan; P. Vippa; M. Thakur and A. Sen. Quadratic electro-optic effect in a nano-optical material based on the nonconjugated conductive polymer, poly(ethylenepyrrolediyl) derivative. *Solid State Commn.*, 143:519, 2007.

[79] Y. Lin and L. Yuzhong. Electrical conductivity in iodine-doped nonconjugated polyanilinefurfural. *Polymer Bulletin*, 38:573, 1997.

[80] M. Thakur; R. Swamy and J. Titus. Quadratic electrooptic effect in a nonconjugated conductive polymer. *Macromolecules*, 37:2667, 2004.

[81] H. Rajagopalan; P. Vippa and M. Thakur. Quadratic electro-optic effect in a nano-optical material based on the nonconjugated conductive polymer poly (? -pinene). *Appl. Phys. Lett.*, 88:033109/1, 2006.

[82] J. Titus and M. Thakur. Two-photon absorption in quantum dots based on a nonconjugated conductive polymer. *Appl. Phys. Lett.*, 90:121111/1, 2007.

[83] A. Luque and S. Hegedus, editors. *Handbook of Photovoltaic Science and Engineering*. John Wiley & Sons.

[84] A. E. Becquerel. *Comt Rend. Academia d. Sciences*, 9:561, 1839.

[85] S. S. Sun and N. S. Sariciftci, editors. *Organic Photovoltaics: Mechanisms, Materials and Devices*. CRC press, 2005.

[86] D Chaplin; C Fuller and G Pearson. A new silicon p?n junction photocell for converting solar radiation into electrical power. *J. Appl.Phys.*, 25:676, 1954.

[87] D. C. Reynolds; G. Leies; L. L. Antes and R. E. Marburger. Photovoltaic effect in cadmium sulfide. *Physics Review Letters*, 96:533, 1954.

[88] D. Jenny; J. Loferski and P. Rappaport. The photovoltaic effect and its utilization. *Phys. Rev. Lett.*, 101:1208, 1956.

[89] D. Cusano. Radiative recombination from gaas directly excited by electron beams. *Solid State Electron*, 6:217, 1963.

[90] J. Lindmayer and J. Allison. The violet cell: An improved silicon solar cell. *COMSAT Tech. Rev.*, 3:1, 1973.

[91] M. Green. In *Proc. 18th IEEE photovoltaic Specialist Conf., pp. 39-42*, 1985.

[92] R Sinton; Y Kwark; P Gruenbaum; R Swanson. In *Proc. 18th IEEE Photovoltaic Specialist Conf.*, 1985.

[93] Renewables in global energy supply - an iea fact sheet. Technical report, OECD, IEA, 2007.

[94] G. A. Chamberlain. Organic solar cells: A review. *Solar Cells*, 8:47, 1983.

[95] R. Even B. Boudjema G. Guillaud J.J. Andre, J. Simon and M. Maitrot. Molecular semiconductors and junction formation: Phthalocyanine derivatives. *Synth*, 18:683, 1987.

[96] H. W. Kroto; J. R. Heath; S. C. O'Brien; R. E. Curl and R E Smalley. C60: Buckminsterfullerene. *Nature*, 318:162, 1985.

[97] C. W. Tang. Two layer organic photovoltaic cell. *Appl. Phys. Lett.*, 48(2):183–185, 1986.

[98] A Paul; Lane; Zakya H. Kafafi. Solid-state organic photovoltaics: A review of molecular and polymeric devices. Technical report, Naval Research Laboratory, Washington, D.C., USA.

[99] R. N. Marks; J. J. M. Halls; D. D. C. Bradley; R. H. Friend and A. B. Holmes. Further evidence for the role of excitons in photogeneration of charges in poly(phenylene vinylene)s. *J.Phys.:Condens. Mat.*, 6(7):1379, 1994.

[100] G. Yu; K. Pakbaz and A. J. Heeger. Semiconducting polymer diodes: Large size, low cost photodetectors with excellent visible?ultraviolet sensitivity. *Appl. Phys. Lett.*, 64(25):3422–3424, 1994.

[101] S. Glenis; G. Horowitz; G. Tourillon and F. Garnier. Electrochemically grown polythiophene and poly(3-methylthiophene) organic photovoltaic cells. *Thin solid Films*, 111:93, 1984.

[102] C. J. Brabec; V. Dyakonov; J. Parisi and N. S. Sariciftci. *Organic Photovoltaics Concepts and Realization*.

[103] N. S. Sariciftci; L. Smilowitz; A. J. Heeger and F. Wudl. Photoinduced electron transfer from a conducting polymer to buckminsterfullerene. *Science*, 258(5087):1474–1476,

1992.

[104] S. Morita; A. A. Zakhidov and K. Yoshino. Doping effect of buckminsterfullerene in conducting polymer: Change of absorption spectrum and quenching of luminescene. *Solid State Commun.*, 82:249, 1992.

[105] S. Morita; S. Kiyomatsu; X. H. Yin; A. A. Zakhidov; T. Noguchi; T. Ohnishi and K. Yoshino. Doping effect of buckminsterfullerene in poly(2,5-dialkoxy-p-phenylene vinylene). *J. Appl. Phys.*, 74:2860, 1993.

[106] S. Günes; D. Baran; G. Günbas; F. Özyurt; A. Fuchsbauer; N. S. Sariciftci and L. Toppare. Photovoltaic and photophysical properties of a novel bis-3-hexylthiophene substituted quinoxaline derivative. *Solar Energy Materials and Solar Cells*, 92:1162, 2008.

[107] V. Y. Butko; J. C. Lashley and A. P. Ramirez. Low-temperature field effect in a crystalline organic material. *Phys. Rev. B*, 72:081312/1, 2005.

[108] C. Reese and Z. Bao. Organic single-crystal field-effect transistors. *Materials Today (Oxford, United Kingdom)*, 10:20, 2007.

[109] S. R. Marder; J. W. Perry and W. P. Schaefer. Synthesis of organic salts with large second-order optical nonlinearities. *Science*, 245:626, 1989.

[110] M. Thakur; S. Katavkar and E. J. Parish. Polyalloocimene, a novel nonconjugated conductive polymer: The correct fundamental basis for conductive polymers. *J. Mac. Mol. Sci. A*, 40, 12:1397, 2003.

[111] K. Uchida; S. Kaneko; S. Omi; C. Hata; H. Tanji; Y. Asahara and A. J. Ikushima. Optical nonlinearities of a high concentration of small metal particles dispersed in glass: copper and silver particles. *J. Opt. Soc. Am. B*, 7:1236, 1994.

[112] M. Thakur and B. S. Elman. Optical and magnetic properties of a nonconjugated conducting polymer. *J. Chem. Phys.*, 90:2042, 1989.

[113] R. Singh and A. K. Narula. Correlation between electron spin resonance and dc conductivity data of polypyrrole, poly(n-methyl pyrrole-pyrrole), and poly(n-methyl pyrrole). *J. Appl. Phys.*, 82:4362, 1997.

[114] J. M. Ballesteros; R. Serna; J. Solis; C. N. Afonso; A. K. Petford-Long, D. H. Osborne, and R.F. Haglund Jr. Pulsed laser deposition of cu:al2o3 nanocrystal thin films with high third-order optical susceptibility. *Appl. Phys. Lett.*, 71:2445, 1997.

[115] C. B. de Araújo; A. Humeau; G. Boudebs; V. D. Del Cacho and L. R. P. Kassab. Giant third-order nonlinearity of lead and germanium based films in the visible and in the infrared. *J. Appl. Phys.*, 101:066103, 2007.

[116] P. Innocenzi and B. Lebeau. Organic–inorganic hybrid materials for non-linear optics. *J. Mater. Chem.*, 15:3821, 2005.

[117] A. Narayanan; A. Palthi and M. Thakur. Electrical and optical properties of a novel nonconjugated conductive polymer, polynorbornene. *J of Macmol. Sci. Part A*, 46-4:455, 2009.

[118] A. Narayanan and M. Thakur. Quadratic electro-optic effect in the nonconjugated conductive polymer iodine-doped poly(?-pinene) measured at longer wavelengths including 1.55 micrometer. *Solid State Commn.*, 150:375, 2010.

[119] N. Del Fatti and F. Vall´ee. Ultrafast optical nonlinear properties of metal nanoparticles. *Appl. Phys. B*, 73:383, 2001.

[120] J. Y. Bigot; J. C. Merle; O. Cregut and A. Daunois. Electron dynamics in copper metallic nanoparticles probed with femtosecond optical pulses. *Phys. Rev. Lett.*, 75(25):4702, 1995.

[121] Q. Li; C. Liu; Z. Liu; and Q. Gong. Broadband optical limiting and two-photon absorption properties of colloidal gaas nanocrystals. *Opt. Express*, 13:1833, 2005.

[122] Q. Wan; C. L. Lin; N. L. Zhang; W. L. Liu; G. Yang and T. H. Wang. Linear and third-order nonlinear optical absorption of amorphous ge nanoclusters embedded in al2o3 matrix synthesized by electron-beam coevaporation. *Appl. Phys. Lett.*, 82:3162, 2003.

[123] Y. Zhu; H. I. Elim; Y. L. Foo; T. Yu; Y. Liu; W. Ji; J. Y. Lee; Z. Shen; A. T. S .Wee; J. T. L. Thong and .C H. Sow. Growth, characterizations and field emission properties of one-dimensional nanostructures. *Adv. Mater.*, 8:587, 2006.

[124] G. Nimtz; P. Marquardt and H. Gleiter. Size-induced metal-insulator transition in metals and semiconductors. *J. of Cryst. Growth*, 86:66, 1988.

[125] Y. Silberberg and G. I. Stegeman. Nonlinear coupling of wave-guide modes. *Appl. Phys. L*, 50:801, 1987.